93-3

Nuclear Magnetic Properties in the Relativistic σ-ω Model

Shingo Ichii

December 1988

Acknowledgement

I express my sincere gratitude to Professor Akito Arima, my thesis advisor, for his ingenious guidance and ceaseless encouragement throughout my graduate career.

I am particularly grateful to Doctor Wolfgang Bentz for his helpful discussions as a collaborator of this work.

I also would like to thank Professors Koichi Yazaki and Takaharu Otsuka, Doctors Kiyotaka Shimizu and Hiroyuki Sagawa for their encouragement and discussions in various occasions.

Finally I wish to thank the members of the Nuclear Theory Group at the University of Tokyo for discussion and interest.

Computer calculation for this thesis was done using HITAC M-680H at the Computer Centre, University of Tokyo and VAX-11/780 at the Meson Science Laboratory, University of Tokyo.

Contents

1 Introduction

In this thesis, nuclear magnetic moments and magnetic form factors are studied within the framework of the relativistic σ-ω model. We focus on the simplest systems available for this purpose, that is, nuclei with an LS closed core plus or minus one nucleon. These systems are simplest in the sense that, in traditional nuclear physics, we can expect the extreme single particle picture to work well for them. In fact, magnetic moments of these nuclei are one of the experimentally most accurately determined quantities, and theoretically the extreme single particle values, the Schmidt values, for isoscalar magnetic moments fall quite near the experimentally measured values [1]. Corrections theoretically expected, such as exchange currents, configuration mixing and the Δ-hole excitation, turn out to be small for isoscalar magnetic moments. (For *isovector* magnetic moments, the small deviations from the Schmidt values result from cancellations between pion exchange currents and configuration mixing effects [1].)

To discuss the small deviations of isoscalar magnetic moments from the Schmidt values, we previously calculated heavier meson exchange currents which had been believed to be less important than the second order configuration mixing effects [2,3]. We found, contrary to this belief, contributions from exchange currents whose order of magnitude are comparable to those from configuration mixing. In the course of the calculation, however, we encountered certain theoretical ambiguities. That is, several parameter sets, which were proposed so as to describe the nuclear force, gave different answers. The ambiguity was severe because many processes gave contri-

butions which were canceling one another. We had no principle to select the most appropriate parameter set. This frustrating situation is inherent to the approach that we took at that time: To derive two body exchange current operators explicitly from meson exchange processes, and then to evaluate the expectation values using the shell model wave functions of nuclei. We had no internal relation between the nuclear wave function and the magnetic moment operators, although both of them can be thought to originally arise from meson exchange processes of the same nature.

Many authors share this uneasy feeling on this (in)consistency between operators and wave functions (for example, concerning isoscalar magnetic moments, see [4]). Most of them try to extract information on two body current operators from conventional two body potentials determined so as to reproduce NN scattering data and the deuteron properties. Though it is true that the current conservation imposes a condition on the longitudinal part of the current, we think that this approach suffers from the following defects: (1) We cannot reproduce properties of finite nuclei from realistic two-body potentials using the many-body techniques at the present stage. Finally one has to resort to harmonic oscillator shell model wave functions. So this approach in fact does not solve the present consistency problem. (2) When we use two-body NN potentials in nonrelativistic quantum mechanics we have lost some information on the underlying meson exchange processes. This loss of information is caused by elimination of meson degrees of freedom and by casting the expression, which represents an essentially relativistic meson exchange phenomenon, into a nonrelativistic form. Therefore we cannot expect that we can extract full information on meson

exchange currents from the two-body potentials commonly used in nuclear physics.

This is why we turned to the apparently unrealistic relativistic σ-ω model [5]. In this model, the medium range attraction between two nucleons is described by the exchange of the fictitious σ meson, which is thought to simulate the 2π exchange to some extent, and the short range repulsion arises from ω meson exchange. This model, when treated in the Hartree approximation, is simple enough to allow a theoretically consistent (in the meaning indicated above, and discussed more profoundly later) treatment of strong and electromagnetic interactions, and capable to reproduce various ground state properties of closed shell nuclei fairly well. We treat meson degrees of freedom explicitly, and if we include the electromagnetic interaction at the lagrangian level we do not encounter the information loss problem stated above. The masses of the σ and ω mesons and their coupling constants to the nucleon field are not very far from, for example, those found in the Bonn OBEP [6,7], and therefore we may regard the model as a schematic model of the relativistic Brückner-Hartree-Fock approaches based on the realistic OBEP [8,9,10].

We first solve the Hartree equations for LS closed nuclei, that is, ^{16}O and ^{40}Ca. Then we can use the wave functions thus obtained to define the electromagnetic current of systems with an LS closed core plus or minus one nucleon. As a first approximation (impulse approximation) one usually assumes that the current is carried entirely by the valence particle or hole. However, since the valence particle interacts with all nucleons in the Fermi sea, it feels some average potential (self energy). Generally, once we adopt

a model for this self energy, the model for the current is fixed, too. This intimate connection between self energy and currents is formally described by the Ward-Takahashi identity [11,12]. In the case of the Hartree approximation for the self energy, the proper current includes the RPA type (ring sum) vertex correction in addition to the single particle current. The fact that we are able to construct explicitly such a current is the strongest point of our approach. In our approach adopted here, however, the vertex corrections are purely isoscalar. This is because we take only isoscalar mesons into account and calculate the RPA type vertex correction around an isoscalar core (we do not include the Coulomb interaction between nucleons). We use the current to calculate isoscalar magnetic moments, which are determined by the currents for momentum transfer near zero. We further study nuclear magnetic form factors in order to investigate also responses to external fields with finite momentum transfer.

We have stated our motivation to investigate magnetic moments from a theoretical side. There is also a more practical side, however, for this. Magnetic moments of nuclei with an LS closed core plus or minus one nucleon were calculated by some authors in the relativistic approach employing the impulse approximation [13,14,15]. The reported values of magnetic moments, especially of ^{15}N, were very far from the Schmidt values (table 1 is an example of such calculations taken from ref. [13]), contrary to the naive expectation that the typical single particle picture should work for these systems.

The deviation from the Schmidt values is attributed to an enhancement of the Dirac part of the current and the magnetic moment. This enhance-

ment can be shown to be mainly due to the small effective mass of a nucleon in the nucleus. This problem was considered as serious since many successes of the relativistic approaches are considered to be due to the smallness of the effective mass.

Taking one of the conclusions of this thesis in advance, it is now widely recognized that the RPA type vertex corrections rescue the difficulties [16,17,18,19] due to several works including ours. We stress that the vertex corrections are a natural consequence of gauge invariance of the electromagnetic interaction, and not an ad-hoc, arbitrarily chosen correction.

Relativistic field theoretical models give rise to effects which are completely absent in the nonrelativistic models: Vacuum fluctuations. In the relativistic approach, a common feature are the very strong scalar and vector potentials for the single nucleon motion. This causes density-dependent quantum fluctuations, which modify the vacuum structure, especially the antinucleon levels, and therefore are expected to affect nuclear properties. Since the presently used σ-ω model is renormalizable, these effects are in principle calculable in a well-defined way. For the renormalization of the nucleon self energy we will follow previous works [20,21]. As for the electromagnetic interaction, we propose the extended VMD (vector meson dominance) model to renormalize the RPA type vertex corrections and applied it in the LDA (local density approximation) to calculate the effect on magnetic properties of finite systems. We are aware of a conceptual problem appearing here, namely that the nucleon is by no means a Dirac particle. Therefore requiring renormalizability of the adopted model lacks solid physical ground. However, we emphasize that we *can* calculate the effect

of the change of vacuum structure on physical quantities in *this* model.

This thesis is organized as follows: In section 2 the relativistic σ-ω model is introduced and used in the Hartree approximation to describe the ground state properties of ^{16}O and ^{40}Ca. We also discuss how to include vacuum fluctuation effects on the nucleon self energy. In section 3 the necessity of vertex corrections and the procedure how to implement them in our model is discussed. The important matter is how to renormalize the vertex correction, which is covered in section 3.3. This formalism is applied to the calculation of nuclear magnetic form factors and magnetic moments in section 3.3.3. Section 4 presents the numerical results both for magnetic moments and for magnetic form factors. There the calculations with and without the effects of vacuum fluctuations are compared. Section 5 is devoted to various discussions. The last section 6 is the summary and conclusion.

2 Relativistic σ-ω Model

In this chapter we introduce the model and discuss how to treat it to obtain nuclear wave functions. We also discuss the prescription to include the effect of vacuum fluctuations on the nucleon self energy.

2.1 Model Lagrangian

The σ-ω model is a renormalizable, relativistic field theoretical model of nucleons interacting via exchange of scalar and vector mesons. With the conventions of Bjorken-Drell [22] its lagrangian is given by

$$\begin{aligned}\mathcal{L} &= \overline{\psi}(i\partial\!\!\!/ - M)\psi + \frac{1}{2}(\partial\sigma)^2 - \frac{1}{2}m_\sigma^2\sigma^2 - \frac{1}{4}G_{\mu\nu}G^{\mu\nu} + \frac{1}{2}m_\omega^2\omega_\mu\omega^\mu \\ &\quad + g_\sigma\overline{\psi}\psi\sigma - g_\omega\overline{\psi}\gamma_\mu\psi\omega^\mu. \end{aligned} \tag{2.1}$$

Here ψ, σ and ω^μ are the field operators for the nucleon, the σ meson and the ω meson with masses M, m_σ and m_ω, respectively. The field strength tensor of the ω meson is defined by $G^{\mu\nu} = \partial^\mu\omega^\nu - \partial^\nu\omega^\mu$. Since we did not include the tensor coupling between the nucleon and the ω meson ($\overline{\psi}\sigma^{\mu\nu}\psi G_{\mu\nu}$), the model is renormalizable. This feature will enable us to discuss the effects of vacuum fluctuations in later sections.

This model lacks the π and ρ mesons. At first sight this seems a serious defect since the π meson is believed to play the most important role in nuclear forces and exchange currents. However, when specifying the model, we anticipate the approximation scheme which we take and the object to which we apply the model. In this particular case, we resort to the Hartree approximation, that is, we retain only direct terms to calculate the self

energy of the nucleon, and we attempt to describe nuclei with an isoscalar core (having the same number of protons and neutrons). In such kinds of nuclei, the pion field may be vanishing in average, and is expected to be not very important for the bulk properties of ground states. However, when we consider vertex corrections to the electromagnetic current in the next chapter, the ring sum type vertex corrections give only isoscalar contributions, which is a direct consequence of the model lagrangian (2.1) and the restriction to the Hartree approximation. To improve this point we have to improve not only the approximation (Hartree-Fock approximation, for example) but also the model itself (inclusion of isovector mesons).

2.2 Hartree Approximation

2.2.1 Mean Field Approximation

We use the model just described to construct the wave functions of ^{16}O and ^{40}Ca. The calculational procedures of treating finite closed shell nuclei are thoroughly discussed in the comprehensive review [5]. Here, for completeness, we briefly describe the method and thereby define notation and terminology.

In the Hartree approximation, the self energy of a nucleon is calculated from the tadpole diagram shown in fig. 1, which plays the role of the average potential used in the Dirac equation that determines the single particle motion. The nucleon line which appears in the loop of fig. 1 should be understood as a propagator which is composed of the fully self-consistent solutions of the present model.

In principle, positive energy occupied states and negative energy anti-

nucleon states should be included in the loop of fig. 1. In this subsection, however, we drop the latter contribution, which is divergent. Since this prescription gives the same answer as the mean field approximation in nuclear matter [23,20], we use this terminology in the following. Handling the divergent parts will be discussed in the next subsection. When we discuss magnetic moments and magnetic form factors in later sections, we will always compare the results obtained in the mean field approximation to those obtained by including the vacuum fluctuation.

In the mean field approximation we should solve the Dirac equation

$$[-i\boldsymbol{\alpha}\cdot\boldsymbol{\nabla}+\beta(M+\Sigma_{\rm s})]\psi=(E-\Sigma_{\rm v})\psi \tag{2.2}$$

with the scalar and vector self energies

$$\Sigma_{\rm s}(\boldsymbol{x}) = -\frac{g_\sigma^2}{4\pi}\int {\rm d}^3x'\,\frac{e^{-m_\sigma|\boldsymbol{x}-\boldsymbol{x}'|}}{|\boldsymbol{x}-\boldsymbol{x}'|}\rho_{\rm s}(x') \tag{2.3}$$

$$\Sigma_{\rm v}(\boldsymbol{x}) = \frac{g_\omega^2}{4\pi}\int {\rm d}^3x'\,\frac{e^{-m_\omega|\boldsymbol{x}-\boldsymbol{x}'|}}{|\boldsymbol{x}-\boldsymbol{x}'|}\rho_{\rm v}(x'), \tag{2.4}$$

where $\rho_{\rm s}$ and $\rho_{\rm v}$ are the scalar and vector densities which depend only on $x'=|\boldsymbol{x}'|$, respectively:

$$\rho_{\rm s}(x')=\frac{1}{4\pi}\sum_{\lambda\in{\rm h}}(2j_\lambda+1)(F_\lambda^2(x')-G_\lambda^2(x')) \tag{2.5}$$

$$\rho_{\rm v}(x')=\frac{1}{4\pi}\sum_{\lambda\in{\rm h}}(2j_\lambda+1)(F_\lambda^2(x')+G_\lambda^2(x'))=\rho_{\rm B}(x'). \tag{2.6}$$

$F_\lambda(x)$ and $G_\lambda(x)$ are the radial parts of the upper and lower components of the Dirac spinor:

$$\psi_{\lambda\mu}=\begin{pmatrix} F_\lambda(x)\chi_\kappa^\mu(\hat{x}) \\ iG_\lambda(x)\chi_{-\kappa}^\mu(\hat{x})\end{pmatrix}, \tag{2.7}$$

and $\lambda = (n, \kappa)$, where n is the principal quantum number and the nonzero integer κ determines j and ℓ. ($j = |\kappa| - \frac{1}{2}, \ell = \kappa - 1$ for $\kappa > 0$ and $\ell = -\kappa$ for $\kappa < 0$.) The χ_κ^μ are spin spherical harmonics with magnetic quantum number μ. The summation in eqs. (2.5) and (2.6) runs over all positive energy occupied states h. The quantity $M^* = M + \Sigma_s$ plays the role of a mass parameter in the Dirac equation. (Note that Σ_s is negative.) It is usually called the "effective mass" though it is different from the one used in the nonrelativistic theory. The vector density is equal to the baryon density ρ_B, as indicated in eq. (2.6).

This theory has essentially three parameters if we employ the experimental values for the masses of the nucleon and the ω meson. We use the parameter set given in ref. [24] (shown in table 2 under the title "MF"). This parameter set reproduces the nuclear matter saturation properties and the rms charge radius of ^{40}Ca. Using these values we solved the equations (2.2) to (2.6) by iteration until self-consistency is achieved to obtain the single particle wave functions for ^{16}O and ^{40}Ca. The calculated scalar and vector densities (see eqs. (2.5) and (2.6)) are shown by the dashed lines in figs.2 and 3.

2.2.2 Inclusion of Vacuum Fluctuations

Next we present a prescription to take the antinucleon excitations into account in the calculation of the nucleon self energy.

There have been several attempts to treat the problem of renormalization in relativistic field theoretical models of nuclear structure. In ref. [20] Chin discussed the procedure to handle vacuum fluctuation effects on the

scalar density in the Hartree approximation in infinite nuclear matter. Horowitz and Serot [21] used Chin's results to estimate the importance of vacuum fluctuations on the properties of finite nuclei in a local density approximation. Recently Perry [25,26] developed a treatment of the vacuum fluctuations without introducing the local density approximation. In this paper, however, we employ the method of ref. [21] to construct the single particle wave functions. An exact treatment of the vacuum fluctuations including their effects on magnetic moments and form factors seems prohibitively complicated at present.

In nuclear matter, the contribution of vacuum fluctuations to the scalar density is given by [20,21]

$$\delta\rho_s = -\frac{1}{\pi^2}M^3\left[\left(\frac{M^*}{M}\right)^3\log\frac{M^*}{M}+\frac{1}{3}-\frac{3}{2}\frac{M^*}{M}+3\left(\frac{M^*}{M}\right)^2-\frac{11}{6}\left(\frac{M^*}{M}\right)^3\right]. \tag{2.8}$$

As discussed in ref. [20], this result is obtained by adding to the lagrangian (2.1) the four counterterms $\sum_{n=1}^{4}(\alpha_n/n!)\sigma^n$, which are required to cancel the one-loop contributions to the Green's functions with one, two, three and four external σ meson lines with momenta equal to zero. That is, the renormalization point for the Green's functions with external σ meson lines is chosen as $q^2 = 0$. Different prescriptions, especially ones where the renormalized self couplings of the σ meson do not vanish at zero momenta, give different nuclear matter properties such as the compressibility [27]. We do not discuss this possibility in this thesis. If we renormalize also the ω meson propagator at $q^2 = 0$, there are no explicit vacuum fluctuation corrections to the vector density. (The case of arbitrary renormalization point for the ω meson will be discussed in section 3.3.3.)

In the local density approximation we make the replacement $M^* \rightarrow M^*(r)$ in eq. (2.8) and add this piece to the valence nucleon (positive energy occupied states) contribution given by eq. (2.5). Since now the scalar density itself depends explicitly on the scalar potential through the effective mass M^*, equation (2.3) now appears as an integral equation which we solve by iteration again.

We use the parameter set determined in ref. [21] to reproduce the nuclear matter saturation point and the rms charge radius of ^{40}Ca as in the previous subsection (shown in table 2 under the title "VF"). Note that both coupling constants become much smaller as compared to their values in the mean field approximation. m_σ is also reduced, which results in a longer range attractive force, compensating to a certain extent the smaller coupling constant. From the nuclear matter picture one can expect that these changes will not affect the isoscalar magnetic moments seriously, since those are determined essentially by the binding energy per nucleon (see section 3.1).

The scalar and vector densities including the vacuum fluctuation effect are shown by solid lines in figs.2 and 3. Note that the vacuum fluctuations modify the vector density only through the change in the wave functions.

In the following part of this thesis, we develop the formalism to calculate the RPA type vertex corrections using the wave functions created in this section and apply it to isoscalar magnetic moments and magnetic form factors.

3 Vertex Corrections

In this section, we develop the formalism to calculate vertex corrections which make the electromagnetic current satisfy the Ward identity within the range of our model, and apply the current, including the impulse one, to calculations of nuclear isoscalar magnetic moments and magnetic form factors. We hereby try to take the effect of vacuum fluctuation into account using the extended vector meson dominance approach.

3.1 General Considerations

The importance of the RPA type vertex corrections in the relativistic approach is now widely recognized. Many authors favor the interpretation of the vertex corrections as the "backflow" current in the Fermi liquid theory due to Landau (see, for example, [28,17]). However, we are on a somewhat different standpoint, which claims that the necessity of the vertex correction derives from a general consideration based upon the Ward-Takahashi identity in the nuclear medium. This point of view is established by Bentz *et al.* [29] (see also [1]). Instead of reproducing their formal discussion here, we discuss the necessity of the RPA type vertex corrections for our particular case.

When we express the quasiparticle current j^μ as

$$j^\mu(p',p) = N_{p'}\overline{f}(p')\Gamma^\mu(p',p)f(p)N_p$$

with $f(p)$ the solution of the Dirac equation including the nucleon self energy

$$S^{-1}f(p) = [\not{p} - M - \Sigma(p)]\, f(p) = 0$$

(we follow the conventions of ref. [22]), where the nucleon self energy $\Sigma = \Sigma_s + \gamma_0 \Sigma_v$ in our model (see eq. (2.2)), the electromagnetic vertex Γ^μ satisfies the following identity:

$$(p' - p)_\mu \Gamma^\mu(p', p) = \frac{1 + \tau_z}{2} \left[S^{-1}(p') - S^{-1}(p) \right]. \tag{3.1}$$

This is the Ward-Takahashi identity [11,12]. It is satisfied by the bare vertex γ^μ and the free propagator $S_F(p) = (\not{p} - M)^{-1}$ trivially. Subtracting the free vertex $\Gamma_0^\mu = \gamma^\mu \frac{1+\tau_z}{2}$ from Γ^μ we have the irreducible vertex correction Λ^μ, which satisfies the identity:

$$(p' - p)_\mu \Lambda^\mu(p', p) = -\frac{1 + \tau_z}{2} \left[\Sigma(p') - \Sigma(p) \right]. \tag{3.2}$$

The identities (3.1) and (3.2) hold due to the gauge invariance properties of the underlying field theory without resorting to any perturbation theoretical argument. Here, however, we remember the perturbative proof of the identities to convince ourselves that, as we repeatedly emphasized, we need the RPA (ring sum) type vertex corrections when we take the Hartree approximation to nucleon self energy $\Sigma(p)$. The key is the very simple observation that $\Lambda^\mu(p', p)$, obtained from $-\Sigma(p)$ by inserting Γ_0^μ which brings in the momentum $p' - p$ into any bare fermion propagator and by summing up all possible insertions, satisfies the identity (3.2). (For its graphical illustration, see p. 301 of ref. [22].) Now that we have $\Sigma(p)$ as composed of the tadpole diagram with the self-consistent nucleon wave functions (fig. 1), what we obtain as Λ^μ by this procedure is of ring sum type (fig. 4).

The advantage of this approach is that, once we decide which approximation we apply to the calculation of Σ, we have determined the explicit

form of Λ. For example, if we take the Hartree-Fock approximation to Σ, we know we have to calculate very complicated diagrams following the same reasonings in order to keep theoretical consistency. They cannot be summarized to any simple form such as the RPA type one. (It is more complicated than the RPA with exchange terms in the interaction.)

In fact, in the Hartree approximation, the vertex correction is not needed for eq. (3.2) to be satisfied, because the nucleon self energy $\Sigma(p)$ does not depend on the momentum of the nucleon p in this approximation. However, when we consider the limiting case in which the momentum transfer $q = p' - p$ goes to zero, or when the Ward, rather than Ward-Takahashi, identity is to be satisfied, the vertex correction is necessary even in the Hartree approximation.

For the general argument concerning this point, we refer to [29] again, and quote the main results. In the nuclear matter model, care should be taken when the limit $q \to 0$ is taken. In order to simulate the fact that there are energy gaps between discrete levels in a finite system, we should first let $\boldsymbol{q}$ go to zero, and then move q^0 to zero. Following this procedure one obtains for the space part of the current at $q = 0$, using (3.1) and the foregoing definition of the current,

$$\boldsymbol{j}(q=0) \equiv \lim_{q^0 \to 0} \lim_{\boldsymbol{q} \to 0} \boldsymbol{j}(q) = \boldsymbol{j}_{\rm vel} + \boldsymbol{j}_{\rm back} \tag{3.3}$$

with

$$\begin{aligned} \boldsymbol{j}_{\rm vel} &= \nabla_p \varepsilon_p \frac{1+\tau_z}{2} \\ \boldsymbol{j}_{\rm back} &= \hat{p} \frac{p^2}{3\pi^3} (f_1 + \tau_z f_1') \,. \end{aligned}$$

Here f_1 and f_1' are two Landau-Migdal parameters [30] characterizing the $\ell = 1$ isospin-independent and isospin dependent part of the spin independent quasiparticle interaction, and ε_p is the quasiparticle energy. The sum can be rewritten as

$$\boldsymbol{j}(q=0) = \frac{\boldsymbol{p}}{\varepsilon_p}\frac{1+\tau_z}{2} - \hat{p}\tau_z\frac{p^2}{3\pi^2}(f_1 - f_1').$$

Note that the isoscalar part of $\boldsymbol{j}$ is determined solely by the quasiparticle energy. From the above form we can further show [29] that the isoscalar part of g_ℓ, the orbital gyromagnetic ratio, is given by

$$g_\ell^{(0)} = \frac{1}{2}\frac{E_{p_F}}{\varepsilon_{p_F}} \tag{3.4}$$

where p_F denotes the Fermi momentum and $E_p = \sqrt{p^2 + M^2}$. Since the binding energy per nucleon in nuclear matter is somewhere around 15 MeV, $g_\ell^{(0)}$ should be very close to $\frac{1}{2}$.

In the Hartree approximation to the σ-ω model we have $\varepsilon_p = E_p^* + \Sigma_v$ with $E_p^* = \sqrt{\boldsymbol{p}^2 + M^{*2}}$. Therefore, the impulse current coincides with

$$\boldsymbol{j}_{\rm vel} = \frac{\boldsymbol{p}}{E_p^*}\frac{1+\tau_z}{2},$$

and $\boldsymbol{j}_{\rm back}$ corresponds to the contribution of the RPA type vertex correction due to nucleon-antinucleon polarization insertions (see fig. 4).

3.2 RPA in the Mean Field Approximation

We use the single particle wave functions obtained in section 2 to construct the electromagnetic current of the valence nucleon or hole outside the $A = 16$ and $A = 40$ core. The current consists of two parts: the impulse

part and the vertex correction. When calculating the RPA type vertex correction, we pay as much respect to the finite geometry as possible. In order to realize this goal, we develop a two-step approach: First, we treat the explicitly density-dependent part of the polarization insertions using the wave functions obtained in section 2.2.1 by the finite system calculation in the Hartree approximation. The calculation of vertex corrections in this step is consistent with the mean field approximation in section 2.2.1, therefore the terminology is applied here too. Next, we incorporate the vacuum fluctuation effects in the framework of a local density approximation. In this step, we use the wave functions obtained in section 2.2.2. By taking this two-step approach we can compare the results of two calculations, one in the mean field approximation and another including the vacuum fluctuation effects. In this subsection we present the outline of calculation of the RPA type vertex corrections in the mean field approximation.

In RPA the current has the form

$$j^{\mu}_{\lambda'\mu',\lambda\mu}(\boldsymbol{z}) = \int \mathrm{d}^3y\, \overline{\psi}_{\lambda'\mu'}(\boldsymbol{y}) \Gamma^{\mu}(\boldsymbol{y},\boldsymbol{z}) \psi_{\lambda\mu}(\boldsymbol{y}), \tag{3.5}$$

where

$$\Gamma^{\mu}(\boldsymbol{y},\boldsymbol{z}) = \Gamma^{\mu}_{0}(\boldsymbol{y})\delta^{(3)}(\boldsymbol{y}-\boldsymbol{z}) + \tilde{\Lambda}^{\mu}(\boldsymbol{y},\boldsymbol{z}) \tag{3.6}$$

is the electromagnetic vertex including the free vertex

$$\Gamma^{\mu}_{0}(\boldsymbol{y}) = e\gamma^{\mu} + \frac{\kappa_{\mathrm{A}}}{2M} \overleftrightarrow{\partial}_{\nu}\, \sigma^{\mu\nu}, \tag{3.7}$$

$$(\overleftrightarrow{\partial}_{\nu}=\overrightarrow{\partial}_{\nu} + \overleftarrow{\partial}_{\nu})$$

and the RPA type vertex correction

$$\tilde{\Lambda}^{\mu}(\boldsymbol{y},\boldsymbol{z}) = -ig_{\omega}\gamma_{\nu}\left(\Lambda^{\nu\mu}(\boldsymbol{y},\boldsymbol{z}) + \int \mathrm{d}^3x \tilde{\Pi}^{\nu}{}_{\lambda}(\boldsymbol{y},\boldsymbol{x})\Lambda^{\lambda\mu}(\boldsymbol{x},\boldsymbol{z})\right). \tag{3.8}$$

In eq. (3.7), e is the charge and κ_A the anomalous magnetic moment of a free nucleon. Disregarding the second term in eq. (3.6) constitutes the impulse approximation as used in this work. The quantities in eq. (3.8) are defined as

$$\tilde{\Pi}^{\mu\nu}(y,x) = \Pi^{\mu\nu}(y,x) + \int \mathrm{d}^3z\, \Pi^{\mu}_{\lambda}(y,z)\tilde{\Pi}^{\lambda\nu}(z,x) \tag{3.9}$$

with

$$\Pi^{\mu\nu}(y,z) = \int \mathrm{d}^3x\, i\Delta^{\mu}_{0\lambda}(y-x)\Pi^{\lambda\nu}_{(\omega\omega)}(x,z), \tag{3.10}$$

and

$$\Lambda^{\mu\nu}(y,z) = \int \mathrm{d}^3x\, i\Delta^{\mu}_{0\lambda}(y-x)\Pi^{\lambda\nu}_{(\omega\gamma)}(x,z). \tag{3.11}$$

$\Delta^{\mu\nu}_0$ in eq. (3.10) and (3.11) means the free ω meson propagator in lowest order, i.e., without polarization insertions. Eq. (3.9) is an integral equation for the $\omega\omega$ correlation function in the ring approximation. (Note that both $\Pi^{\mu\nu}$ and $\tilde{\Pi}^{\mu\nu}$ include one external ω propagator $\Delta^{\mu\nu}_0$.)

In order to introduce the mean field approximation, we split up (see fig. 5)

$$\Pi^{\mu\nu}_{(\omega\omega)} = \Pi^{\mu\nu}_{(\omega\omega)\mathrm{D}} + \Pi^{\mu\nu}_{(\omega\omega)\mathrm{F}} \tag{3.12}$$

with $\Pi^{\mu\nu}_{(\omega\omega)\mathrm{D}}$ being that (finite) part of the $\omega\omega$-polarization operator $\Pi^{\mu\nu}_{(\omega\omega)}$ which explicitly depends on the Fermi distribution function. More precisely, starting from its definition, we have the following expression for $\Pi^{\mu\nu}_{(\omega\omega)}$ [31]:

$$\begin{aligned}
\Pi^{\mu\nu}_{(\omega\omega)} &= \int_{-\infty}^{\infty} \frac{\mathrm{d}\varepsilon}{2\pi} \mathrm{tr}\left[\Gamma^{\mu} S(x,z,\varepsilon)\Gamma^{\nu} S(z,x,\varepsilon - q^0)\right] \\
&= i\sum_{\alpha} \mathrm{tr}[\frac{\Gamma^{\mu}u_{\alpha}(x)\overline{u}_{\alpha}(z)\Gamma^{\nu}u_{\beta}(z)\overline{u}_{\beta}(x)}{q^0 + \varepsilon_{\beta} - \varepsilon_{\alpha} + i\delta}(1-n_{\alpha})n_{\beta} \\
&+ \frac{\Gamma^{\mu}u_{\alpha}(x)\overline{u}_{\alpha}(z)\Gamma^{\nu}u_{\beta}(z)\overline{u}_{\beta}(x)}{\varepsilon_{\alpha} - q^0 - \varepsilon_{\beta} + i\delta}(1-n_{\beta})n_{\alpha}
\end{aligned}$$

$$
\begin{aligned}
&+ \frac{\Gamma^\mu u_\alpha(x)\overline{u}_\alpha(z)\Gamma^\nu v_\beta(z)\overline{v}_\beta(x)}{q^0-\overline{\varepsilon}_\beta-\varepsilon_\alpha+i\delta}(1-n_\alpha) \\
&+ \frac{\Gamma^\mu v_\alpha(x)\overline{v}_\alpha(z)\Gamma^\nu u_\beta(z)\overline{u}_\beta(x)}{-\overline{\varepsilon_\alpha}-q^0-\varepsilon_\beta+i\delta}(1-n_\beta)] \qquad (3.13) \\
&= i[\sum_{\mathrm{p,h}}(\frac{<\mathrm{h}|\Gamma^\mu(x)|\mathrm{p}><\mathrm{p}|\Gamma^\nu(z)|\mathrm{h}>}{q^0+\varepsilon_\mathrm{h}-\varepsilon_\mathrm{p}+i\delta} \\
&+ \frac{<\mathrm{p}|\Gamma^\mu(x)|\mathrm{h}><\mathrm{h}|\Gamma^\nu(z)|\mathrm{p}>}{\varepsilon_\mathrm{h}-q^0-\varepsilon_\mathrm{p}+i\delta}) \\
&+ \sum_{\mathrm{N},\overline{\mathrm{p}}}(\frac{<\overline{\mathrm{p}}|\Gamma^\mu(x)|\mathrm{N}><\mathrm{N}|\Gamma^\nu(z)|\overline{\mathrm{p}}>}{q^0+\overline{\varepsilon}_{\overline{\mathrm{p}}}-\varepsilon_\mathrm{N}+i\delta} \\
&+ \frac{<\mathrm{N}|\Gamma^\mu(x)|\overline{\mathrm{p}}><\overline{\mathrm{p}}|\Gamma^\nu(z)|\mathrm{N}>}{-\overline{\varepsilon}_{\overline{\mathrm{p}}}-q^0-\varepsilon_\mathrm{N}+i\delta}) \\
&- \sum_{\mathrm{h},\overline{\mathrm{p}}}(\frac{<\overline{\mathrm{p}}|\Gamma^\mu(x)|\mathrm{h}><\mathrm{h}|\Gamma^\nu(z)|\overline{\mathrm{p}}>}{q^0-\overline{\varepsilon}_{\overline{\mathrm{p}}}-\varepsilon_\mathrm{h}+i\delta} \\
&+ \frac{<\mathrm{h}|\Gamma^\mu(x)|\overline{\mathrm{p}}><\overline{\mathrm{p}}|\Gamma^\nu(z)|\mathrm{h}>}{-\overline{\varepsilon}_{\overline{\mathrm{p}}}-q^0-\varepsilon_\mathrm{h}+i\delta})]. \qquad (3.14)
\end{aligned}
$$

Here S is the nucleon propagator, $u_\alpha(x)$ and $v_\alpha(x)$ stand for the Dirac spinors with eigenvalues $\varepsilon_\alpha > 0$ and $\overline{\varepsilon}_\alpha < 0$, respectively, and n_α is one (zero) if the state α is below (above) the Fermi surface. $\Gamma^\mu = -ig_\omega\gamma^\mu$ denotes the ω-nucleon vertex. In eq. (3.14) we used the simplified notation

$$< \alpha|\Gamma^\mu(x)|\beta >= \overline{u}_\alpha(x)\Gamma^\mu u_\beta(x)$$

and

$$< \overline{\mathrm{p}}|\Gamma^\mu(x)|\beta >= \overline{v}_{\overline{\mathrm{p}}}(x)\Gamma^\mu u_\beta(x).$$

The terms in the first and the second line of eq. (3.13) correspond to particle-hole excitations, which are rewritten to the first and second line of eq. (3.14). The terms in the last two lines of eq. (3.13) correspond to particle-antinucleon excitations. A naive calculation of the latter diverges

because of the infinite summation of the particle and antinucleon states. To deal with these terms we devise the following procedure. The sum over the particle states can be divided into two kinds of terms, one involving a sum over all positive energy states N (for nucleon, as opposed to antinucleon) which is given in the third and forth line of eq. (3.14) and will be denoted by $\Pi^{\mu\nu}_{(\omega\omega)\mathrm{F}}$, and one involving a sum over occupied positive energy states h (for "hole") given in the last two lines of (3.14). The terms involving a sum over h make up $\Pi^{\mu\nu}_{(\omega\omega)\mathrm{D}} = \Pi^{\mu\nu}_{(\omega\omega)} - \Pi^{\mu\nu}_{(\omega\omega)\mathrm{F}}$. They are characterized as the explicitly density-dependent terms, since each of them depends on the Fermi distribution function n_α explicitly and vanishes as the latter goes to zero. $\Pi^{\mu\nu}_{(\omega\omega)\mathrm{D}}$ is finite because the summation over h runs only over a finite number of states. When q^0 is small enough not to cause real $\mathrm{N\overline{N}}$ excitations, $\Pi^{\mu\nu}_{(\omega\omega)\mathrm{D}}$ is expressed in a relatively compact form [32]:

$$\begin{aligned}\Pi^{\mu\nu}_{(\omega\omega)\mathrm{D}} &= i\sum_{\mathrm{h}}\{\overline{u}_{\mathrm{h}}(\boldsymbol{x})\Gamma^{\mu}S(\boldsymbol{x},\boldsymbol{z},q^0+\varepsilon_{\mathrm{h}})\Gamma^{\nu}u_{\mathrm{h}}(\boldsymbol{z}) \\ &+ [\overline{u}_{\mathrm{h}}(\boldsymbol{x})\Gamma^{\mu}S(\boldsymbol{x},\boldsymbol{z},-q^0+\varepsilon_{\mathrm{h}})\Gamma^{\nu}u_{\mathrm{h}}(\boldsymbol{z})]^*\}. \qquad (3.15)\end{aligned}$$

Here S is again the nucleon propagator and the sum extends over the occupied positive-energy states h. Because $q^0 = 0$ for the calculation of magnetic moments and elastic magnetic form factors, $\Pi^{\mu\nu}_{(\omega\omega)\mathrm{D}}$ is simply determined by the real part of the first term in the bracket of eq. (3.15).

The treatment of the divergent term $\Pi^{\mu\nu}_{(\omega\omega)\mathrm{F}}$ (the "Feynman part") in an infinite system will be discussed in the next subsection.

Similarly to eq. (3.12) we split up the $\omega\gamma$ polarization operator into its explicitly density dependent part and Feynman part (fig. 6)

$$\Pi^{\mu\nu}_{(\omega\gamma)} = \Pi^{\mu\nu}_{(\omega\gamma)\mathrm{D}} + \Pi^{\mu\nu}_{(\omega\gamma)\mathrm{F}}, \qquad (3.16)$$

where the former is used to construct the quantity $\Lambda^{\mu\nu}$ of eq. (3.11). All two-point functions ($P(\boldsymbol{x},\boldsymbol{y})$) in eqs. (3.9), (3.10) and (3.11) are defined by $P(\boldsymbol{x},\boldsymbol{y}) \equiv P(\boldsymbol{x},\boldsymbol{y},q_0=0)$, where $P(\boldsymbol{x},\boldsymbol{y},q_0)$ is the Fourier transform of $P(x,y)$ with respect to (x^0-y^0).

The vertex correction (3.8) is graphically shown in fig. 4. [1] Note that in the definition of the vertex correction there enter only the explicitly density dependent parts of the polarization operators. Within this approximation, which is consistent with the mean field approximation adopted for the nucleon self energy, the positive and negative energy continuum states can be treated exactly ("continuum RPA"). Calculational details are collected in Appendix A. The Feynman parts of the polarization operators will be re-included into the calculation in section 3.3.3.

[1] In eq. (3.8) we already used the fact that for an external magnetic field (M1, M3,...) only the ω meson (and, in particular only its space component ω^i) contributes to the vertex correction.

3.3 Renormalization

Anticipating the application to the RPA type vertex corrections, in this section we discuss the renormalization of nucleon loop diagrams associated with the ω meson exchange processes. As discussed later, only the space components of the ω meson contribute to ring diagrams for elastic magnetic processes. We first discuss the renormalization of the ω meson propagator, and then proceed to the case where the electromagnetic interaction is turned on. The common procedure to handle renormalization and to assess its effects on nuclear properties is as follows: Renormalization is performed in the vacuum. That is, counterterms which render physical quantities finite are determined in the vacuum. Then the density dependence is evaluated in the nuclear matter model. And at last, the calculation in finite systems is done by employing a local density approximation. Details of this last procedure for vertex corrections will be discussed in the subsection 3.3.3.

3.3.1 ω Meson Propagator

In this subsection we discuss the renormalization of the ω meson propagator. The divergent part of the polarization insertion caused by $N\overline{N}$ excitation has, in nuclear matter, the same form as in free space with the nucleon mass replaced by the effective nucleon mass M^*:

$$\Pi^{\mu\nu}_{(\omega\omega)\mathrm{F}}(q) = -2ig_\omega^2 \int \frac{\mathrm{d}^4k}{(2\pi)^4} \mathrm{tr}\,\gamma^\nu \frac{1}{\not{k}+\not{q}-M^*+i\epsilon}\gamma^\mu \frac{1}{\not{k}-M^*+i\epsilon}.$$

An overall factor 2 accounts for the isospin multiplicity. In the dimensional regularization scheme we have [33]

$$\begin{aligned} \Pi^{\mu\nu}_{(\omega\omega)\mathrm{F,reg}}(q) &= -\frac{g_\omega^2}{\pi^2}\left(-g^{\mu\nu}+\frac{q^\mu q^\nu}{q^2}\right)q^2 \\ &\times \left[\frac{1}{6\epsilon}-\frac{1}{6}\gamma-\int_0^1 \mathrm{d}x\, x(1-x)\log\frac{M^{*2}-x(1-x)q^2}{\lambda^2}\right] \end{aligned} \tag{3.17}$$

where $\epsilon = (4-d)/2$ with d the number of dimensions, γ is the Euler number, and λ is an arbitrary mass scale which appears in the procedure of dimensional regularization.

To carry out the renormalization in the omega-nucleon sector of our model, we interpret as usual all quantities in the lagrangian (2.1) as unrenormalized ones (characterized by a subscript 0) and make the scale transformations

$$\omega^\mu_{(0)} = \sqrt{Z_\omega}\omega^\mu,\ \psi_{(0)} = \sqrt{Z_\mathrm{N}}\psi,\ m^2_{\omega_0} = \frac{m^2_\omega + \delta m^2_\omega}{Z_\omega},\ g_{\omega_0} = \frac{g_\omega Z_g}{\sqrt{Z_\omega}Z_\mathrm{N}}. \tag{3.18}$$

Here Z_ω is the wave funcion renormalization constant and δm^2_ω the mass counterterm for the ω meson, and Z_g is the ωNN vertex renormalization constant. Since in the present Hartree model there is no correction to the nucleon propagator for zero density, the wave function renormalization constant Z_N for the nucleon is equal to one. Putting eq. (3.18) into eq. (2.1) we obtain the lagrangian in the omega-nucleon sector,

$$\begin{aligned} \mathcal{L}_{\omega\mathrm{N}} &= \overline{\psi}(i\partial\!\!\!/ - M)\psi - \frac{1}{4}G_{\mu\nu}G^{\mu\nu} + \frac{m^2_\omega}{2}\omega_\mu\omega^\mu - \frac{1}{4}(Z_\omega - 1)G_{\mu\nu}G^{\mu\nu} \\ &+ \frac{\delta m^2_\omega}{2}\omega_\mu\omega^\mu - Z_g g_\omega \overline{\psi}\gamma_\mu\psi\omega^\mu. \end{aligned} \tag{3.19}$$

The renormalized polarization $\Pi^{\mu\nu}_{(\omega\omega)\mathrm{F,r}}$ is now obtained by adding the wave function and mass renormalization counterterm contributions $-(Z_\omega -$

$1)(q^\mu q^\nu - g^{\mu\nu}q^2) - \delta m_\omega^2 g^{\mu\nu}$ to eq. (3.17) and replacing $g_\omega \to Z_g g_\omega$:

$$\Pi^{\mu\nu}_{(\omega\omega)\mathrm{F,r}}(q) = \left(-g^{\mu\nu} + \frac{q^\mu q^\nu}{q^2}\right)\Pi_{(\omega\omega)}(q^2) - \frac{q^\mu q^\nu}{q^2}\delta m_\omega^2 \tag{3.20}$$

with

$$\begin{aligned}\Pi_{(\omega\omega)}(q^2) &= -q^2\frac{(g_\omega Z_g)^2}{\pi^2}\left[\frac{1}{6\epsilon} - \frac{1}{6}\gamma - \int_0^1 \mathrm{d}x\, x(1-x)\log\frac{M^{*2} - x(1-x)q^2}{\lambda^2}\right] \\ &\quad - (Z_\omega - 1)q^2 + \delta m_\omega^2. \end{aligned}\tag{3.21}$$

The ω meson propagator including the Feynman part of the polarization operator is then obtained from Dyson's equation as

$$\Delta^{\mu\nu}(q) = \left(-g^{\mu\nu} + \frac{q^\mu q^\nu}{q^2}\right)\Delta(q^2) + \frac{q^\mu q^\nu}{q^2}\frac{1}{m_\omega^2 + \delta m_\omega^2}, \tag{3.22}$$

$$\Delta(q^2) = \frac{1}{q^2 - m_\omega^2 - \Pi_{(\omega\omega)}(q^2)}. \tag{3.23}$$

This propagator is graphically represented by fig. 7. Denoting the renormalization point by μ^2 we impose the conditions

$$\begin{aligned}\Pi_{(\omega\omega)}(q^2)|_{q^2=\mu^2, M^*=M} &= 0 \\ \frac{\partial\Pi_{(\omega\omega)}(q^2)}{\partial q^2}|_{q^2=\mu^2, M^*=M} &= 0,\end{aligned}$$

from which Z_ω and δm_ω^2 are determined as

$$Z_\omega - 1 = -\frac{(g_\omega Z_g)^2}{\pi^2}\left[\frac{1}{6\epsilon} - \frac{1}{6}\gamma - \int_0^1 \mathrm{d}x\, x(1-x)\log\frac{M^2 - x(1-x)\mu^2}{\lambda^2}\right] - C_\omega, \tag{3.24}$$

$$\delta m_\omega^2 = -\mu^2 C_\omega \tag{3.25}$$

with

$$C_\omega = \mu^2\frac{(g_\omega Z_g)^2}{\pi^2}\int_0^1 \mathrm{d}x\, \frac{\{x(1-x)\}^2}{M^2 - x(1-x)\mu^2}. \tag{3.26}$$

Note that δm_ω^2 is finite. This can also be shown by a more formal discussion given in Appendix C of ref. [34]. As is clear from eq. (3.18), however, the bare ω meson mass is infinite since Z_ω^{-1} diverges. To fix the remaining renormalization constant Z_g we follow ref. [35]. We define g_ω in such a way that the ωNN source vertex $\Gamma^\mu_{\omega S}(q)$ for $q \to 0$, zero density ($\rho = 0$) and on mass shell external nucleon legs with momenta $p' = p$ satisfies

$$\Gamma^\mu_{\omega S}(q)|_{\rho=0} \to -ig_\omega \gamma^\mu \text{ as } q \to 0,\ \not{p} \to M. \tag{3.27}$$

The source vertex is defined via the total ωNN Green's function with amputated nucleon lines $\Gamma^\mu_\omega(q)$ by

$$\Gamma^\mu_\omega(q) = i\Delta^\mu_{0\nu}(q)\Gamma^\nu_{\omega S}(q), \tag{3.28}$$

where $\Delta_0^{\mu\nu}(q)$ is the free propagator in lowest order (i.e., eq. (3.22) with $\Pi_{(\omega\omega)} = \delta m_\omega^2 = 0$). With the requirement (3.27), the Ward-Takahashi identity for baryon current conservation gives the following relation between the renormalization constants

$$Z_g = Z_N \left(1 + \frac{\delta m_\omega^2}{m_\omega^2}\right), \tag{3.29}$$

which corresponds to eq. (3.11) of ref. [35]. For the proof, see Appendix B. In our case $Z_N = 1$, and Z_g is completely determined by mass renormalization. In our present Hartree model, $\Gamma^\mu_{\omega S}$ is modified due to the RPA type vertex corrections, and eq. (3.29) ensures the validity of (3.27) and the conservation of the baryon current. Note that g_ω is not the observed ωNN coupling constant, which is defined via the source vertex at $q^2 = m_\omega^2$ rather than $q^2 = 0$ [36]. The resulting renormalized transverse vacuum

polarization is obtained from eqs. (3.21), (3.24), and (3.25) as

$$\Pi_{(\omega\omega)}(q^2) = C_\omega(q^2 - \mu^2) + q^2 Z_g P(q^2) \tag{3.30}$$

with

$$P(q^2) = \frac{g_\omega^2 Z_g}{\pi^2} \int_0^1 \mathrm{d}x\, x(1-x) \log \frac{M^{*2} - q^2 x(1-x)}{M^2 - \mu^2 x(1-x)}. \tag{3.31}$$

Due to eqs. (3.25) and (3.29) we can write the transverse part of the propagator (3.23) as

$$\Delta(q^2) = \frac{1}{Z_g} \frac{1}{q^2 - m_\omega^2 - q^2 P(q^2) - \frac{C_\omega}{Z_g} q^2 \left(1 - \frac{\mu^2}{m_\omega^2}\right)}. \tag{3.32}$$

Note that the last term in the denominator of eq. (3.32) is zero if we choose $\mu^2 = m_\omega^2$ or $\mu^2 = 0$ which gives zero to C_ω.

It is easy to see that the ω meson propagator (3.32) has an unphysical pole at spacelike $q^2 < 0$. The same pole occurs in QED and is sometimes referred to as "Landau ghost" [37]. It implies a breakdown of perturbation theory for high $|q^2|$. While in QED this pole occurs for extremely high $|q^2|$, the problem is much more serious in our case due to the large coupling constant. Thus, finally we will have to introduce a phenomenological ωNN vertex form factor to dump $\Pi_{(\omega\omega)}(q^2)$ at high $|q^2|$. The determination of this vertex form factor as well as the choice of the renormalization point μ^2 will be discussed in section 3.3.3.

3.3.2 Electromagnetic Interactions

In the previous subsection we discussed the renormalized form of the ω meson propagator. We now turn to the renormalization of the meson-photon polarization $\Pi^{\mu\nu}_{(\omega\gamma)}$ shown in fig. 6. The vacuum fluctuation effects to

be discussed below will eventually be incorporated into a density dependent form factor $\tilde{F}_{1s}(q^2)$ (see eq. (4.1) below), which is folded into the isoscalar Dirac part of the free vertex in (3.6), i.e.,

$$\frac{1}{2}\gamma^\mu\delta^{(3)}(y-z) \to \int \frac{\mathrm{d}^3q}{(2\pi)^3}\frac{1}{2}\gamma^\mu\tilde{F}_{1s}(q^2)\exp iq\cdot(y-z). \tag{3.33}$$

This modified vertex is then used in the impulse approximation as well as in the RPA type vertex correction. Thus, our aim is to replace the isoscalar Dirac form factor of a free nucleon by the density dependent form factor $\tilde{F}_{1s}$ calculated within the present model. Since due to gauge invariance the present Hartree model does not allow for any vertex corrections besides the RPA type one, one might calculate the nucleon form factor by summing up the diagrams shown in the first row of fig. 8, i.e., those pieces which are obtained from the zero density expressions by the replacement $M \to M^*$. However, as we will see later, the form factor calculated in this way behaves as a constant for $|q^2| \to \infty$ and therefore is unable to account for the properties of a free nucleon. This is one of the reasons why in this work we follow the generalized vector meson dominance model (GVMD) [35,36] and include the possibility of a direct $\omega\gamma$ coupling, which gives rise to the diagrams shown in the second row of fig. 8. A further advantage of this model is that the renormalization prescription discussed in the previous section for the strong interaction determines also the electromagnetic vertex of fig. 8 without introducing any further conditions.

The photon-nucleon vertices in the diagrams of fig. 8 are understood to contain the Dirac part only. In this way this set of diagrams renormalizes the Dirac part of the current by multiplying a form factor which in free space

reduces to the Dirac-Pauli form factor F_{1s}. In the present Hartree model we cannot generate the anomalous magnetic moment coupling consistently. In the mean field calculation of the vertex correction, this coupling may be introduced phenomenologically. This method cannot be applied here, since this coupling term would make the theory unrenormalizable. However, the contribution of the isoscalar anomalous magnetic moment term to the corrections to nuclear magnetic moments and to the nuclear form factors is small. Thus, for our purpose, the inadequacy of the present model to generate the isoscalar anomalous magnetic moment coupling has no serious consequences. Our concern therefore is to use the diagrams of fig. 8 to calculate the free space Dirac-Pauli form factor F_{1s}, which is associated with the isoscalar Dirac part of the current, and to investigate how it is changed in the nuclear medium.

Following ref. [35], we extend our lagrangian (3.19) to obtain the lagrangian in the omega-nucleon-photon sector:

$$\mathcal{L}_{\omega N\gamma} = \mathcal{L}_{\omega N} + \mathcal{L}_{e},$$

where, in terms of unrenormalized quantities,

$$\mathcal{L}_{e} = -\frac{1}{4}F_{(0)\mu\nu}F^{\mu\nu}_{(0)} - e_0\overline{\psi}_{(0)}\gamma_\mu\psi_{(0)}A^{\mu}_{(0)} - \frac{e_0}{2g_{\omega 0}}F_{(0)\mu\nu}G^{\mu\nu}_{(0)}. \tag{3.34}$$

Here $F^{\mu\nu} = \partial^\mu A^\nu - \partial^\nu A^\mu$ is the electromagnetic field strength tensor. The second term in eq. (3.34) describes the nucleon-photon coupling and the third term, which is gauge invariant by itself, the omega-photon coupling. This special form of the coupling has been chosen to reproduce the current-field identity (CFI), as we will see later. Since in our present calculation we

do not take into account the electromagnetic field renormalization (which is of order e^2 or higher), we have $A^\mu_{(0)} = A^\mu$ and $e_0 = e$. The other quantities in (3.34) are renormalized according to eq. (3.18) and we obtain

$$\mathcal{L}_e = -\frac{1}{4}F_{\mu\nu}F^{\mu\nu} - eZ_N\overline{\psi}\gamma_\mu\psi A^\mu - \frac{e}{2g_\omega}F_{\mu\nu}G^{\mu\nu} - \frac{e}{2g_\omega}(Z_{0\omega}-1)F_{\mu\nu}G^{\mu\nu}. \quad (3.35)$$

Here we introduced the constant

$$Z_{0\omega} = \frac{Z_\omega Z_N}{Z_g} = \frac{m^2_\omega}{m^2_{\omega 0}}, \quad (3.36)$$

where the second equality follows from eq. (3.29) and (3.18). In the actual Hartree calculation we have again $Z_N = 1$.

The CFI can now be shown as follows: From $\mathcal{L}_{\omega N}$ of eq. (3.19) we derive the ω meson field equation

$$\partial_\mu G^{\mu\nu} + m^2_\omega \omega^\nu = j^\nu_{\omega S} \quad (3.37)$$

with the renormalized source

$$j^\nu_{\omega S} = g_\omega Z_N \overline{\psi}\gamma^\nu\psi - (Z_{0\omega}-1)\partial_\mu G^{\mu\nu}. \quad (3.38)$$

Here we used again the relation (3.29). We therefore can write $\mathcal{L}_e$ in the form

$$\mathcal{L}_e = -\frac{1}{4}F_{\mu\nu}F^{\mu\nu} - \frac{e}{g_\omega}\left(j^\mu_{\omega S}A_\mu + \frac{1}{2}F_{\mu\nu}G^{\mu\nu}\right), \quad (3.39)$$

where we left out a total derivative term. From eq. (3.39) follows the Maxwell equation

$$\partial_\mu F^{\mu\nu} = \frac{e}{g_\omega}(j^\nu_{\omega S} - \partial_\mu G^{\mu\nu}) = e\frac{m^2_\omega}{g_\omega}\omega^\nu \equiv 2ej^\nu_s, \quad (3.40)$$

which establishes the CFI

$$j_s^\nu = \frac{m_\omega^2}{2g_\omega}\omega^\nu \tag{3.41}$$

between the isoscalar electromagnetic current j_s^ν and the ω meson field. The CFI (3.41) together with the field equation (3.37) gives the following relation between the matrix elements for arbitrary states A and B

$$< B|j_s^\mu|A >= \frac{1}{2g_\omega}\frac{-m_\omega^2}{q^2 - m_\omega^2} < B|j_{\omega S}^\nu|A > . \tag{3.42}$$

where q is the difference between the total momenta of A and B.

Let us now calculate the RPA type vertex shown in fig. 8 using the lagrangian $\mathcal{L}_{\omega N\gamma}$ given by the sum of eqs. (3.19) and (3.35). The new ingredient is the Feynman part of the $\omega\gamma$ polarization which has the renormalized form (cf. eq. (3.20))

$$\Pi^{\mu\nu}_{(\omega\gamma)F,r}(q) = \left(-g^{\mu\nu} + \frac{q^\mu q^\nu}{q^2}\right)\Pi_{(\omega\gamma)}(q^2) \tag{3.43}$$

with

$$\begin{aligned}\Pi_{(\omega\gamma)}(q^2) &= -q^2\frac{g_\omega Z_g}{\pi^2}\left[\frac{1}{6\epsilon} - \frac{1}{6}\gamma - \int_0^1 \mathrm{d}x\, x(1-x)\log\frac{M^{*2} - x(1-x)q^2}{\lambda^2}\right] \\ &\quad - \left[(Z_\omega - 1) - \frac{\delta m_\omega^2}{m_\omega^2}\right]\frac{q^2}{g_\omega Z_g}.\end{aligned} \tag{3.44}$$

The counterterm contributions in eq. (3.44) have been derived from the lagrangian (3.35) using

$$Z_{0\omega} - 1 = \frac{1}{Z_g}\left[(Z_\omega - 1) - \frac{\delta m_\omega^2}{m_\omega^2}\right],$$

as follows from eqs. (3.36) and (3.29) with $Z_N = 1$. The wave function and mass renormalization constants have been determined in eqs. (3.24) and

(3.25). Using these forms we obtain (cf. eq. (3.30))

$$\Pi_{(\omega\gamma)}(q^2) = \frac{q^2}{g_\omega}\left(\frac{C_\omega}{Z_g}\left(1-\frac{\mu^2}{m_\omega^2}\right)+P(q^2)\right), \tag{3.45}$$

where C_ω and $P(q^2)$ are given by eqs. (3.26) and (3.31). We now add the contribution due to the direct $\omega\gamma$ coupling, which is derived from the third term of eq. (3.35) as

$$\left(-g^{\mu\nu}+\frac{q^\mu q^\nu}{q^2}\right)\frac{-q^2}{g_\omega}$$

to obtain the total renormalized $\omega\gamma$ interaction

$$Q^{\mu\nu}_{(\omega\gamma)}(q) = \left(-g^{\mu\nu}+\frac{q^\mu q^\nu}{q^2}\right)Q_{(\omega\gamma)}(q^2) \tag{3.46}$$

with

$$Q_{(\omega\gamma)}(q^2) = -\frac{1}{g_\omega}q^2\left(1-P(q^2)-\frac{C_\omega}{Z_g}\left(1-\frac{\mu^2}{m_\omega^2}\right)\right). \tag{3.47}$$

Using this result together with the ω meson propagator as given by eqs. (3.22) and (3.32) we are now able to calculate the isoscalar part of the RPA type vertex shown in fig. 8:

$$\begin{aligned}\Gamma_s^\mu(q) &= -\frac{i}{2}\left\{\gamma^\mu + g_\omega Z_g \gamma_\nu \Delta^{\nu\sigma} Q^{\ \mu}_{(\omega\gamma)\sigma}\right\} \\ &= -\frac{i}{2}\left\{\gamma^\mu - \left(\gamma^\mu - \frac{q^\mu \not{q}}{q^2}\right) Z_g \Delta(q^2) q^2 \left(1-P(q^2)-\frac{C_\omega}{Z_g}\left(1-\frac{\mu^2}{m_\omega^2}\right)\right)\right\} \\ &= -\frac{i}{2}\left\{\left(\gamma^\mu - \frac{q^\mu \not{q}}{q^2}\right) F_{1s}(q^2) + \frac{q^\mu \not{q}}{q^2}\right\}\end{aligned} \tag{3.48}$$

with

$$\begin{aligned}F_{1s}(q^2) &= -Z_g m_\omega^2 \Delta(q^2) \\ &= \frac{-m_\omega^2}{q^2 - m_\omega^2 - q^2 P(q^2) - \frac{C_\omega}{Z_g} q^2 \left(1-\frac{\mu^2}{m_\omega^2}\right)}.\end{aligned} \tag{3.49}$$

In the last step of eq. (3.48) and in eq. (3.49) we used the form of Δ as given by eq. (3.32). Eq. (3.49) constitutes our result for the isoscalar Dirac-Pauli form factor in the medium, which is an extension of the well-known vector meson dominance result $-m_\omega^2/(q^2-m_\omega^2)$ to include the contribution due to the RPA type ring sum. Note that if we do not include the direct $\omega\gamma$ coupling (i.e., the graphs in the second row of fig. 8), the numerator of eq. (3.49) gets an additional term q^2.

We can also see that the result (3.48) is consistent with the CFI (3.41): The source vertex of the ω meson can be expressed by inverting eq. (3.28):

$$\Gamma^\mu_{\omega S}(q) = i\left(\Gamma^\mu_\omega(q)(q^2-m_\omega^2) - q^\mu q_\nu \Gamma^\nu_\omega\right), \tag{3.50}$$

where the ωNN Green's function Γ^μ_ω is given by the diagrams in the first line of fig. 8 with the photon line replaced by an ω meson line, i.e.,

$$\Gamma^\mu_\omega = g_\omega Z_g \gamma_\nu \Delta^{\nu\mu}_\omega. \tag{3.51}$$

Using eq. (3.51) and (3.22) in (3.50) we obtain for the source vertex

$$\Gamma^\mu_{\omega S}(q) = (-i)g_\omega \left\{ \left(\gamma^\mu - \frac{q^\mu \not{q}}{q^2}\right) Z_g \Delta(q^2)(q^2-m_\omega^2) + \frac{q^\mu \not{q}}{q^2} \right\}. \tag{3.52}$$

Comparing eq. (3.52) with (3.48) we see that the longitudinal parts of both the isoscalar γNN vertex and the ωNN source vertex are not renormalized, while their transverse parts satisfy

$$\Gamma^\mu_{s,t}(q) = \frac{1}{2g_\omega}\frac{-m_\omega^2}{q^2-m_\omega^2}\Gamma^\mu_{\omega S,t}(q) \tag{3.53}$$

in accordance with CFI.

3.3.3 Application to Magnetic Form Factors

In this section we describe our method to implement the vacuum fluctuation effects discussed in the last two sections into the finite system calculation of magnetic form factors and magnetic moments.

Before presenting the implementation of the vacuum fluctuation effects into the vertex correction calculations, we discuss two points which were left out in the previous subsection. Let us consider the choice of the renormalization point. For the σ meson we followed previous works [20,21] and used $q^2 = 0$ as the renormalization point. For theoretical completeness, we discussed the renormalization in the omega-nucleon-photon sector of our model for arbitrary renormalization point μ^2. In this scheme, the vector density is related to the baryon density by

$$\rho_{\rm v} = \left(1 + \frac{\delta m_\omega^2}{m_\omega^2}\right) \rho_{\rm B} \tag{3.54}$$

instead of $\rho_{\rm v} = \rho_{\rm B}$ as in eq. (2.6). In the vector self energy (2.4) this means effectively to replace

$$g_\omega^2 \to Z_g g_\omega^2 \tag{3.55}$$

on account of eq. (3.29). The replacement (3.55) is also evident following the more formal discussion given in Appendix C of ref. [34], where it is shown that in nuclear matter the vector self energy becomes $g_\omega^2 Z_g \rho_{\rm B}/m_\omega^2$ and the ω meson contribution to the Hartree energy density becomes $g_\omega^2 Z_g \rho_{\rm B}^2/(2m_\omega^2)$. In previous works in the literature [20,21] the renormalization point was chosen as $\mu^2 = 0$. In this case we have $\delta m_\omega^2 = 0$ and $Z_g = 1$ from eqs. (3.25) and (3.29). Thus, the coupling constant $g_{\omega,\rm HS}$ of ref. [21] is related to our

g_ω by

$$g^2_{\omega,\mathrm{HS}} = Z_g \cdot g^2_\omega. \tag{3.56}$$

If we renormalize at the physical ω meson mass ($\mu^2 = m^2_\omega$) and use $g^2_{\omega,\mathrm{HS}} = 102.77$ from ref [21], we obtain $Z_g = 0.78$ and $\delta m^2_\omega / m^2_\omega = -0.22$ from eqs. (3.25) and (3.26). In our numerical calculations we will choose $\mu = 0$ for the following reasons, though: First it facilitates the comparison with previous works [20,21], and second many formulae given in the previous sections simplify. We note that with this choice the ω meson propagator (3.32) in free space does not have a pole at $q^2 = m^2_\omega$.

The second point we wish to discuss is the unphysical pole at spacelike $q^2 < 0$ of the ω meson propagator (3.32) and the form factor (3.49). As mentioned in section 3.3, a pole of the same kind, but of course at much higher $-q^2$, occurs in the photon propagator of QED. Since our applications here will require the Fourier transform of the ω meson propagator into the coordinate space, we have to avoid this pole by damping the self energy at high $-q^2$. This will actually be done by introducing an ad-hoc ωNN form factor $f_\Lambda(q^2)$, which, due to our renormalization condition (3.27), should satisfy $f_\Lambda(0) = 1$. We choose the dipole form

$$f_\Lambda(q^2) = \left(\frac{1}{1 - q^2/\Lambda^2} \right) \tag{3.57}$$

and modify the ω meson self energy (3.30) by multiplying it with f^2_Λ, i.e.,

$$\Pi_{(\omega\omega)}(q^2) \to \Pi_{(\omega\omega)}(q^2) f^2_\Lambda(q^2) \tag{3.58}$$

In addition, due to the coupling to the external nucleon line, the transverse part of the ωNN source vertex should be multiplied by the same $f_\Lambda(q^2)$. Due

to the CFI, which requires eq. (3.53) to be valid, we must also multiply our form factor (3.49) by $f_A(q^2)$. Physically this means that we use the same "intrinsic" form factor for the ωNN and the γNN coupling.

Combining our discussions up to this point, we will use the following forms for the transverse part of the ω meson propagator and the isoscalar Dirac-Pauli form factor:

$$\tilde{\Delta}(q^2) = \frac{1}{q^2 - m_\omega^2 - \tilde{\Pi}_{(\omega\omega)}(q^2)}, \tag{3.59}$$

$$\tilde{F}_{1s}(q^2) = -f_A(q^2) m_\omega^2 \tilde{\Delta}(q^2) \tag{3.60}$$

and

$$\tilde{\Pi}_{(\omega\omega)}(q^2) = q^2 P(q^2) f_A^2(q^2) \tag{3.61}$$

where $P(q^2)$ is given by eq. (3.31) with $\mu^2 = 0$ and $Z_g = 1$. The tilde is to distinguish these forms from the original ones (eqs. (3.32) and (3.49)). In the section 4.2 we will determine the cut off mass Λ by requiring that the form factor (3.60) for zero density ($M^* = M$) reproduces the experimental slope at $q^2 = 0$ of the isoscalar Dirac-Pauli form factor $F_{1s}(q^2)$ of a free nucleon. We note that the introduction of "intrinsic" form factors seems inevitable in all studies of the free nucleon form factors based on the vector meson dominance principle [38,39] in order to fit the experimental data. This is because the form factors in the vector meson dominance model fall off with q^{-2}, while the experimentally observed ones show a q^{-4} behavior.

In order to use the results (3.60) and (3.61) in finite nuclei, we use a local density approximation (LDA). In finite nuclei the effective mass M^*

is position dependent. We will use the average

$$< M^* >_\alpha = \int_0^\infty r^2 \mathrm{d}r \, M^*(r) \rho^\alpha_{\mathrm{val}}(r), \tag{3.62}$$

where $\rho^\alpha_{\mathrm{val}}(r) = \frac{1}{4\pi}(2j_\alpha + 1)(F^2_\alpha + G^2_\alpha)$ is the probability distribution of the valence nucleon in the state α, in eq. (3.31) to obtain the ω meson propagator and the single nucleon form factor to be used for the finite system calculation. Though we will not indicate it explicitly, the quantities (3.60) and (3.61) then depend on the state of the valence nucleon.

We have now all ingredients to implement the vacuum fluctuation effects into the finite system calculation. We employ the following recipe:

1. Add the vacuum fluctuation correction $\delta\rho_{\mathrm{s}}$ of eq. (2.8) to the valence nucleon contribution of eq. (2.5) and use eq. (2.3) (together with $M^* = M + \Sigma_{\mathrm{s}}$) to calculate the scalar self energy. This is then used in the Dirac equation (2.2) to obtain the new single particle wave functions.

2. In the calculation of the RPA type vertex (3.6), replace the lowest order ω meson propagator $\Delta^{\mu\nu}_0(\boldsymbol{x})$ in eqs. (3.10) and (3.11) by $-g^{\mu\nu}\tilde{\Delta}(\boldsymbol{x})$, where $\tilde{\Delta}(\boldsymbol{x})$ is the Fourier transform of eq. (3.59) for $q^2 = -\boldsymbol{q}^2$. Graphically this means to replace the dashed ω meson lines in fig. 4 by the propagator shown in fig. 7.

3. Fold the single nucleon form factor (3.60) into the isoscalar Dirac part of the elementary vertex according to eq. (3.33). Graphically this means that the bare γNN vertex in the impulse approximation

and the vertices at point z in fig. 4 are replaced by the vertex shown in fig. 8.

It is not difficult to convince oneself that due to points 2 and 3 the RPA type vertex correction will finally include all possible combinations of explicitly density dependent pieces (D) and vacuum fluctuation pieces (F) of the polarization insertions. We finally must add some comments here: First, in the present framework we can only generate the isoscalar Dirac part of the current and its associated form factor (F_{1s}). In the actual calculation we therefore continue to use the form factors determined semi-phenomenologically in ref. [39] except for F_{1s}, which we replace by the density dependent form factor (3.60). As we show in the next section, for zero density (3.60) reproduces F_{1s} of ref. [39]. Secondly, the prescriptions 2 and 3 given above imply that the terms $\sim q^\mu q^\nu$ in the ω meson propagator (3.22) or the terms $\sim q^\mu \not{q}$ in the single nucleon vertex (3.48) can be dropped. These terms do not contribute as we explain in Appendix A. Our third comment concerns the use of the average value of the effective mass, eq. (3.62). There is an ambiguity, among others, since instead of using an average value one can also choose a suitably fixed position at which the value of M^* is calculated. Some authors [40,17] have chosen the point y in fig. 4 for a LDA to the total vertex correction in the mean field approximation. Applying an analogous prescription to the quantum fluctuation pieces would lead to a single nucleon form factor which is inevitably position dependent and therefore somewhat inconvenient to handle and to interpret. In order to avoid these and similar complications in the ω meson propagator we will use the average value (3.62). These ambiguities in the prescription

to implement the LDA should not influence the results seriously due to the short range nature of the ω meson exchange process.

4 Numerical Results

In this section we present numerical results of our calculation of isoscalar magnetic moments and magnetic form factors. We present first the results in mean field approximation, that is, those calculated by using only the explicitly density dependent terms in the loops in the RPA diagrams and in the nucleon self energy of fig. 1. Then we show the results of our "full" calculation taking the vacuum fiuctuation effects into account, and compare the two.

4.1 Mean Field Approximation

We first discuss our numerical results on isoscalar magnetic moments in the mean field approximation. As already pointed out the vertex correction eq. (3.8) is purely isoscalar. The results for the isoscalar magnetic moments are listed in table 3. In this table we list the single particle (impulse) values which are obtained by neglecting $\tilde{\Lambda}^{\mu}$ in eq. (3.6), the RPA type vertex corrections, the sum of these two contributions and the nonrelativistic Schmidt values. Contributions due to the Dirac part and the anomalous part of the magnetic moment operator are shown separately. A detailed discussion of these results using the LDA will be given in the section 5.1. Here we just note that the effect of the vertex corrections is to cancel the large enhancements relative to the Schmidt values which appeared in the impulse approximation. These corrections arise almost entirely from the particle-antinucleon ($p\overline{N}$) parts of the polarization insertions in fig. 4. In a nuclear matter picture, these corrections reduce the isoscalar current from

the impulse value ($\doteq$ velocity) $\sim \boldsymbol{p}/M^*$ to $\boldsymbol{p}/\epsilon_p$, where $\boldsymbol{p}$ is the momentum of the particle and ϵ_p its energy, and thus correspond to the "backflow" in the Landau Fermi liquid theory [28]. The vertex correction does not affect the anomalous part much. In fact, these contributions vanish if calculated in the nuclear matter model. The resulting differences between the nonrelativistic Schmidt values and our final results including the vertex corrections roughly correspond to the effect of exchange currents due to σ and ω mesons in the nonrelativistic treatment [31,2] (There is, however, a delicate difference in finite systems due to the radial dependencies of the scalar self energy, see section 5.2). The present calculation results in isoscalar magnetic moments which in most cases are extremely close to the Schmidt values or even smaller. This result disagrees with the nuclear matter picture or with usual exchange current calculations performed in the nonrelativistic framework [2], where always an enhancement is obtained. We discuss this point further in section 5.2. The isovector magnetic moments can be obtained from the isoscalar ones of table 3 by multiplying the contributions "Anomalous" in the impulse approximation by $-3.7/0.12 = -30.83$ while leaving the Dirac part unchanged, and setting the vertex corrections equal to zero. For convenience we also list these values in table 3.

Next we turn to the magnetic form factors. In the actual calculation we employed the single nucleon form factors determined in ref. [39] in the impulse approximation as well as at the photon vertices of fig. 4. In the region of q relevant for our purposes, the parameterization of these form factors is based on the vector meson dominance principle supplemented by "intrinsic" form factors. The results for ^{15}N, ^{17}O and ^{39}K are shown in

figs. 9, 10 and 11, respectively. We show the results of the impulse approximation (dashed-dotted curves) as well as the results obtained by adding the RPA type vertex corrections (full curves). For comparison the results of the nonrelativistic impulse approximation using harmonic oscillator wave functions [41,42,43,44] are also shown (dotted lines). Consider first the proton hole states ^{15}N and ^{39}K. The difference between the nonrelativistic and the relativistic impulse approximation results can be partially attributed to the enhancement of the relativistic impulse current due to the small effective mass. For $q \lesssim 1$ fm^{-1} the RPA type vertex corrections cancel these enhancements in the isoscalar part of the current and thus bring the form factors closer to the nonrelativistic results. As in the case of the magnetic moments, the p$\overline{\text{N}}$ excitation processes in the polarizations of fig. 4 are responsible for this cancellation. For higher momentum transfer, however, the particle-hole (ph) excitation processes become increasingly important and enhance the impulse current. This point, which has also been noted in ref. [18], will be discussed in more detail in the next section. Note that for both ^{15}N and ^{39}K the RPA type corrections vanish in the momentum region around the maximum of the form factors ($q \simeq 1$ fm^{-1}). Next let us turn to the neutron-particle state ^{17}O. In this case the impulse current has no Dirac part, and the difference between the relativistic and the nonrelativistic results can be partially ascribed to relativistic correction terms proportional to G^2 (G is the radial part of the small component), see the discussion in the section 5.1. The RPA type vertex corrections involve also (and mainly) a Dirac part and enhance the relativistic impulse value for low q in accordance with the enhancement of the magnetic moment of ^{17}O

(see table 3). For $q \simeq 1$ fm^{-1} the vertex correction changes sign for the same reason as discussed above. In the momentum region around the second maximum the vertex correction contributes only little. Note that in the magnetic form factors shown here, isoscalar and isovector contributions are not separated. As in the case of the magnetic moments, the present model is certainly not refined enough to make a meaningful comparison with experiment. In particular the second order core polarization, which plays an extremely important role for nuclear magnetic properties [1,45], is absent in the present calculation.

4.2 Effects of Vacuum Fluctuations

Now we present the numerical results for magnetic moments and form factors including the effects of the vacuum fluctuations. According to our recipe given in section 3.3.3, the vacuum fluctuations change the results of the previous subsection in three respects: The single particle wave functions are changed, the ω meson propagator is modified by self-energy insertions, and the single nucleon form factor becomes density dependent. Let us first discuss these three points separately.

As mentioned earlier, the inclusion of the term (2.8) in the scalar density leads to a rather drastic reduction of the coupling constants (see table 2) in order to fit the nuclear matter saturation point and the rms charge radius of ^{40}Ca [21]. The calculation shows that the self consistent scalar and vector potentials for ^{16}O and ^{40}Ca show a radial shape very similar to the one in the mean field approximation while their magnitude is reduced. We can thus expect that both the deviations of the relativistic impulse

approximation results from the nonrelativistic ones and the magnitude of the RPA type vertex corrections will be reduced as compared to the mean field approximation.

Consider next the single nucleon form factor (3.60) in free space, which for $q_0 = 0$ can be written in the form

$$\tilde{F}_{1s}(q^2) = f_\Lambda(q^2)\frac{{m_\omega}^2}{{m_\omega}^2 + q^2}\left(1 + \frac{\tilde{\Pi}_{(\omega\omega)}(q^2)}{q^2 + {m_\omega}^2}\right)^{-1} \tag{4.1}$$

with $q^2 = -q^2$. The derivative at $q^2 = 0$ takes the form

$$\tilde{F}'_{1s}(0) = -\left(\frac{1}{{m_\omega}^2} + \frac{2}{\Lambda^2} + \frac{\tilde{\Pi}'_{(\omega\omega)}(0)}{{m_\omega}^2}\right) \tag{4.2}$$

$$= -\left(\frac{1}{{m_\omega}^2} + \frac{2}{\Lambda^2} - \frac{1}{3}\left(\frac{g_\omega}{m_\omega \pi}\right)^2 \log\frac{M^*}{M}\right). \tag{4.3}$$

Due to our renormalization prescription the last term in (4.2) vanishes for zero density. If we fix the cut-off mass so as to reproduce the experimental value of the slope of F_{1s} at $q^2 = 0$, which is -0.092 fm^2, we obtain $\Lambda = 1.65$ GeV. The resulting form factor for zero density is shown in fig. 12 in comparison with the one of ref. [39] (dashed line) which we used in the calculation of section 4.1. We see that the two form factors agree very well in the range of momentum transfers considered here, in spite of their different analytical forms. By varying the derivative at $q^2 = 0$ freely even a better overall agreement could be attained. We also show the result of the analysis of ref. [38] (dotted line) which includes small contributions due to the ϕ meson[2]. Note that with the present choice of g_ω, the last factor

[2] ϕ is a vector-isoscalar meson with a mass of 1020 MeV. Both $\omega$and ϕ mesons are often included in the phenomenological analysis using the vector meson dominance model.

in (4.1) for $M^* = M$ differs from unity only by a negligible amount, at least in the range of q^2 relevant for our purposes. This is shown by the dashed line in fig. 13.

The form factor (4.1) depends on the density via the average effective mass $< M^* >$. Due to

$$\tilde{\Pi}_{(\omega\omega)}(q^2)\,|_{M^*<M} > \tilde{\Pi}_{(\omega\omega)}(q^2)\,|_{M^*=M},$$

the form factor is quenched in the nucleus. This is shown in fig. 13, where we plot the last factor in (4.1) for the case $A = 15$ ($M^*/M = 0.85$) as well as its ratio to the value for zero density. This ratio, which is shown by the solid line in fig. 13, is the quenching factor of the single nucleon isoscalar Dirac form factor due to $M^* < M$. The resulting single nucleon form factor for $A = 15$ is shown by the dashed-dotted line in fig. 12. Associated with this quenching is an enhancement of the slope at $q^2 = 0$, as is clear from eq. (4.3). This can be interpreted as a change of the "isoscalar charge radius" $< r^2 >_{\rm s}$ defined by

$$\tilde{F}'_{1{\rm s}}(0) = -\frac{1}{6} < r^2 >_{\rm s} - \frac{\kappa_{\rm s}}{4M^2} \tag{4.4}$$

with $\kappa_{\rm s} = -0.12$ and

$$< r^2 >_{\rm s} = < r^2 >_{\rm p} + < r^2 >_{\rm n} . \tag{4.5}$$

Values for the isoscalar charge radius are given in table 4.

Once we have fixed the value of the cut-off mass as described above, we can calculate the ω meson exchange potential in coordinate space by a Fourier transformation of $\tilde{\Delta}(q^2)$, eq. (3.59). The results are shown in fig. 14,

where we compare the Yukawa form used in section 4.1 with the potential for zero density ($M^* = M$, dashed-dotted line), $A = 15$ ($M^*/M = 0.85$, dotted line) and $A = 17$ ($M^*/M = 0.91$, dashed line). The asymptotic form of the potential is determined by the pole of (3.59) for timelike real q^2. The values of the pole positions are listed in table 4 in the entry "$m_\omega{}^*$". Note that since the renormalization point has been chosen as $\mu^2 = 0$, the self energy in (3.59) causes a shift of the pole position also for zero density. For $q^2 > 0$ the self energy (3.59) is negative and becomes smaller as M^* decreases. Therefore the shift of the pole position is largest for the smallest M^*, i.e., for $A = 39$ in table 4. According to this shift, the ω meson exchange potential has now a longer range, as can be seen from fig. 14. For distances between 0.5 and 1 fm the potentials of fig. 14 drop below the Yukawa curve. This can be understood from the fact that the integral of $\tilde{\Delta}(r)$ over the whole space must be equal to $1/m_\omega{}^2$, since the self energy vanishes at $q = 0$.

The results for the isoscalar magnetic moments are listed in table 5, which should be compared with the mean field results of table 3. We see that due to the weaker scalar potential the magnetic moments in the impulse approximation are less enhanced than in the mean field model. Nevertheless, the impulse values considered alone are still unreasonably large especially for hole states, and the RPA type vertex correction continues to play an essential role in reducing them to reasonable values. For these vertex corrections we listed in parenthesis also the results obtained by using the Yukawa form for the ω meson exchange potential. Therefore the difference between the values in parenthesis in table 5 and the ones in table 3

is only due to the difference in the scalar and vector potentials. We see that this difference in the one-body potentials has almost no influence on the final results for the isoscalar magnetic moments of the particle states, while it leads to a 4 % reduction for $A = 15$ and a 2 % enhancement for $A = 39$. The effect of the vacuum fluctuations in the ω meson exchange potential is to decrease the vertex corrections in magnitude and thereby to enhance the isoscalar magnetic moments by some small amount, typically 1 to 2 %. This small reduction of the vertex correction has its origin in the depression of the ω meson exchange potential for distances below 1 fm as compared to the Yukawa form (see fig. 14). Altogether, the inclusion of vacuum fluctuations leads to a decrease (increase) of the isoscalar magnetic moment of $A = 15$ ($A = 39$) by about 3 %, while the values for $A = 17$ and $A = 41$ are enhanced by a smaller amount.

We see from the above discussion that the inclusion of vacuum fluctuations leads only to minor changes of the overall picture concerning the isoscalar magnetic moments in the present model. This was anticipated already in section 3.1. Although the results differ in details from the intuitive expectations based on the nuclear matter picture, the overall conclusion is that a consistent description leads to isoscalar magnetic moments which differ from the Schmidt values by not more than a few percent, which is in accordance with the results based on the more traditional concept of meson exchange currents.

We now turn to discuss the results for the magnetic form factors including the vacuum fluctuation effects. The magnetic form factors of ^{15}N, ^{17}O and ^{39}K are shown in fig. 15, 16 and 17, which should be compared

with the results based on the mean field approximation (figs. 9, 10 and 11). Consider first the proton hole states ^{15}N and ^{39}K. Figs. 15 and 17 show the enhancement of the form factor in the relativistic impulse approximation (dashed-dotted line) relative to the nonrelativistic one (dotted line), which is partially due to the enhancement of the isoscalar Dirac part of the current. The RPA type vertex corrections reduce the form factors for $q \lesssim 1\text{fm}^{-1}$ but give rise to an enhancement for larger q. This is qualitatively the same situation as observed in the mean field approximation. Quantitatively, however, both the deviations caused by the enhanced isoscalar impulse current and the corrections due to the RPA type diagrams are much less significant than in the mean field approximation. Figs. 18 to 20 show a comparison between the form factors including the effect of the vacuum fluctuations (full lines) with those based on the mean field approximation (dashed lines). We see that the form factors of both ^{15}N and ^{39}K are considerably reduced in magnitude when the vacuum fluctuations are included. In order to understand the reason for this difference from the mean field results, we have also carried out a calculation including the vacuum fluctuation effects only in the single particle wave functions but not in the single nucleon form factor F_{1s} and in the ω meson propagator. These results, which differ from the mean field results only due to the smaller scalar and vector potentials, are shown by the dashed-dotted lines in figs. 18 to 20. We see that almost the whole difference to the mean field results comes from the difference in the single particle potentials. Moreover, as is clear from figs. 9, 11 and 15, 17, the vertex corrections are very small around the maxima of the form factors. Therefore, in this region of q, the reduction of

the form factors shown in figs. 15, 16 and 17 is simply due to the fact that according to the smaller scalar potential the impulse approximation leads to less enhancement of the form factors when the vacuum fluctuations are taken into account.

For the case of ^{17}O, the Dirac part of the current does not contribute in the impulse approximation, and therefore the difference in the scalar potential does not change the impulse approximation result very much. This is seen by comparing figs. 10 and 16. As we discussed previously, the RPA type vertex corrections enhance the form factor around the first maximum but are almost zero around the second maximum. Due to the weaker scalar potential, this enhancement around the first maximum becomes weaker when the vacuum fluctuations are included. Fig. 19 shows the comparison to the result based on the mean field theory and also demonstrates that almost all of the difference comes from the change of the single particle potentials.

The above discussion shows that among the three effects caused by the vacuum fluctuations mentioned at the beginning of this section, only the first one, i.e., the change of the single particle potentials, shows up significantly in the results for the magnetic form factors and leads to a quenching of the form factors for all three nuclei (except for ^{17}O in the high q region). As for the other two effects, we have confirmed that the small differences between the dashed-dotted and the full lines in figs. 18, 19 and 20 come from the quenching of the isoscalar Dirac-Pauli form factor F_{1s} (see fig. 12), while the effect due to the renormalization of the ω meson propagator (see fig. 14) is completely negligible in the present context. The former effect

leads to a reduction of the isoscalar Dirac parts of the total nuclear form factors (impulse plus vertex corrections) by a q-dependent factor shown by the full line in fig. 13. Due to the presence of the large contributions from the anomalous term, however, this quenching cannot be seen directly in the nuclear form factors, and in fact is hardly visible on a logarithmic scale. Thus, while these two effects caused by the vacuum fluctuations are of physical interest by themselves and must be taken into account to achieve theoretical consistency within the present framework, they actually contribute only little to the nuclear magnetic form factors. Their role in different contexts, for example in the quenching of the Coulomb sum rule, remains to be investigated.

5 Discussion

The aim of this section is to gain more understanding of our results for the magnetic moments and form factors in the mean field approximation presented in table 3 and figs. 9, 10 and 11. In the first subsection 5.1 the connection between the present calculation and the nuclear matter model is investigated. A comparison with the exchange current effects in nonrelativistic treatments is presented in subsection 5.2.

5.1 Connection to the nuclear matter model

Let us briefly recall some results obtained in nuclear matter [29,31]. Let $\boldsymbol{j}_{\rm f}$, $\boldsymbol{j}_{\rm I}$ and $\boldsymbol{j}$ be the isoscalar currents for zero momentum transfer of a free nucleon, a bound nucleon in the impulse approximation, and of a bound nucleon including the vertex corrections.[3] Then we have the following relations,

$$\boldsymbol{j}_{\rm I} = \frac{E_p}{E_p^*}\boldsymbol{j}_{\rm f} \simeq \frac{M}{M^*}\boldsymbol{j}_{\rm f} \tag{5.1}$$

$$\boldsymbol{j} = \frac{E_p^*}{\varepsilon_p}\boldsymbol{j}_{\rm I} = \frac{E_p}{\varepsilon_p}\boldsymbol{j}_{\rm f} \simeq \frac{M}{\varepsilon}\boldsymbol{j}_{\rm f}. \tag{5.2}$$

Here $E_p = \sqrt{M^2 + \boldsymbol{p}^2}$, $E_p^* = \sqrt{M^{*2} + \boldsymbol{p}^2}$, ε_p is the quasiparticle energy, and $\varepsilon = \varepsilon_{p=0}$. Eq. (5.1) shows the enhancement of the impulse current by a factor M/M^*, while eq. (5.2) tells that the total current is only slightly enhanced ($\varepsilon \lesssim M$). As discussed in ref. [29], the same relations hold for the isoscalar angular momentum g-factor. For the special case of the σ-

[3] In this section, all currents (j) and magnetic moments (m) refer to the isoscalar Dirac parts only. The current $\boldsymbol{j}$ (without arguments) stands for the nuclear matter result at $q = 0$ ($\boldsymbol{j} = \boldsymbol{j}(q = 0)$), while $\boldsymbol{j}(\boldsymbol{x})$ denotes the current in a finite system.

ω model in the Hartree approximation, however, analogous relations hold also for the isoscalar magnetic moments m (including the spin part) for the following reason: First, the current $\boldsymbol{j}_{\rm I}(q)$ for finite q is obtained from $\boldsymbol{j}_{\rm f}(q)$ by replacing $M \to M^*$. Thus, a relation analogous to (5.1) holds between $m_{\rm I}$ and $m_{\rm f}$. Second, since the ω meson couples to the nucleon in the same way as the photon, the current $\boldsymbol{j}(q)$ including the RPA type vertex correction of fig. 4 is obtained from $\boldsymbol{j}_{\rm I}(q)$ by multiplying a form factor $F(\boldsymbol{q}^2)$ with $F(0) = E_p^*/\varepsilon_p$. Explicitly, the transverse part of the current, including the vertex correction caused by the space components of the ω meson field, becomes

$$\boldsymbol{j}(q) = \boldsymbol{j}_{\rm I}(q) \cdot F(\boldsymbol{q}^2) \tag{5.3}$$

with

$$F(\boldsymbol{q}^2) = \frac{\boldsymbol{q}^2 + {m_\omega}^2}{\boldsymbol{q}^2 + {m_\omega}^2 + \Pi_{\rm t}(\boldsymbol{q}^2, q_0)}, \tag{5.4}$$

where $\Pi_{\rm t}$ is the transverse (with respect to the three vector $\boldsymbol{q}$) part of $\Pi^{ij}_{(\omega\omega){\rm D}}$ and is given analytically in ref. [46]. In eq. (5.4) we left the q_0-dependence in $\Pi_{\rm t}$, since the limit $q \to 0$ must be taken by letting first $\boldsymbol{q} \to 0$ and then $q_0 \to 0$. Since the $\boldsymbol{q}$-dependence of this form factor does not enter into the magnetic moment ($\boldsymbol{m} = -\frac{\rm i}{2}[\nabla_q \times \boldsymbol{j}(q)]_{q=0}$), a relation analogous to (5.2) holds between m, $m_{\rm I}$ and $m_{\rm f}$.

Let us compare these results with our values for the isoscalar magnetic moments obtained in the previous section. In the first row of table 6 we list the expectation values of $M/M^*(r)$ for the various single particle states, and in the second row we reproduce the ratios $m_{\rm I}/m_{\rm S}$, where $m_{\rm S}$ is the Schmidt value, from table 3. We see that for hole states this ratio is larger

than $< M/M^* >$, while for particle states it is smaller. This fact can be explained as follows: Using the Dirac equation (2.2) we can perform a Gordon decomposition of the isoscalar impulse current with the result

$$\boldsymbol{j}_{\rm I}(r) = \frac{1}{2}\overline{\psi}(r)\gamma\psi(r) = \frac{M}{M^*(r)}\boldsymbol{j}_{\rm f}(r) \tag{5.5}$$

with

$$\boldsymbol{j}_{\rm f}(r) = \frac{1}{4M}\overline{\psi}(r)(\vec{\boldsymbol{p}} - \overleftarrow{\boldsymbol{p}} + \overleftrightarrow{\boldsymbol{\nabla}} \times \boldsymbol{\Sigma})\psi(r). \tag{5.6}$$

Here $\vec{\boldsymbol{p}} = -i\,\vec{\boldsymbol{\nabla}}$, $\overleftrightarrow{\boldsymbol{\nabla}} = \vec{\boldsymbol{\nabla}} + \overleftarrow{\boldsymbol{\nabla}}$, and $\boldsymbol{\Sigma}$ is the Dirac matrix

$$\boldsymbol{\Sigma} = \begin{pmatrix} \boldsymbol{\sigma} & 0 \\ 0 & \boldsymbol{\sigma} \end{pmatrix}.$$

$\boldsymbol{j}_{\rm f}(r)$ has the same functional form as the current of a free nucleon. Eq. (5.5) now corresponds to eq. (5.1) for the nuclear matter model. However, the magnetic moment calculated from eq. (5.5) becomes (in unit of $e/2M$)

$$\begin{aligned} \boldsymbol{m}_{\rm I} &= M\int {\rm d}^3r\, \boldsymbol{r} \times \boldsymbol{j}_{\rm I}(r) \\ &= \frac{1}{2}\int {\rm d}^3r\, \frac{M}{M^*(r)}\overline{\psi}\{\boldsymbol{L} + \boldsymbol{\Sigma}\left(1 - \frac{1}{3}\frac{r(M^*)'}{M^*}\right) \\ &\quad - \frac{\sqrt{8\pi}}{6}\left[Y^{(2)}(\hat{r}) \times \Sigma^{(1)}\right]^{(1)}\frac{r(M^*)'}{M^*}\}\psi, \end{aligned} \tag{5.7}$$

where $\boldsymbol{L} = \boldsymbol{r} \times \boldsymbol{p}$, and $(M^*)' = {\rm d}M^*/{\rm d}r$. We see that, in addition to one piece which shows the characteristic enhancement factor M/M^*, there are certain spin dependent terms which arise from the radial dependence of the scalar potential. Further explicit evaluation for a single particle orbit with angular momentum j gives, using the spinors (2.7),

$$m_{\rm I} = \tilde{m}_{\rm I} + \frac{2j+1}{j+1}\frac{\varpi}{8}\int_0^\infty r^3{\rm d}r\,(F^2 + G^2)\frac{M(M^*)'}{(M^*)^2} \tag{5.8}$$

with

$$\begin{aligned} \tilde{m}_{\rm I} &= \frac{1}{2}\int {\rm d}^3r\, \frac{M}{M^*}\overline{\psi}(L_{\rm z}+\Sigma_{\rm z})\psi \\ &= m_{\rm S}\int_0^\infty r^2{\rm d}r\, \frac{M}{M^*}\left(F^2-\left(\frac{j+1}{j}\right)^{\varpi}G^2\right). \end{aligned} \tag{5.9}$$

Here $m_{\rm S}$ is the isoscalar Schmidt value (which is equal to $\frac{1}{2}(j+\frac{1}{2})$ for $j=\ell+\frac{1}{2}$ and $\frac{j(2j+1)}{4(j+1)}$ for $j=\ell-\frac{1}{2}$), and $\varpi=-1(+1)$ for $j=\ell+\frac{1}{2}(\ell-\frac{1}{2})$. The values for $\tilde{m}_{\rm I}/m_{\rm s}$ are listed in the third row of table 6. They are close to the values for $< M/M^* >$, being somewhat smaller due to the term proportional to G^2 in eq. (5.9). (Thus, it is eq. (5.9) with M/M^* replaced by 1, rather than the nonrelativistic Schmidt value, which corresponds to $m_{\rm f}$ of our nuclear matter discussion.) The most important point to note, which we mentioned already in section 3.3.3, is that due to $(M^*)' = (\Sigma_{\rm s})' > 0$ in the average (the scalar potential goes from negative values to zero for increasing r), the second term in eq. (5.8) gives a positive (negative) contribution for hole (particle) states. Thus, the fact that in finite nuclei the relativistic impulse value of the magnetic moment is enhanced by a factor larger than $< M/M^* >$ for hole states and smaller than $< M/M^* >$ for particle states is due to the radial dependence of the scalar potential.

Next we turn to a discussion of our final values for isoscalar magnetic moments including the vertex corrections. In the fourth row of table 6 we list the expectation values of $M/\varepsilon(r)$ ($\varepsilon(r) = M^*(r) + \Sigma_{\rm v}(r)$ in the present model), and below that we reproduce our values for $m/m_{\rm S}$ from table 3. We see that the latter ratio is practically equal to 1 and therefore less than $< M/\varepsilon >$, except for the case $A = 15$. In order to investigate the reason for this, let us first try to understand our values for $m/m_{\rm S}$ in

terms of a simple local density approximation (LDA). The nuclear matter relation (5.2) suggests the use of the following current [17,40]:

$$\boldsymbol{j}_{\rm LDA}(r) = \frac{M^*(r)}{\varepsilon(r)} \boldsymbol{j}_{\rm I}(r), \tag{5.10}$$

where $\boldsymbol{j}_{\rm I}$ is given by eq. (5.5). The choice (5.10) for the current is not unique, since one can fix the point at which the correction factor M^*/ε is calculated anywhere "between" $\boldsymbol{y}$ and $\boldsymbol{z}$ of fig. 4. This ambiguity, however, should not influence the results seriously since the ω meson exchange process is of sufficiently short range. The magnetic moments $m_{\rm LDA}$ calculated by using the current (5.10) are listed in the last but one row of table 6. We see that except for $A = 15$ the values agree very well with the results of the exact calculation. Following now the same steps which lead from eq. (5.5) to (5.8), we obtain the following expression for the isoscalar magnetic moment in the LDA:

$$m_{\rm LDA} = \tilde{m}_{\rm LDA} + \frac{2j+1}{j+1}\frac{\varpi}{8}\int_0^\infty r^3 {\rm d}r\,(F^2+G^2)\frac{M\varepsilon'}{\varepsilon^2} \tag{5.11}$$

$$\begin{aligned} \tilde{m}_{\rm LDA} &= \frac{1}{2}\int {\rm d}^3 r \frac{M}{\varepsilon(r)}\overline{\psi}(L_z+\Sigma_z)\psi \\ &= m_{\rm S}\int_0^\infty r^2 {\rm d}r\,\frac{M}{\varepsilon(r)}\left(F^2 - \left(\frac{j+1}{j}\right)^{\varpi} G^2\right) \end{aligned} \tag{5.12}$$

with $\varepsilon' = {\rm d}\varepsilon/{\rm d}r$. The values for $\tilde{m}_{\rm LDA}/m_{\rm S}$ are listed in the last row of table 6. We see that the corresponding values in the last two rows of table 6 are very close to each other, which tells that the second term in eq. (5.11) is very small. Therefore we see that if also the ω meson is taken into account in the magnetic moment, the radial dependence of the combined potential

$\Sigma_s + \Sigma_v$ has only a very small effect on the magnetic moment. In other words, $\varepsilon' = \Sigma_s' + \Sigma_v' \gtrsim 0$ in the average. The fact that the ratio $m_{\rm LDA}/m_s$ is smaller than $< M/\varepsilon >$ can then be simply traced back to the presence of the last term in eq. (5.12), which arises from the small components. In this way one can see that m/m_s is smaller than $< M/\varepsilon >$ due to relativistic effects for all cases except for $A = 15$, where the LDA does not seem to work well. We do not have a good explanation for this case. The above discussion shows that the RPA type vertex corrections cancel not only the enhancement of the magnetic moments due to the small effective mass, but also the large contributions from the second term in eq. (5.8), which is related to the LS-force [47].

A similar comparison between the results including vacuum fluctuations presented in section 4.2 and the expectations based on the nuclear matter picture is presented in table 7, which can be compared with table 6 for the mean field case discussed above. Again we list the expectation values of M/M^* and compare them with the ratios of the relativistic impulse approximation values to the Schmidt values. (Note that all magnetic moments in table 7 refer to the isoscalar Dirac part only.) These latter ratios are larger (smaller) than $< M/M^* >$ for hole (particle) states, which is ascribed to the second term in eq. (5.8). The first term in (5.8) leads again to magnetic moments which are close to (but smaller than) $< M/M^* >$ times the Schmidt value. The expectation values of $< M/\varepsilon >$ are close to the mean field values shown in table 6, which is due to the fact that both parameters sets employed in the two calculations lead to the same binding energy per particle in nuclear matter. Below the values for $< M/\varepsilon >$ we reproduce

from table 5 the ratios of the isoscalar Dirac parts m/m_S, and in parenthesis the ratios calculated by neglecting the vacuum fluctuations in the ω meson potential. Except for $A = 15$, these latter values are smaller than $< M/\varepsilon >$. The results of a LDA based on eqs. (5.11) and (5.12) are given in the last but one row and seem to reproduce the values in parenthesis quite well except for $A = 15$. The last row in table 7 demonstrates again that the magnetic moments in the LDA are determined mainly by the first term in eq. (5.11) and are therefore somewhat smaller than $< M/\varepsilon >$ times the Schmidt value due to the term involving G^2 in eq. (5.12).

Let us now turn to discuss the results for the form factors in the mean field approximation shown in figs. 9, 10 and 11. In order to keep the discussion as parallel as possible to the magnetic moment case, let us introduce a quantity $\mu^J(q)$ which for $J = 1$ and $q \to 0$ becomes the magnetic moment. $\mu^J(q)$ is related to M^J in Appendix A by the formula:

$$M^J = \sqrt{\frac{(j+1)(2j+1)}{j}} \frac{iq}{2M\sqrt{6\pi}} \mu^J(q)$$

Corresponding to eq. (5.11), the form of $\mu^J(q)$ in the impulse approximation is:

$$\mu_I^J(q) = \tilde{\mu}_{ID}^J(q) + C_j^J \frac{\varpi}{q}(2J+1) \int_0^\infty r^2 \mathrm{d}r \, (F^2 + G^2) j_J(qr) e \frac{M(M^*)'}{(M^*)^2} + \mu_{IA}(q) \tag{5.13}$$

with

$$\tilde{\mu}_{ID}^J(q) = C_j^J(2j+1) \int_0^\infty r^2 \mathrm{d}r \, e \frac{M}{M^*} \{(F^2 + G^2)[j_{J-1}(qr) \left(1 - \frac{\varpi J}{2j+1}\right) + j_{J+1}(qr) \left(1 + \frac{\varpi(J+1)}{2j+1}\right)] - 2G^2(j_{J+1}(qr) + j_{J-1}(qr))\}, \tag{5.14}$$

$$\mu^J_{\rm IA}(q) = -C^J_j \kappa_{\rm A} \varpi \int_0^\infty r^2 {\rm d}r \{(F^2+G^2)[j_{J-1}(qr)(J+1)\left(1-\frac{\varpi J}{2j+1}\right) - j_{J+1}(qr)J\left(1+\frac{\varpi(J+1)}{2j+1}\right)] + G^2 \frac{2\varpi J(J+1)}{2j+1}(j_{J-1}(qr)+j_{J+1}(qr))\}, \quad (5.15)$$

and

$$C^J_j = i^{J+1}(2j+1)\left[\frac{3j}{2(j+1)J(J+1)(2J+1)}\right]^{\frac{1}{2}} < Jj0\frac{1}{2}|j\frac{1}{2} > .$$

Here $e = \frac{1+\tau_z}{2}$ is the charge and $\kappa_{\rm A}$ the anomalous magnetic moment of the valence nucleon. $j_J(x)$ is the spherical Bessel function of J-th order. The first two terms in eq. (5.13) are due to the Dirac part of the current and the last term is due to the anomalous part. For $J = 1$ and $q \to 0$ the isoscalar Dirac part of (5.13) reduces to (5.8). The expression for the nonrelativistic impulse approximation is obtained by replacing M/M^* by 1, (F^2+G^2) by the square of the nonrelativistic wave function and setting the terms proportional to G^2 equal to zero.

Within the LDA, the quantity $\mu^J(q)$ including the effect of the RPA type vertex correction can be obtained from the expressions (5.13), (5.14) and (5.15) by the replacements

$$e\frac{M}{M^*(r)} \to \frac{1}{2}\left(\frac{M}{\epsilon(\boldsymbol{q}^2,r)} + \tau_z \frac{M}{M^*(r)}\right) \quad (5.16)$$

$$e\frac{M(M^*)'}{(M^*)^2} \to \frac{1}{2}\left(\frac{M\epsilon'(\boldsymbol{q}^2,r)}{\epsilon^2(\boldsymbol{q}^2,r)} + \tau_z \frac{M(M^*)'}{(M^*(r))^2}\right) \quad (5.17)$$

with

$$\frac{M}{\epsilon(\boldsymbol{q}^2,r)} = \frac{M}{M^*(r)} \cdot F(\boldsymbol{q}^2,r), \quad (5.18)$$

where the form factor $F(q^2, r)$ is obtained from the nuclear matter result (5.4) by replacing $M^* \rightarrow M^*(r)$. With the effect of the vertex corrections introduced according to (5.16), the isoscalar Dirac part of $\mu^1(0)$ is identical to (5.11) provided that we replace again $F(0,r) = E^*_{\rm pF}(r)/\epsilon_{\rm pF}(r)$ by $M^*(r)/\epsilon(r)$.

Eqs. (5.13) to (5.18) can be used to get an understanding of the numerical results show in figs. 9 to 11. Let us first discuss the proton-hole state ^{15}N. In this case we have $J = 1$, $j = \frac{1}{2}$, $\varpi = 1$, $\tau_z = 1$ and $\kappa_{\rm A} = 1.79$. The dotted line in fig. 21 shows the form factor obtained by setting $M^* = M$ and neglecting the terms proportional to G^2 in eq. (5.13), (5.14) and (5.15). When we include the factor M/M^* in eq. (5.14) we obtain the result shown by the dashed-dotted line. In the present case the coefficient of $(F^2 + G^2)$ in eq. (5.14) is $\frac{1}{2}(j_0 + 4j_2)$, and this term gives a positive contribution to the integral for all values of q. The dashed line shows the result when the terms proportional to G^2 are included. These terms give a negative contribution to $\mu_I(q)$, and their effect is appreciable especially for higher values of q. Finally, the full line shows the result obtained by including also the second term in eq. (5.13). For low and medium q, this term is positive and reinforces the M/M^* enhancement in the same way as for the isoscalar magnetic moment. For $q \geq 2.1$ fm^{-1}, however, it becomes negative due to the presence of $j_1(qr)$. The full line in fig. 21 is the total relativistic impulse form factor and is the same as the dashed-dotted line in fig. 9. Altogether, we see that the relativistic correction terms in eq. (5.13), (5.14) and (5.15) enhance the form factor for low and medium values of q, but at higher q the M/M^* enhancement is canceled by the terms proportional to G^2 and the

term involving $(M^*)'$ in eq. (5.13). In this way one can understand why the relativistic impulse approximation result in fig. 9 approaches the nonrelativistic one after the maximum. (Note, however, that after the maximum the dotted lines in fig. 9 and 21 differ appreciably.)

When we now introduce the replacement (5.16) to account for the vertex corrections, the term $\tilde{\mu}^J_{\rm ID}$ is changed qualitatively as follows: For low q, where the $\rm p\overline{N}$ contributions to the ω meson self energy are dominant, we have $\Pi_{\rm t} > 0$ in eq. (5.4) and hence $F < 1$, i.e., the form factor in eq. (5.18) reduces the enhancement caused by the small effective mass. For higher q the ph terms in the ω meson self energy become important such that beyond some value of q we have $\Pi_{\rm t} < 0$ and $F > 1$. Thus, the modification (5.16) causes a quenching (enhancement) of $\tilde{\mu}^J_{\rm ID}$ below (above) some value of q. The replacement (5.17), when inserted into the second term in (5.13), works into the same direction. This is the reason for the crossing between the relativistic impulse approximation curve and the full result in fig. 9. The vertex correction changes sign at $q \gtrsim 1\text{fm}^{-1}$. The LDA form factor (5.4) predicts this sign changes at too low values of q [18], which is an indication of the fact that ph excitation processes cannot be described well in the LDA. Moreover, a finite value of q_0 is needed in the LDA form factor in order to account qualitatively for the result in finite nuclei. We therefore refrain from giving more quantitative discussions on the role of the RPA type vertex correction for finite q. We wish to point out, however, that with a realistic residual interaction this ph excitation process mentioned above, which is nothing but the well known first order core polarization or the Arima-Horie effect [1], gives rise to a quenching of the form factor instead

of an enhancement [41,42,43,44,45] for all the cases ^{15}N, ^{17}O and ^{39}K.

For the proton-hole state ^{39}K we have to use $j = \frac{3}{2}$, $\varpi = 1$, $\tau_z = 1$, $\kappa_A = 1.79$ and $J = 1, 3$. It turns out that for this case we have almost exactly the same situation as discussed above for ^{15}N: For low and medium q the relativistic correction terms give rise to an enhancement of the form factor, while for higher q they tend to cancel each other. Also the role of the RPA type vertex correction is similar: It introduces a quenching up to $q \simeq 1$ fm^{-1} and beyond that an enhancement. This explains the qualitative features shown in fig. 11.

For the neutron-particle state ^{17}O we have to use $j = \frac{5}{2}$, $\varpi = -1$, $\tau_z = -1$, $\kappa_A = -1.91$ and $J = 1, 3, 5$. In the impulse approximation the form factor is determined by the anomalous term (5.15). The second term in this expression, being proportional to G^2, reduces the contribution due to the first term somewhat for all three values of J. However, this effect turns out to be quite small and cannot explain the full difference between the relativistic and nonrelativistic impulse approximation results shown in fig. 10. If the RPA type vertex corrections are introduced according to eqs. (5.16), (5.17) and (5.18), also the Dirac parts in (5.13) contribute. For low q, the expression on the right hand side of (5.16) is negative and thus gives a negative Dirac contribution when inserted into (5.14). Since the anomalous contribution (5.15) is also negative, the absolute value of the form factor becomes enhanced at low q due to the vertex corrections. This enhancement is reduced somewhat due to the modification (5.17), which gives a positive contribution when inserted into the second term of (5.13). The enhancement of the form factor for low q is completely analogous to the

enhancement of the magnetic moment of ^{17}O, as can be seen from table 3. For reasons discussed above, the right hand side of (5.16) becomes positive at some value of q, which leads to a sign change of the vertex correction and to the crossing between the relativistic impulse curve and the full result in fig. 10 around $q \simeq 1$ fm^{-1}. In the region around the second maximum the vertex correction is very small.

5.2 Connection to exchange currents

In this subsection we discuss the connection between the relativistic framework used in section 4.1 and the concept of meson exchange currents used in nonrelativistic calculations. We shall restrict ourselves to study the implications for magnetic moments.

In a nonrelativistic treatment of isoscalar currents, the starting point is the Schrödinger current

$$\boldsymbol{j}_{\rm f}^{\rm (NR)}(r) = \frac{1}{4M}\psi^{+}\left(\vec{\boldsymbol{p}} - \overleftarrow{\boldsymbol{p}} + \overleftrightarrow{\boldsymbol{\nabla}} \times \boldsymbol{\sigma}\right)\psi. \tag{5.19}$$

Corrections to this current are conventionally calculated in lowest order perturbation theory by averaging the two-body pair current operators [2,1] due to σ and ω meson exchange with respect to one of the two nucleons over all states in the Fermi sea. Let us briefly recapitulate the forms of the resulting currents in nuclear matter at $q = 0$ [2,1]: The pair current due to the σ meson gives the effective single particle current

$$\boldsymbol{j}_{\sigma}^{\rm (NR)} = -\frac{\Sigma_{\rm s}}{M}\boldsymbol{j}_{\rm f}^{\rm (NR)},$$

and therefore we have

$$\boldsymbol{j}_{\rm I}^{\rm (NR)} \equiv \boldsymbol{j}_{\rm f}^{\rm (NR)} + \boldsymbol{j}_{\sigma}^{\rm (NR)} = \left(1 - \frac{\Sigma_{\rm s}}{M}\right) \boldsymbol{j}_{\rm f}^{(NR)}, \tag{5.20}$$

which agrees with eq. (5.1) in lowest order perturbation theory. The pair current due to the ω meson gives

$$\boldsymbol{j}_{\omega}^{\rm (NR)} = -\frac{\Sigma_{\rm v}}{M} \boldsymbol{j}_{\rm f}^{\rm (NR)},$$

and therefore

$$j^{\rm (NR)} \equiv \boldsymbol{j}_{\rm I}^{\rm (NR)} + \boldsymbol{j}_{\omega}^{\rm (NR)} = \left(1 - \frac{\Sigma_{\rm s}}{M} - \frac{\Sigma_{\rm v}}{M}\right) \boldsymbol{j}_{\rm f}^{\rm (NR)}, \tag{5.21}$$

in accordance with eq. (5.2). As explicitly shown in ref. [2], analogous results hold for the isoscalar magnetic moments as well. Thus, in nuclear matter, the exchange current approach and the fully relativistic approach agree (besides kinematical corrections) to lowest order perturbation theory. However, differences occur in finite systems: If we use the direct terms of the two-body pair current operators given in ref. [2], we obtain the effective single particle currents

$$\boldsymbol{j}_{\sigma}^{\rm (NR)}(r) = -\frac{\Sigma_{\rm s}(r)}{M} \boldsymbol{j}_{\rm f}^{\rm (NR)}(r) + \frac{1}{4M^2} \left(\psi^{+} \boldsymbol{\sigma} \psi\right) \times \boldsymbol{\nabla} \Sigma_{\rm s}(r) \tag{5.22}$$

$$\boldsymbol{j}_{\omega}^{\rm (NR)}(r) = -\frac{1}{M} \int {\rm d}^3 r_1 \, \boldsymbol{j}_{\rm f}^{\rm (NR)}(\boldsymbol{r}_1) \Sigma_{\rm v}(\boldsymbol{r}_1, \boldsymbol{r}). \tag{5.23}$$

Here the nonrelativistic scalar and vector potentials have the same forms as the relativistic expressions (2.3) and (2.4) with $\rho_{\rm s}(r) = \rho_{\rm v}(r) = \sum_{\rm occ} \psi_i^{+}(r) \psi_i(r)$, and $\Sigma_{\rm v}(\boldsymbol{r}, \boldsymbol{r}')$ is defined by

$$\Sigma_{\rm v}(r) = \int {\rm d}^3 r' \, \Sigma_{\rm v}(\boldsymbol{r}, \boldsymbol{r}').$$

Let us first discuss the σ meson contribution (5.22). We see that the resulting nonrelativistic impulse current

$$\boldsymbol{j}_{\rm I}^{\rm (NR)}(r) = \boldsymbol{j}_{\rm f}^{\rm (NR)}(r) + \boldsymbol{j}_{\sigma}^{\rm (NR)}(r) = \left(1 - \frac{\Sigma_{\rm s}}{M}\right) \boldsymbol{j}_{\rm f}(r) + \frac{1}{4M^2} \left(\psi^{+} \boldsymbol{\sigma} \psi\right) \times \boldsymbol{\nabla} \Sigma_{\rm s} \tag{5.24}$$

disagrees with the lowest order term of the relativistic impulse current (5.5) due to the last term in (5.24). One can, however, easily show that the last term ($\delta \boldsymbol{j}$) in (5.24) does not destroy current conservation, i.e., $\boldsymbol{\nabla} \cdot \delta \boldsymbol{j} = 0$ for diagonal matrix elements. The magnetic moment due to $\boldsymbol{j}_{\rm I}^{\rm (NR)}$ becomes

$$\begin{aligned} \boldsymbol{m}_{\rm I}^{\rm (NR)} &= M \int {\rm d}^3 r \, \boldsymbol{r} \times \boldsymbol{j}_{\rm I}^{\rm (NR)}(r) \\ &= \frac{1}{2} \int {\rm d}^3 r \left(1 - \frac{\Sigma_{\rm s}(r)}{M}\right) \psi^{+}(r) \left(\boldsymbol{L} + \boldsymbol{\sigma}\right) \psi(r) \end{aligned} \tag{5.25}$$

Comparing eqs. (5.5) and (5.24) for the currents and eqs. (5.7) and (5.25) for the magnetic moments, we see that in the relativistic approach it is the *current* while in the nonrelativistic exchange current approach it is the *magnetic moment* which shows the M/M^* enhancement. Thus, except for higher order terms in the perturbation expansion, the σ meson contributions in the exchange current approach give a M/M^* enhancement of the magnetic moment, which is less (more) enhancement for hole states (particle states) than in the relativistic approach.

The ω meson contribution (5.23), on the other hand, corresponds directly to the first term on the right hand side of our vertex correction (3.8). It can be obtained from the expression for $\Pi^{\mu\nu}_{(\omega\gamma){\rm D}}$ (eq. (A.1)) by replacing the full propagator S of eq. (A.1) by the negative frequency part of the Feynman propagator in free space and retaining only terms of lowest order in $1/M$.

From the above discussion we conclude that while the ω meson contributions are basically equivalent in the relativistic calculation and the nonrelativistic exchange current approach, differences occur for the σ meson.

In nuclear matter $j_\sigma^{(\mathrm{NR})}$ can be considered to arise from the admixture of free negative energy solutions into the wave function of the valence nucleon due to the interaction with the nucleons in the core [2,1], i.e., in lowest order perturbation theory the solution to the Dirac equation can be written in the form $f(p) = u(p) + S_-(p)\Sigma_s(p)u(p)$ with $u(p)$ the free solution. The differences mentioned above are due to the fact that in a finite system it is strictly speaking not possible to express the solution to the Dirac equation in an analogous form.

6 Summary and Conclusion

In this work we attempted a theoretically consistent description of magnetic properties of nuclei with an LS closed core plus or minus one nucleon in the framework of a relativistic field theoretical model. The model, where nucleons interact via the exchange of scalar and vector mesons, was treated in the Hartree approximation.

As a first step, we used the mean field approximation to the explicitly density-dependent part of the polarization insertions in the RPA type vertex correction so as to account fully for the finite geometry of the system. At this stage the calculation is consistent with the mean field approximation applied to the Hartree calculation of nuclear wave functions. The RPA type vertex correction was found to play an essential role in reducing the isoscalar magnetic moments to reasonable values. For the magnetic form factors of actual nuclei the effect of the vertex correction is less well pronounced, since first it does not affect the isovector part of the current, and second its magnitude decreases as we move away from the photon point and even changes its sign at $q \simeq 1$ fm^{-1} for the cases considered here. As a result, the magnetic form factors of ^{15}N, ^{17}O and ^{39}K around their maxima are practically unaffected by the vertex corrections and therefore are still enhanced considerably in comparison to the nonrelativistic result. In section 5 we discussed in detail how the large differences between the relativistic and the nonrelativistic impulse approximation results can be understood from the average value and the radial dependence of the effective mass. There we also compared the relativistic mean field calculation with

the nonrelativistic exchange current approach and pointed out that, while the two approaches agree in nuclear matter in lowest order perturbation theory, differences occur in finite systems.

We then continued to include the effects of the vacuum fluctuations by using a local density approximation. We pointed out that the vacuum fluctuations change the results based on the mean field approximation in three respects: First, the single particle potentials and accordingly the single particle wave functions are changed due to an additional term in the scalar density which describes the antinucleon contribution in the loop of fig. 1. After readjusting the parameters of the model in order to reproduce the nuclear matter saturation point, the single particle potentials are found to be much weaker than in the mean field approximation. Second, the isoscalar Dirac part of the single nucleon form factor (F_{1s}) calculated in the ring approximation becomes reduced in the nuclear medium (see fig. 12), which in particular leads to an enhancement of the "isoscalar nucleon charge radius" inside the nucleus. To calculate this modified single nucleon form factor, we followed the vector meson dominance principle and included a direct $\omega\gamma$ coupling term in the lagrangian. Note that our present definition of the "single nucleon form factor inside the nucleus" includes only the effects of vacuum fluctuations; the other contributions, which come from the "density parts" of the polarization operators, are already included in the mean field calculation. Since there is no definite or natural definition of the nucleon radius in nuclei, we by no means claim that our results of the enhancement of the isoscalar nucleon charge radius stated above can be considered to be valid in other contexts. (We believe our definition is

quite natural in the context of our discussion, though.) Third, the ω meson propagator used in the calculation of the RPA type vertex correction is modified by vacuum polarizations, leading to a depression of the propagator at distances $r \lesssim 1$ fm and to an enhancement for larger distances according to the reduced effective mass of the ω meson in the medium (see fig. 14). We found that these vacuum fluctuation effects have only little influence on the isoscalar magnetic moments, since those are determined roughly speaking by the binding energy per nucleon. The overall corrections we found were about 3 % for the hole states ($A = 15$ and $A = 39$) and less for the particle states. The magnetic form factors, however, were found to be considerably quenched, see figs. 18, 19 and 20. We pointed out that most of this reduction is simply a consequence of the larger nucleon effective mass. The effect of the reduced isoscalar single nucleon form factor works in the same direction for $A = 15$ and $A = 39$, but finally leads to no significant corrections to the form factors of ^{15}N, ^{17}O and ^{39}K which include also the isovector contributions. Even less contribution comes from the modification of the ω meson propagator used in the calculation of the vertex correction.

We emphasize again that the present investigation should be considered merely as a first step in the description of nuclear magnetic properties in the framework of a relativistic field theory. The results show how far one can account for magnetic moments and form factors of nuclei with an LS closed core plus or minus one nucleon in the Hartree approximation. The present description is still too simple-minded to allow a meaningful comparison with experiment. For this, one should at least include the Fock terms both in the single particle potentials and in the electromagnetic vertex in

a manner consistent with gauge invariance. Furthermore, higher order corrections like the second order core polarization, which is known to be very important from nonrelativistic studies, should also be included in relativistic descriptions. Within a renormalizable model the divergences associated with these higher order corrections can be handled in a well defined way. One advantage of using relativistic models is that it is in principle possible to achieve consistency between the single particle potential and the electromagnetic vertex in the sense that one employs the same meson exchange mechanisms to account for both. This guarantees that the calculation is consistent with gauge invariance. We regard this fact as one of the most important motivations to pursue and extend the study of nuclear magnetic properties in models based on relativistic field theory.

Appendices

A Explicit formulae for the calculation of magnetic moments and magnetic form factors

In this appendix we show explicit formulae to calculate the RPA type vertex correction in the mean field approximation. We start from eqs. (3.5) to (3.11) of the main part. The explicitly density-dependent part of the $\omega\gamma$ polarization operator has the following form (see eq. (3.15))

$$\begin{aligned} \Pi^{\mu\nu}_{(\omega\gamma)\mathrm{D}}(\boldsymbol{x},\boldsymbol{z}) &= i\sum_{\mathrm{h}}\{\overline{u}_{\mathrm{h}}(\boldsymbol{x})\,(-ig_\omega\gamma^\mu)\,S(\boldsymbol{x},\boldsymbol{z},q_0+\varepsilon_{\mathrm{h}})\Gamma^\nu_0(\boldsymbol{z})u_{\mathrm{h}}(\boldsymbol{z}) \\ &+ [\overline{u}_{\mathrm{h}}(\boldsymbol{x})\,(-ig_\omega\gamma^\mu)\,S(\boldsymbol{x},\boldsymbol{z},-q_0+\varepsilon_{\mathrm{h}})\Gamma^\nu_0(\boldsymbol{z})u_{\mathrm{h}}(\boldsymbol{z})]^*\}, \end{aligned} \tag{A.1}$$

where the spinors $u_{\mathrm{h}}(\boldsymbol{x})$ for the occupied positive energy states h satisfy the Dirac equation (2.2) with eigenvalues ε_{h}, and the Hartree propagator S is a solution to

$$(\varepsilon + i\boldsymbol{\alpha}\cdot\boldsymbol{\nabla}_x - \beta(M+\Sigma_{\mathrm{s}}) - \Sigma_{\mathrm{v}})\,S(\boldsymbol{x},\boldsymbol{z},\varepsilon) = \beta\delta^{(3)}(\boldsymbol{x}-\boldsymbol{z}) \tag{A.2}$$

with the continuous energy variable ε. The $\omega\omega$ polarization operator $\Pi^{\mu}_{(\omega\omega)\mathrm{D}}$ is obtained from eq. (A.1) by replacing the free electromagnetic vertex $\Gamma^\nu_0(z)$ (see eq. (3.7)) by $(-ig_\omega\gamma^\nu)$. By using (2.2) and (A.2) one easily verifies that

$$q_0\Pi^{0\nu}_{(\omega\gamma)\mathrm{D}}(\boldsymbol{x},\boldsymbol{z}) + i\nabla_{xi}\Pi^{i\nu}_{(\omega\gamma)\mathrm{D}}(\boldsymbol{x},\boldsymbol{z}) = 0, \tag{A.3}$$

and similar for $\Pi^{\mu\nu}_{(\omega\omega)\mathrm{D}}$. From this equation it follows that the terms proportional to $q^\mu q^\nu$ in the ω meson propagator $\Delta^{\mu\nu}_0$ do not contribute in

eqs. (3.10) and (3.11), as is verified by performing a partial integration. Therefore in the actual calculation we can replace $\Delta_0^{\mu\nu}(\boldsymbol{x}) \rightarrow g^{\mu\nu}\Delta_0(\boldsymbol{x})$ with the Yukawa function $\Delta_0(\boldsymbol{x})$ given in eq. (A.9) below. For the same reason we can drop the second term in the ω meson propagator (3.22) when the vacuum fluctuations are included. Also, the terms proportional to $q^\mu \not{q}$ in the vertex (3.48) do not contribute when used in the calculation of the $\omega\gamma$ polarization operator (A.1). The Hartree propagator S can be expressed by using the regular ($\psi_{\kappa\mu}$) and irregular ($\psi^{(+)}_{\kappa\mu}$) solutions of the Dirac equation as follows:

$$\begin{aligned} S(\boldsymbol{x},\boldsymbol{z},\varepsilon) &= -(\theta(x-z)\sum_{\kappa\mu}\frac{1}{W_\kappa(\varepsilon)}\psi^{(+)}_{\kappa\mu}(\boldsymbol{x},\varepsilon)\overline{\psi}_{\kappa\mu}(\boldsymbol{z},\varepsilon) \\ &\quad + \theta(z-x)\sum_{\kappa\mu}\frac{1}{W_\kappa(\varepsilon)}\psi_{\kappa\mu}(\boldsymbol{x},\varepsilon)\overline{\psi}^{(+)}_{\kappa\mu}(\boldsymbol{z},\varepsilon)). \end{aligned} \tag{A.4}$$

The solutions ψ and $\psi^{(+)}$ can be written in the form (2.7) with the radial functions $f_\kappa(r,\varepsilon)$, $g_\kappa(r,\varepsilon)$ and $f^{(+)}_\kappa(r,\varepsilon)$, $g^{(+)}_\kappa(r,\varepsilon)$. The wronskian W_κ is given by

$$W_\kappa(\varepsilon) = r^2\left(f^{(+)}_\kappa(r,\varepsilon)g_\kappa(r,\varepsilon) - g^{(+)}_\kappa(r,\varepsilon)f_\kappa(r,\varepsilon)\right) \tag{A.5}$$

independent of r. By writing the propagator in the form (A.2) it is possible to treat the positive and negative energy continuum states exactly.

Magnetic moments or elastic magnetic form factors with multipolarity J are obtained from the matrix element

$$< \lambda\mu|T^J_{\mu_J}(q)|\lambda\mu >= \int \mathrm{d}^3x\, \boldsymbol{j}_{\lambda\mu,\lambda\mu}(\boldsymbol{x})\cdot \boldsymbol{Y}^{JJ1}_{\mu_J}(\hat{x})j_J(qx), \tag{A.6}$$

where the current of the valence nucleon is given by (3.5), and the single particle state is characterized by $\lambda = (n,\kappa)$ with corresponding angular

momentum $j = |\kappa| - \frac{1}{2}$, and the magnetic quantum number μ. In the following we give formulae for the reduced matrix element

$$M^J(q) =< \lambda||T^J(q)||\lambda >\equiv M_{\rm I}^J(q) + \delta M^J(q). \tag{A.7}$$

The contribution due to the impulse approximation is

$$M_{\rm I}^J(q) = \sqrt{\frac{(j+1)(2j+1)}{j}}\frac{iq}{2M\sqrt{6\pi}}\left(\mu_{\rm ID}^J(q) + \mu_{\rm IA}^J(q)\right). \tag{A.8a}$$

with

$$\mu_{\rm ID}^J(q) = \frac{4M}{q}C_j^J\varpi(2J+1)e\int_0^\infty r^2{\rm d}r\, F\cdot G j_J(qr), \tag{A.8b}$$

and $\mu_{\rm IA}^J(q)$ given by (5.15). The factor C_j^J is given below eq. (5.15), and $\varpi = -1$ $(+1)$ for $j = \ell + \frac{1}{2}$ $(\ell - \frac{1}{2})$. Using the relations

$$r^2F\cdot G = \frac{[r^2(F^2+G^2)]'}{4M^*} - \frac{\kappa r}{2M^*}(F^2-G^2),\ \kappa = -\frac{\varpi}{2}(2j+1),$$

one can show that the Dirac part (A.8a) is equivalent to the first two terms on the right hand side of eq. (5.13) in the main text. In order to calculate the contribution of the vertex correction $(\delta M^J(q))$, one expresses the ω meson propagator $g^{\mu\nu}\Delta(\boldsymbol{x})$ in terms of combinations of the spherical Bessel and Hankel functions in the usual way:

$$\begin{aligned}\Delta(\boldsymbol{x}-\boldsymbol{x}') &= \frac{1}{4\pi}\frac{e^{-m_\omega|\boldsymbol{x}-\boldsymbol{x}'|}}{|\boldsymbol{x}-\boldsymbol{x}'|}\\ &= im_\omega\sum_{\ell m} j_\ell(im_\omega x_<)h_\ell^{(+)}(im_\omega x_>)Y_m^{\ell *}(\hat{x})Y_m^\ell(\hat{x}').\end{aligned} \tag{A.9}$$

The nucleon propagator has already been expanded in eq. (A.4). The actual calculation is considerably simplified due to the fact that only the space components of the ω meson propagator with multipolarity J contribute.

In other words, the intermediate states containing one ω meson in fig. 4 have all the same multipolarity J. In this way we obtain the following contribution due to the vertex correction $\tilde{\Lambda}$ of eq. (3.8):

$$\delta M^J(q) = \int_0^\infty y^2 \mathrm{d}y \int_0^\infty z^2 \mathrm{d}z \, \tilde{\Lambda}^J(y,z) j_J(qz), \tag{A.10}$$

where

$$\begin{aligned} \tilde{\Lambda}^J(y,z) &= -ig_\omega < \overline{u}_\lambda(\boldsymbol{y}) || \left[Y^J(\hat{y}) \times \gamma^{(1)} \right]^J || u_\lambda(\boldsymbol{y}) > \\ &\times \left(\Lambda^J(y,z) + \int_0^\infty x^2 \mathrm{d}x \, \tilde{\Pi}^J(y,x) \Lambda^J(x,z) \right), \end{aligned} \tag{A.11}$$

$$\tilde{\Pi}^J(y,x) = \Pi^J(y,x) + \int_0^\infty z^2 \mathrm{d}z \, \Pi^J(y,z) \tilde{\Pi}^J(z,x), \tag{A.12}$$

$$\begin{aligned} \Lambda^J(y,z) &= 2m_\omega g_\omega \delta_{LJ} \sum_{\mathrm{h}} \sum_{\alpha} \int_0^\infty y'^2 \mathrm{d}y' \, j_L(im_\omega y_<) h_L^{(+)}(im_\omega y_>) \\ &\times \frac{1}{2J+1} (-1)^{j_\mathrm{h} - j_\alpha + L - J} \mathrm{Re}[-\frac{\theta(y'-x)}{W_\alpha} < \overline{u}_\mathrm{h}(\boldsymbol{y}') || \left[Y^L \times \gamma^{(1)} \right]^J || \psi_\alpha^{(+)}(\boldsymbol{y}') > \\ &\times < \overline{\psi}_\alpha(\boldsymbol{z}) || \left[Y^L \times \Gamma_0^{(1)} \right]^J || u_\mathrm{h}(\boldsymbol{z}) > \\ &\times -\frac{\theta(x-y')}{W_\alpha} < \overline{u}_\mathrm{h}(\boldsymbol{y}') || \left[Y^L \times \gamma^{(1)} \right]^J || \psi_\alpha(\boldsymbol{y}') > \\ &\times < \overline{\psi}_\alpha^{(+)}(\boldsymbol{z}) || \left[Y^L \times \Gamma_0^{(1)} \right]^J || u_\mathrm{h}(\boldsymbol{z}) >] \end{aligned} \tag{A.13}$$

and Π^J is given by replacing the free electromagnetic vertex $\Gamma_0^{(1)}$ by $-ig_\omega \gamma^{(1)}$ in eq. (A.13). In eq. (A.13), for every fixed occupied positive-energy state h the sum over α runs over all states allowed by angular momentum conservation[4]. $y_<$ ($y_>$) means the smaller (larger) of the variables y, y'. The reduced matrix elements in eq. (A.13) are easily evaluated by first expressing them in

[4]Performing the sum over the isospin quantum numbers means simply to replace $\Gamma_0^{(1)}$ by its isoscalar part and to multiply a factor 2.

two-dimensional Pauli spinor space and them applying the standard composition formulae for reduced matrix elements. Π^J and Λ^J defined above are the building blocks of the RPA calculation. The Dyson equation (A.12) is solved by matrix inversion, discretizing the coordinate variables into 15 Gauss points. From $\tilde{\Pi}^J$ we obtain $\tilde{\Lambda}^J$ and δM^J from eqs. (A.11) and (A.10).

We employ the single nucleon form factors of ref. [39]. For this we first split up M^J into the Dirac and anomalous parts, and M_I^J further into the isoscalar and isovector parts, and then multiply the single nucleon form factors $F_{1\mathrm{s}}$, $F_{1\mathrm{v}}$, $F_{2\mathrm{s}}$ or $F_{2\mathrm{v}}$ separately. Using the "bare bone" form factor M^J thus obtained we calculate the nuclear form factor F^J by the following formula:

$$|F^{(J)}(q)|^2 = |M^J(q)|^2 \exp\left(\frac{b^2}{2A}q^2\right)\frac{4\pi}{Z^2}\frac{1}{2j+1} \tag{A.14}$$

where the exponential factor is the conventional center of mass correction with b the b-parameter of the harmonic oscillator shell model. Summing finally over all values of J allowed by angular momentum conservation, the transverse form factor $|F_\mathrm{T}(q)|^2$ is obtained. The magnetic moment is related to $M^{J=1}$ by

$$\mu = 2M \cdot \sqrt{6\pi}\sqrt{\frac{j}{(j+1)(2j+1)}}\lim_{q\to 0}\frac{1}{iq}M^1(q). \tag{A.15}$$

B Conservation of the baryon current

In this appendix we present the proof of eq. (3.29) making use of the Ward-Takahashi identities for ωNN vertices which follow from baryon current conservation. For definiteness we refer to the lagrangian (2.1) (or (3.19) after renormalization). The discussion applies for nuclear matter.

Consider first the identities for unrenormalized quantities (denoted by a subscript (0)). We define, as usual, the ωNN Green's function $\Gamma^{\mu}_{\omega(0)}$ with amputated nucleon legs by

$$\begin{aligned} &< 0|\mathrm{T}\left(\psi_{(0)}(x)\overline{\psi}_{(0)}(x')\omega^{\mu}_{(0)}(y)\right)|0> \\ &= \int \mathrm{d}^4u \int \mathrm{d}^4u' S_{(0)}(x'-u)\Gamma^{\mu}_{\omega(0)}(u'-y,u-y)S_{(0)}(u-x). \end{aligned} \quad \text{(B.1)}$$

Here S is the nucleon propagator. Operating on (B.1) with $\partial/\partial y^{\mu}$ and using the definition of the T-product we encounter equal time commutators of the form $[\omega^0_{(0)}(x), \psi_{(0)}(x')]$, which can be evaluated as follows: From the equation of motion derived from the lagrangian (2.1) with unrenormalized quantities we have

$$\omega^0_{(0)} = \frac{1}{m^2_{\omega 0}}\left(g_{\omega 0} j^0_{\mathrm{B}} - \partial_i G^{i0}_{(0)}\right) \quad \text{(B.2)}$$

with the baryon current

$$j^{\mu}_{\mathrm{B}} = \overline{\psi}_{(0)}\gamma^{\mu}\psi_{(0)}. \quad \text{(B.3)}$$

The physical degrees of freedom are the fields ω^i and ψ with their conjugate momenta $E^i = G^{i0}$ and ψ^+. Therefore E^i commutes with the nucleon field, and we obtain from (B.2)

$$[\omega^0_{(0)}(x), \psi_{(0)}(x')] = -\frac{g_{\omega 0}}{m^2_{\omega 0}}\psi_{(0)}(x)\delta^{(3)}(\boldsymbol{x}-\boldsymbol{x}')$$

at equal times. Using further the transversality condition $\partial_{\mu}\omega^{\mu}_{(0)} = 0$ which follows from baryon current conservation, we arrive at the Ward-Takahashi identity in momentum space

$$q_{\mu}\Gamma^{\mu}_{\omega(0)}(p',p) = \frac{g_{\omega 0}}{m^2_{\omega 0}}\left(S^{-1}_{(0)}(p') - S^{-1}_{(0)}(p)\right). \quad \text{(B.4)}$$

Here $q = p' - p$. Renormalizing the fields and the propagator $S_{(0)}$ in eq. (B.1) by applying eq. (3.18), and defining the renormalized Green's function Γ^{μ}_{ω} by an equation similar to (B.1) without the subscripts (0), we obtain

$$\Gamma^{\mu}_{\omega(0)} = \frac{\sqrt{Z_\omega}}{Z_{\rm N}} \Gamma^{\mu}_{\omega}.$$

Therefore, eq. (B.4) reads in terms of renormalized quantities

$$q_\mu \Gamma^{\mu}_{\omega}(p', p) = \frac{Z_g}{Z_{\rm N}} \frac{g_\omega}{m_\omega^2 + \delta m_\omega^2} \left(S^{-1}(p') - S^{-1}(p) \right). \tag{B.5}$$

Using eq. (3.50) we then obtain the identity for the ωNN source vertex

$$q_\mu \Gamma^{\mu}_{\omega {\rm S}}(p', p) = -i g_\omega \frac{Z_g}{Z_{\rm N}(1 + \delta m_\omega^2 / m_\omega^2)} \left(S^{-1}(p') - S^{-1}(p) \right). \tag{B.6}$$

The differential form of this identity in free space and the renormalization prescription (3.27) then gives the relation (3.29) between the renormalization constants:

$$Z_g = Z_{\rm N} \left(1 + \frac{\delta m_\omega^2}{m_\omega^2} \right). \tag{B.7}$$

(Note that in the Hartree model $Z_{\rm N} = 1$ and $S^{-1}(p') - S^{-1}(p) = \not{q}$.)

References

[1] A. Arima, K. Shimizu, W. Bentz, and H. Hyuga. Adv. in Nucl. Phys., 18, 1, (1987).

[2] S. Ichii. *Isoscalar currents and nuclear magnetic moments.* Master's thesis, University of Tokyo, January 1986.

[3] S. Ichii, W. Bentz, and A. Arima. Nucl. Phys., A464, 575, (1987).

[4] D. O. Riska. Physica Scripta, 31, 107, (1985).

[5] B. J. Serot and J. D. Walecka. Adv. in Nucl. Phys., 16, 1, (1986).

[6] K. Holinde. Phys. Rep., 68, 121, (1981).

[7] R. Machleidt, K. Holinde, and Ch. Elster. Phys. Rep., 149, 1, (1987).

[8] L. S. Celenza and C. M. Shakin. *Relativistic Nuclear Physics.* World Scientific, Singapore, (1986).

[9] R. Brockmann and R. Machleidt. Phys. Lett. B, 149, 283, (1984).

[10] H. Müther, R. Machleidt, and R. Brockmann. Phys. Lett. B, 202, 483, (1988).

[11] J. C. Ward. Phys. Rev., 78, 1824, (1950).

[12] Y. Takahashi. Nuovo Cimento, 6, 370, (1957).

[13] L. D. Miller. Ann. Phys. (N. Y.), 91, 40, (1975).

[14] A. Bouyssy, S. Marcos, and J. F. Mathiot. Nucl. Phys., A415, 497, (1984).

[15] M. Bawin, C. Hughes, and G. Strobel. Phys. Rev. C, 28, 456, (1983).

[16] S. Ichii, W. Bentz, A. Arima, and T. Suzuki. Phys. Lett. B, 192, 11, (1987).

[17] J. A. McNeil, R. D. Amado, C. J. Horowitz, and M. Oka. Phys. Rev. C, 34, 746, (1986).

[18] J. R. Shepard, E. Rost, C.-Y. Cheng, and J. A. McNeil. Phys. Rev. C, 37, 1130, (1988).

[19] R. J. Furnstahl. Phys. Rev. C, 38, 370, (1988).

[20] S. A. Chin. Ann. Phys. (N. Y.), 108, 301, (1977).

[21] C. J. Horowitz and B. D. Serot. Phys. Lett. B, 140, 181, (1984).

[22] J. D. Bjorken and S. D. Drell. *Relativistic Quantum Fields.* McGraw-Hill, New York, (1965).

[23] J. D. Walecka. Ann. Phys. (N. Y.), 83, 491, (1974).

[24] C. J. Horowitz and Brian D. Serot. Nucl. Phys., A368, 503, (1981).

[25] R. J. Perry. Phys. Lett. B, 182, 269, (1986).

[26] R. J. Perry. Nucl. Phys., A467, 717, (1987).

[27] J. Boguta. Phys. Lett. B, 106, 250, (1981).

[28] G. E. Brown, W. Weise, G. Baym, and J. Speth. Comments on Nucl. Part. Phys., 17, 39, (1987).

[29] W. Bentz, A. Arima, H. Hyuga, K. Shimizu, and K. Yazaki. Nucl. Phys., A436, 593, (1985).

[30] A. B. Migdal. *Theory of finite Fermi systems and applications to atomic nuclei.* Wiley, New York, (1967).

[31] A. Arima, W. Bentz, and S. Ichii. In K. Takahashi *et al.*, eds., *Rationale of Beings*, p. 205, World Scientific, Singapore, (1986).

[32] S. Nishizaki, H. Kurasawa, and T. Suzuki. Phys. Lett. B, 171, 1, (1986).

[33] P. Ramond. *Field Theory: A Modern Primer.* Benjamin/Cummings, Reading, (1981).

[34] S. Ichii, W. Bentz, A. Arima, and T. Suzuki. Nucl. Phys., A487, 493, (1988).

[35] N. M. Kroll, T. D. Lee, and B. Zumino. Phys. Rev., 157, 1376, (1967).

[36] J. J. Sakurai. *Currents and Mesons.* The University of Chicago Press, Chicago, (1969).

[37] N. N. Bogoliubov and D. V. Shirkov. *Introduction to the Theory of Quantized Fields.* John Wiley & Sons, New York, (1959).

[38] F. Iachello, A. D. Jackson, and A. Lande. Phys. Lett. B, 43, 191, (1973).

[39] M. Gari and W. Krümpelmann. Z. Phys. A, 322, 689, (1985).

[40] R. J. Furnstahl and B. D. Serot. Nucl. Phys., A468, 539, (1987).

[41] T. Suzuki, H. Hyuga, A. Arima, and K. Yazaki. Nucl. Phys., A358, 421c, (1981).

[42] A. Arima, Y. Horikawa, H. Hyuga, and T. Suzuki. Phys. Rev. Lett., 40, 1001, (1978).

[43] A. Arima, Y. Horikawa, H. Hyuga, and T. Suzuki. Phys. Rev. Lett., 42, 1186, (1979).

[44] T. Suzuki. Phys. Lett. B, 120, 27, (1983).

[45] P. G. Blunden and B. Castel. Nucl. Phys., A445, 742, (1985).

[46] H. Kurasawa and T. Suzuki. Nucl. Phys., A445, 685, (1985).

[47] S. Nishizaki, H. Kurasawa, and T. Suzuki. Phys. Lett. B, 209, 6, (1988).

[48] R. P. Singhal *et al.*. Phys. Rev. C, 28, 513, (1983).

[49] M. V. Hynes *et al.*. Phys. Rev. Lett., 42, 1444, (1979).

[50] L. Lapikás. In *Lecture Notes in Physics, vol. 108*, Springer, Berlin, (1979).

Table captions

1. Miller's calculation of magnetic moments in the relativistic approach. Taken from ref.[13].

2. Various parameters. For explanation, see text.

3. Magnetic moments obtained in the mean field approximation.

4. Nuclear isoscalar charge radius as determined from eqs. (4.4) and (4.3), and the pole position of the ω meson propagator (3.59).

5. Magnetic moments including the effects of vacuum fluctuations. The values in parenthesis show the results when the vacuum fluctuation effects are included only in the single particle wave functions.

6. Isoscalar Dirac parts of the magnetic moments in the mean field approximation in comparison with the expectation values of $M/M^*(r)$ and $M/\varepsilon(r)$ between single particle states ($\varepsilon(r) = M^*(r) + \Sigma_v(r)$. For explanation, see text.

7. Same as table 6 when the vacuum fluctuations are taken into account.

Figure captions

1. Self-energy of a nucleon in the Hartree approximation.
   The dashed line represents the exchanged meson (σ or ω). All states below the Fermi surface (positive and negative energy) are counted

in the loop. In the mean field approximation, however, only positive energy occupied states are retained.

2. Scalar density of ^{16}O calculated using the wave functions obtained by the self-consistent calculations.
   The dashed line is the result in the mean field approximation, and the full line is that includes the vacuum fluctuation effects. For the latter, the valence nucleon contribution ((2.5)) and that from the vacuum fluctuation ((2.8)) in the local density approximation are displayed separately (dot-dashed line for the former, and the dotted for the latter with the sign changed).

3. Vector density of ^{16}O calculated using the wave functions obtained by the self-consistent calculations.
   The dashed line and the solid line are the result in the mean field approximation and the result of the calculation including the vacuum fluctuation effects. The difference comes only from the change in the wave functions.

4. Graphical representation of the RPA type vertex correction eq. (3.8). Symbols for the polarization insertions are defined in figs. 5 and 6. The dashed line represents the free ω meson propagator in lowest order ($\Delta_0^{\mu\nu}$).

5. $\omega\omega$-polarization operator $\Pi^{\mu\nu}_{(\omega\omega)}$.
   It is splitted up into two parts as in eq. (3.12). For explanation, see text.

6. $\omega\gamma$-polarization operator $\Pi^{\mu\nu}_{(\omega\gamma)}$.
   It is splitted up into two parts as in eq. (3.16).

7. Graphical representation of the ω meson propagator eq. (3.22) including the Feynman part (F) of the polarization operator.
   This propagator will replace the lowest order one (dashed lines) in the vertex correction fig. 4 of the mean field model.

8. Electromagnetic vertex of a nucleon including the Feynman parts (F) of the polarization operator (see eq. (3.48)).
   This vertex will replace the bare γNN vertices at point z in fig. 4 and in the impulse approximation.

9. Magnetic form factor of ^{15}N in the mean field approximation.
   The dashed-dotted curve is the result of the relativistic impulse approximation, while the full curve includes the RPA type vertex corrections. For comparison we also show the result of the nonrelativistic impulse approximation using harmonic oscillator wave functions (dotted line). The experimental data are taken from ref. [48].

10. Magnetic form factor of ^{17}O in the mean field approximation.
    For explanation of the curves, see the caption to fig. 9. The experimental data are taken from ref. [49].

11. Magnetic form factor of ^{39}K in the mean field approximation.
    For explanation of the curves, see the caption to fig. 9. The experimental data are taken from ref. [50].

12. Isoscalar Dirac part of the single nucleon form factor (F_{1s}).
    The full line gives the form factor (3.60) for zero density, while the results of refs [39] and [38] are shown by the dashed and the dotted lines, respectively. (The dotted line refers to the fit with $\beta_\varphi = 0.112$ in table 1 of ref. [38].) The dashed-dotted and dashed-doubledotted lines show the form factor (3.60) for $A = 17$ and $A = 15$, respectively.

13. The dashed and dashed-dotted lines show the last factor in eq. (4.1) for zero density and for $A = 15$, respectively, while their ratio is shown by the full line.
    The full line represents the quenching factor of the isoscalar Dirac part of the single nucleon form factor.

14. The ω meson exchange potential as determined by a Fourier transformation of eq. (3.59) for $q_0 = 0$.
    The results for zero density, $A = 15$ and $A = 17$ are given by the dashed-dotted, the dotted and the dashed lines, respectively. The full line shows Yukawa form.

15. Magnetic form factor of ^{15}N including vacuum fluctuation effects.
    The dashed-dotted curve is the impulse approximation. The solid curve includes the RPA type vertex corrections. The dotted curve is the nonrelativistic impulse approximation using harmonic oscillator wave functions.

16. Magnetic form factor of ^{17}O including vacuum fluctuation effects.

Legends are the same as of fig. 15.

17. Magnetic form factor of ^{39}K including vacuum fluctuation effects.
    Legends are the same as of fig. 15.

18. Comparison of the magnetic form factors of ^{15}N obtained in the mean field approximation (dashed line) and including vacuum fluctuation effects (solid line).
    The dashed-dotted line shows the results of a calculation where the vacuum fluctuation effects are included only in single particle wave functions. The dotted line is the nonrelativistic impulse approximation.

19. Same as fig. 18 for ^{17}O

20. Same as fig. 18 for ^{39}K

21. Various contributions to the magnetic form factor of ^{15}N in the impulse approximation based on eqs. (5.13).
    The dotted line shows the result obtained by setting $M^* = M$ and neglecting the terms proportional to G^2 in eqs. (5.13), (5.14) and (5.15). When the factor M/M^* in eq. (5.14) is included, one obtains the dashed-dotted line. The dashed line shows the results when the terms proportional to G^2 are included. The total form factor in the impulse approximation is given by the full line.

Table 1

	^{15}N			^{15}O		
	Dirac	Anomalous	Sum	Dirac	Anomalous	Sum
Calc.	0.716	-0.623	0.093	0	0.665	0.665
Schmidt	0.333	-0.598	-0.265	0	0.637	0.637
Exp.			-0.28			0.72

Table 2

	MF	VF
$g_\sigma^2/4\pi$	8.72	4.32
$g_\omega^2/4\pi$	15.15	8.18
m_σ [MeV]	520	458
m_ω [MeV]	783	783
M [MeV]	939	939
reference	[24]	[21]

Table 3

A	15	17	39	41
1. Isoscalar				
Impulse				
(Dirac)	0.3308	1.6430	0.9939	2.3379
(Anomalous)	0.0209	-0.0597	0.0367	-0.0597
(Sum)	0.3517	1.5833	1.0306	2.2782
RPA type vertex correction				
(Dirac)	-0.1457	-0.1466	-0.3888	-0.3458
(Anomalous)	0.0001	-0.0001	0.0003	0.0000
(Sum)	-0.1456	-0.1467	-0.3885	-0.3458
Impulse + RPA type vertex correction				
(Dirac)	0.1851	1.4964	0.6051	1.9921
(Anomalous)	0.0210	-0.0598	0.0370	-0.0597
(Sum)	0.2061	1.4366	0.6421	1.9324
Schmidt values				
(Dirac)	0.1667	1.5	0.6	2.0
(Anomalous)	0.0200	-0.0600	0.0360	-0.0600
(Sum)	0.1867	1.4400	0.6360	1.9400
Experiment				
	0.2179	1.4141	0.7066	1.9206
2. Isovector				
Impulse				
(Dirac)	0.3308	1.6430	0.9939	2.3379
(Anomalous)	-0.6444	1.8407	-1.1316	1.8407
(Sum)	-0.3136	3.4837	-0.1377	4.1786
Schmidt values				
(Dirac)	0.1667	1.5	0.6	2.0
(Anomalous)	-0.6167	1.8500	-1.1100	1.8500
(Sum)	-0.4500	3.3500	-0.5100	3.8500
Experiment				
	-0.5000	3.3065	-0.3142	3.5073

Table 4

A	free	15	17	39	41
$\sqrt{< r^2 >_s}$ (fm)	0.74	0.88	0.82	0.90	0.86
m^*_ω (MeV)	666.9	534.7	576.7	519.4	546.0

Table 5

A	15	17	39	41
1. Isoscalar				
Impulse				
(Dirac)	0.2410	1.5639	0.7834	2.1630
(Anomalous)	0.0206	-0.0598	0.0364	-0.0598
(Sum)	0.2610	1.5041	0.8198	2.1032
RPA type vertex correction				
(Dirac)	-0.0625	-0.0618	-0.1559	-0.1392
	(-0.0643)	(-0.0660)	(-0.1671)	(-0.1570)
(Anomalous)	0.0001	0.0000	0.0002	0.0001
	(0.0001)	(-0.0000)	(0.0002)	(0.0000)
(Sum)	-0.0624	-0.0618	-0.1556	-0.1391
	(-0.0642)	(-0.0660)	(-0.1669)	(-0.1570)
Impulse + RPA type vertex correction				
(Dirac)	0.1785	1.5021	0.6275	2.0238
	(0.1767)	(1.4979)	(0.6163)	(2.0060)
(Anomalous)	0.0207	-0.0598	0.0367	-0.0597
	(0.0207)	(-0.0598)	(0.0366)	(-0.0598)
(Sum)	0.1992	1.4423	0.6642	1.9643
	(0.1974)	(1.4381)	(0.6530)	(1.9463)
Schmidt values				
(Dirac)	0.1667	1.5	0.6	2.0
(Anomalous)	0.0200	-0.0600	0.0360	-0.0600
(Sum)	0.1867	1.4400	0.6360	1.9400
2. Isovector				
Impulse				
(Dirac)	0.2410	1.5639	0.7834	2.1630
(Anomalous)	-0.6352	1.8438	-1.1122	1.8438
(Sum)	-0.3942	3.4077	-0.3288	4.0068
Schmidt values				
(Dirac)	0.1667	1.5	0.6	2.0
(Anomalous)	-0.6167	1.8500	-1.1100	1.8500
(Sum)	-0.4500	3.3500	-0.5100	3.8500

Table 6

A	15	17	39	41
$< M/M^* >$	1.375	1.221	1.455	1.330
$m_{\rm I}/m_{\rm S}$	1.985	1.097	1.658	1.169
$\tilde{m}_{\rm I}/m_{\rm S}$	1.195	1.191	1.312	1.285
$< M/\varepsilon >$	1.044	1.031	1.053	1.043
$m/m_{\rm S}$	1.110	0.997	1.008	0.996
$m_{\rm LDA}/m_{\rm S}$	1.008	0.996	0.998	0.996
$\tilde{m}_{\rm LDA}/m_{\rm S}$	0.941	1.005	0.969	1.007

Table 7

A	15	17	39	41
$< M/M^* >$	1.191	1.110	1.226	1.166
$m_{\rm I}/m_{\rm S}$	1.446	1.044	1.306	1.082
$\tilde{m}_{\rm I}/m_{\rm S}$	1.111	1.086	1.161	1.133
$< M/\varepsilon >$	1.040	1.027	1.047	1.039
$m/m_{\rm S}$	1.071	0.962	1.046	1.012
	(1.060)	(0.999)	(1.027)	(1.003)
$m_{\rm LDA}/m_{\rm S}$	1.029	0.997	1.017	1.000
$\tilde{m}_{\rm LDA}/m_{\rm S}$	0.978	1.005	0.996	1.008

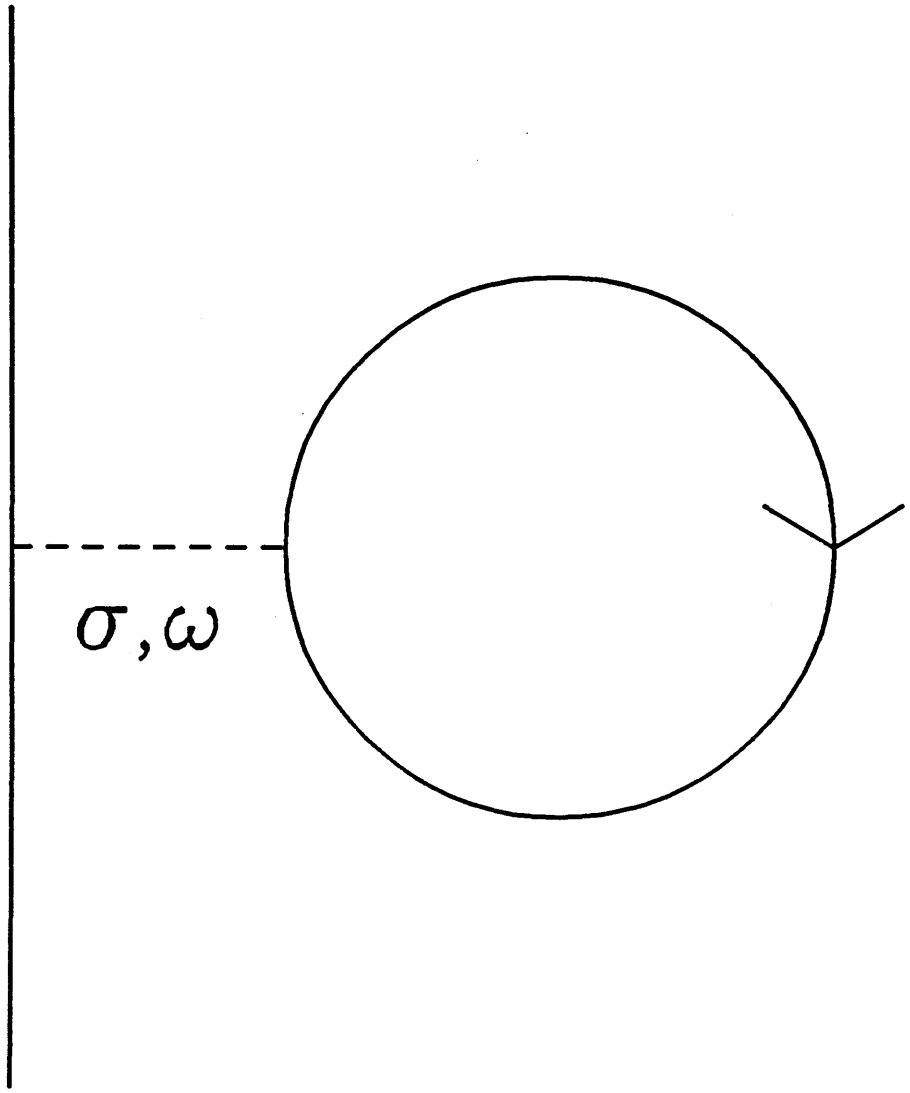

Figure 1

Figure 2

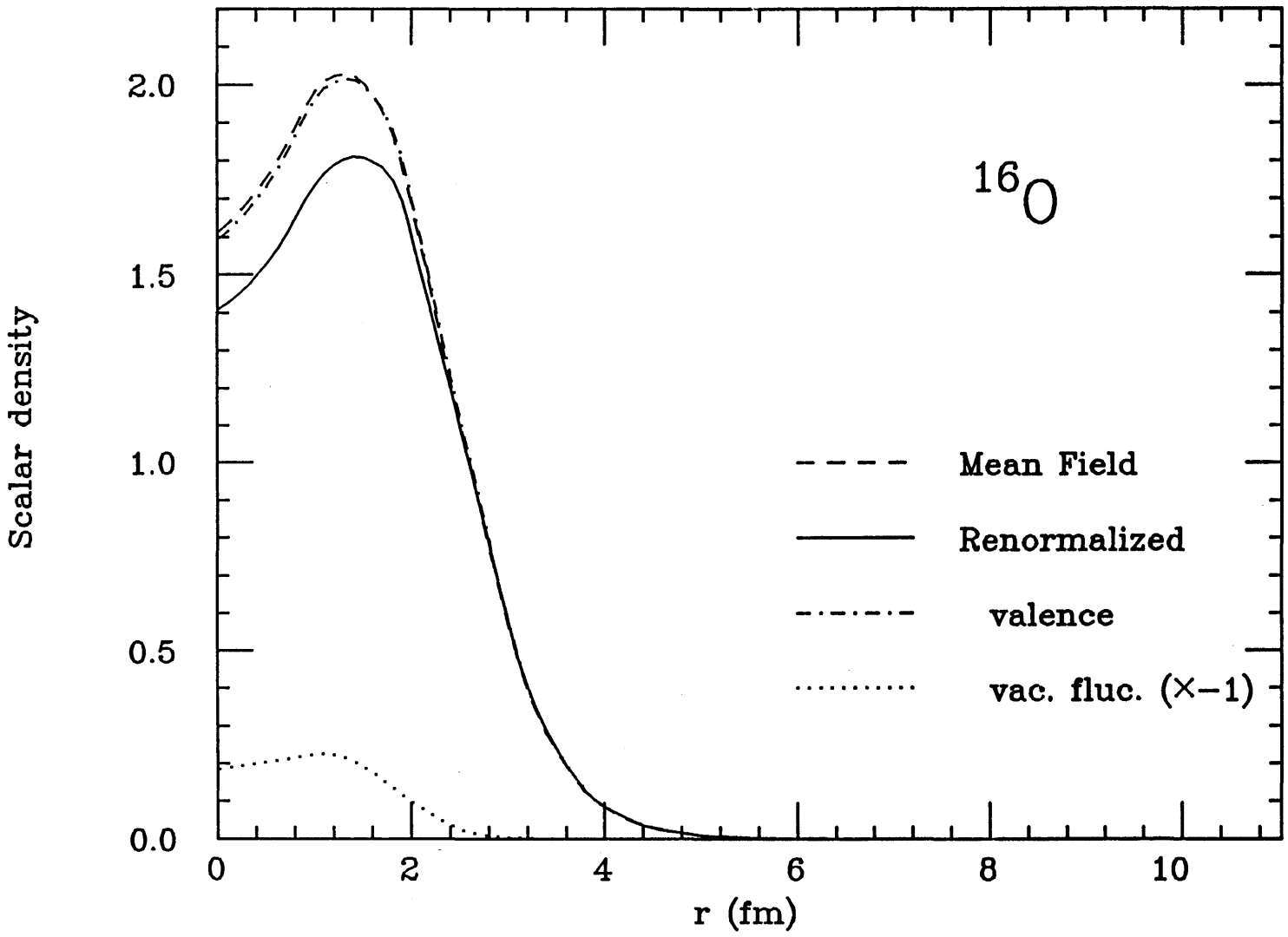
Scalar density
2.0
1.5
1.0
0.5
0.0
0
2
4
6
8
10
r (fm)
^{16}O
Mean Field
Renormalized
valence
vac. fluc. (×−1)

Figure 3

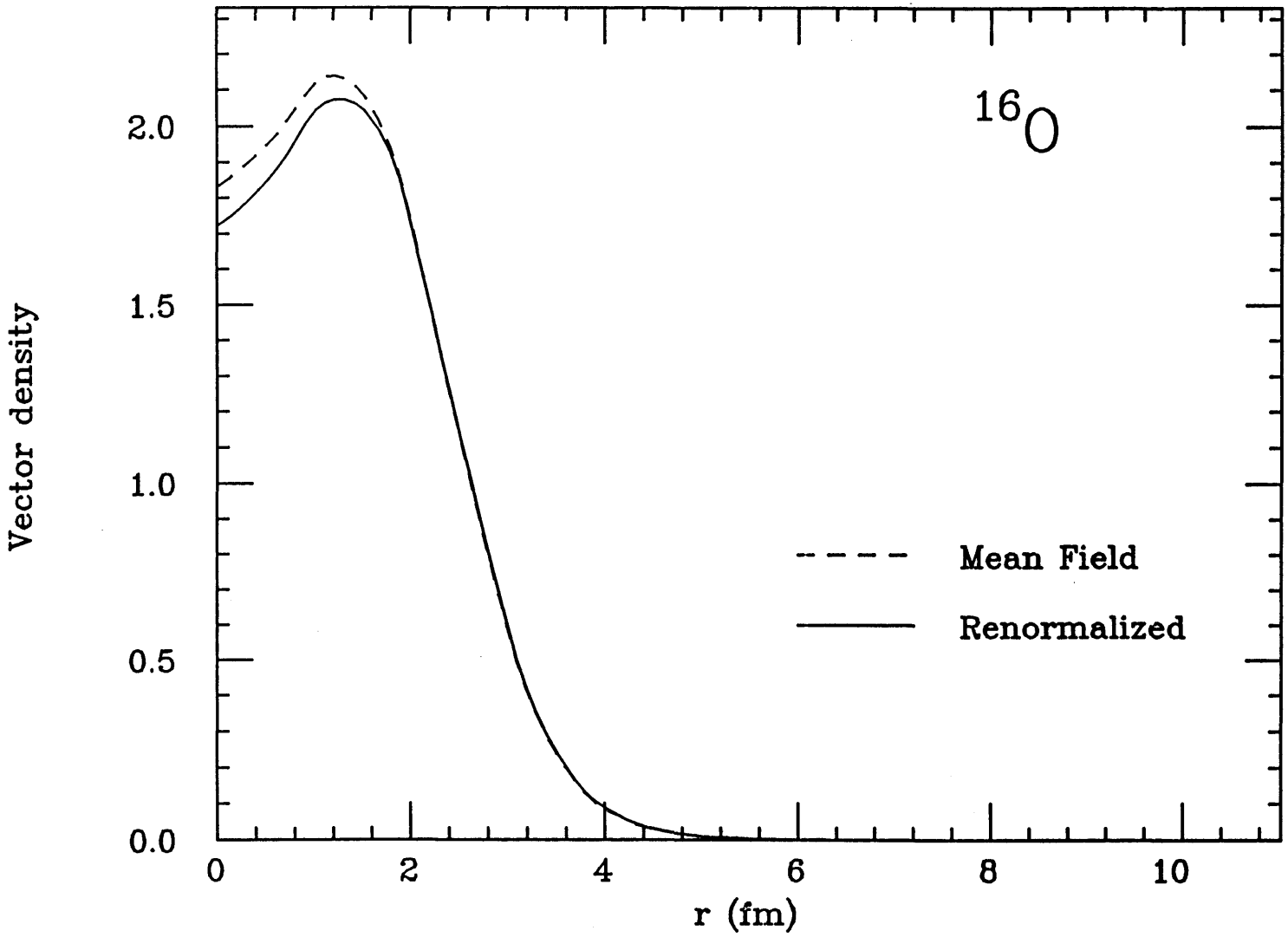
^{16}O
Vector density
2.0
1.5
1.0
0.5
0.0
0
2
4
6
8
10
r (fm)
Mean Field
Renormalized

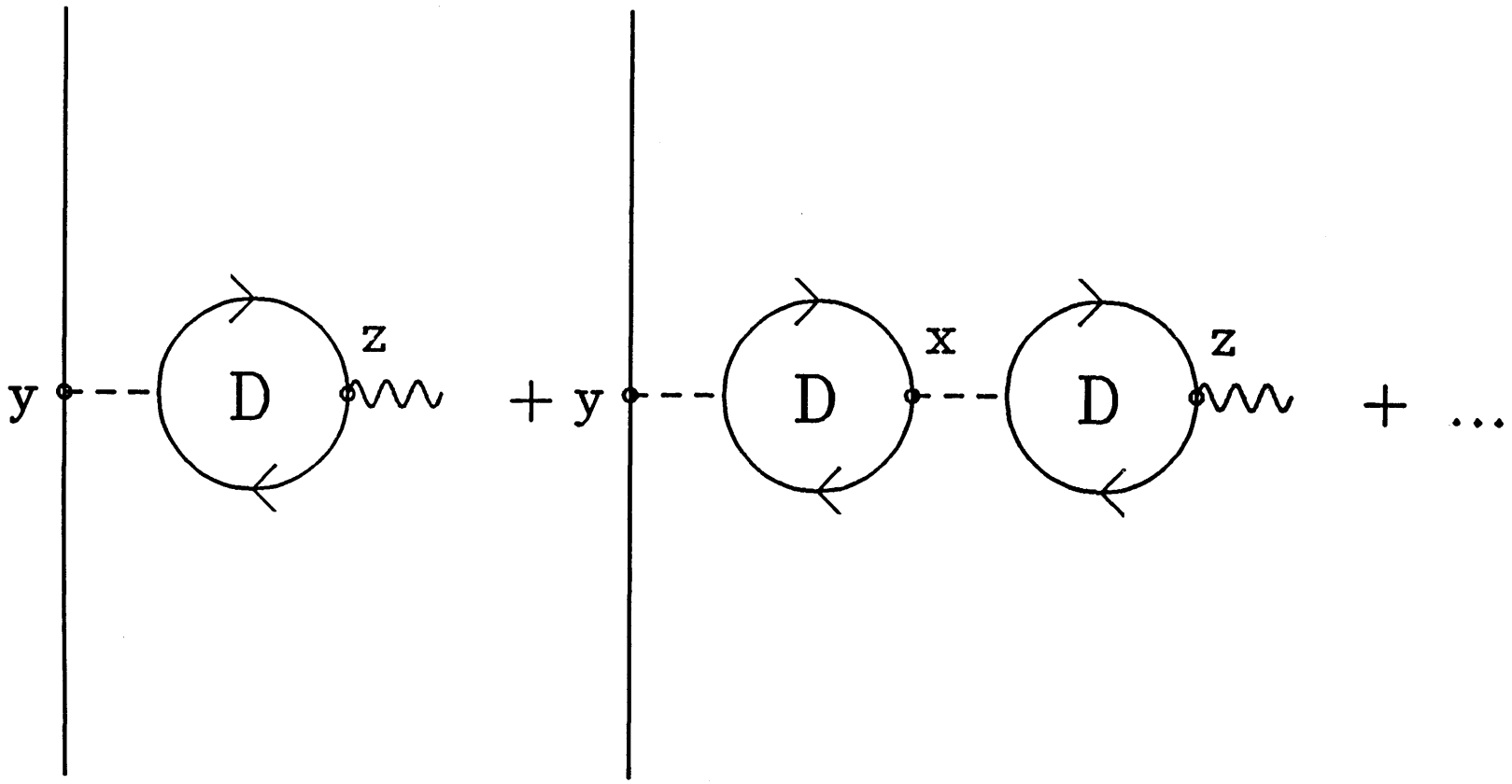

Figure 4

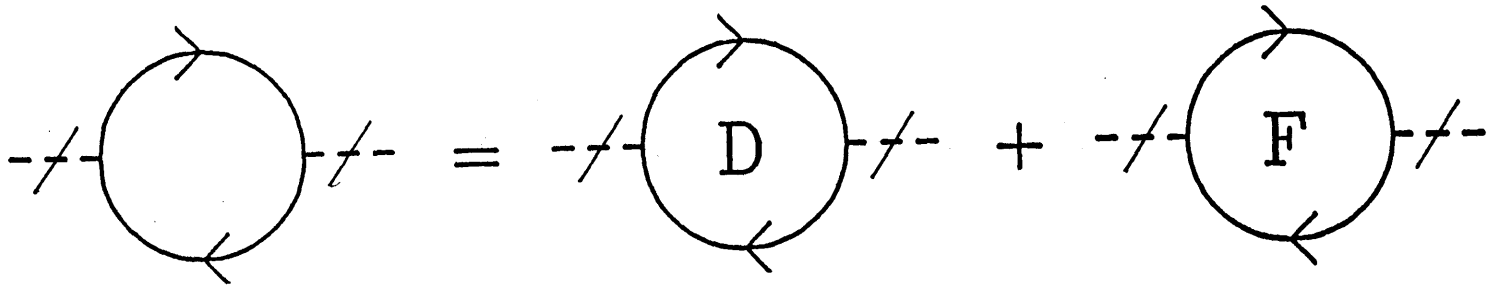

Figure 5

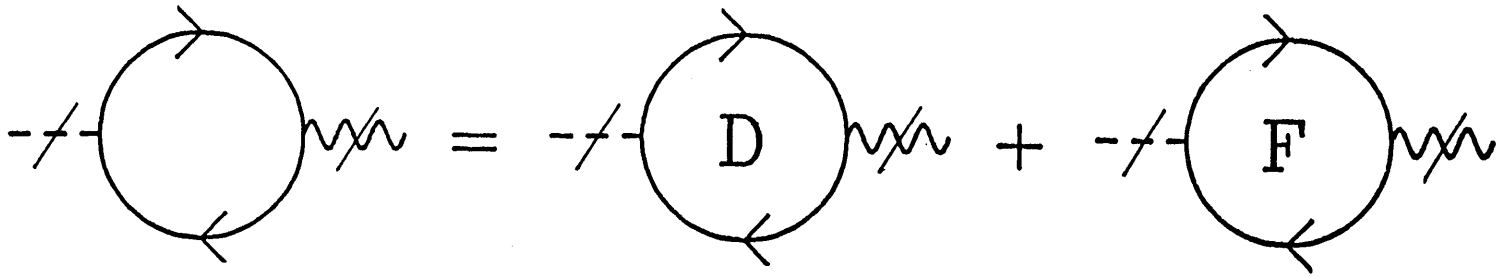

Figure 6

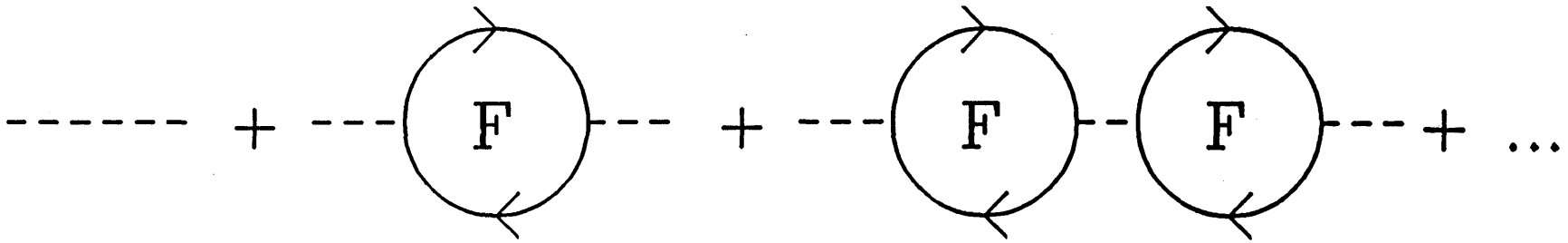

Figure 7

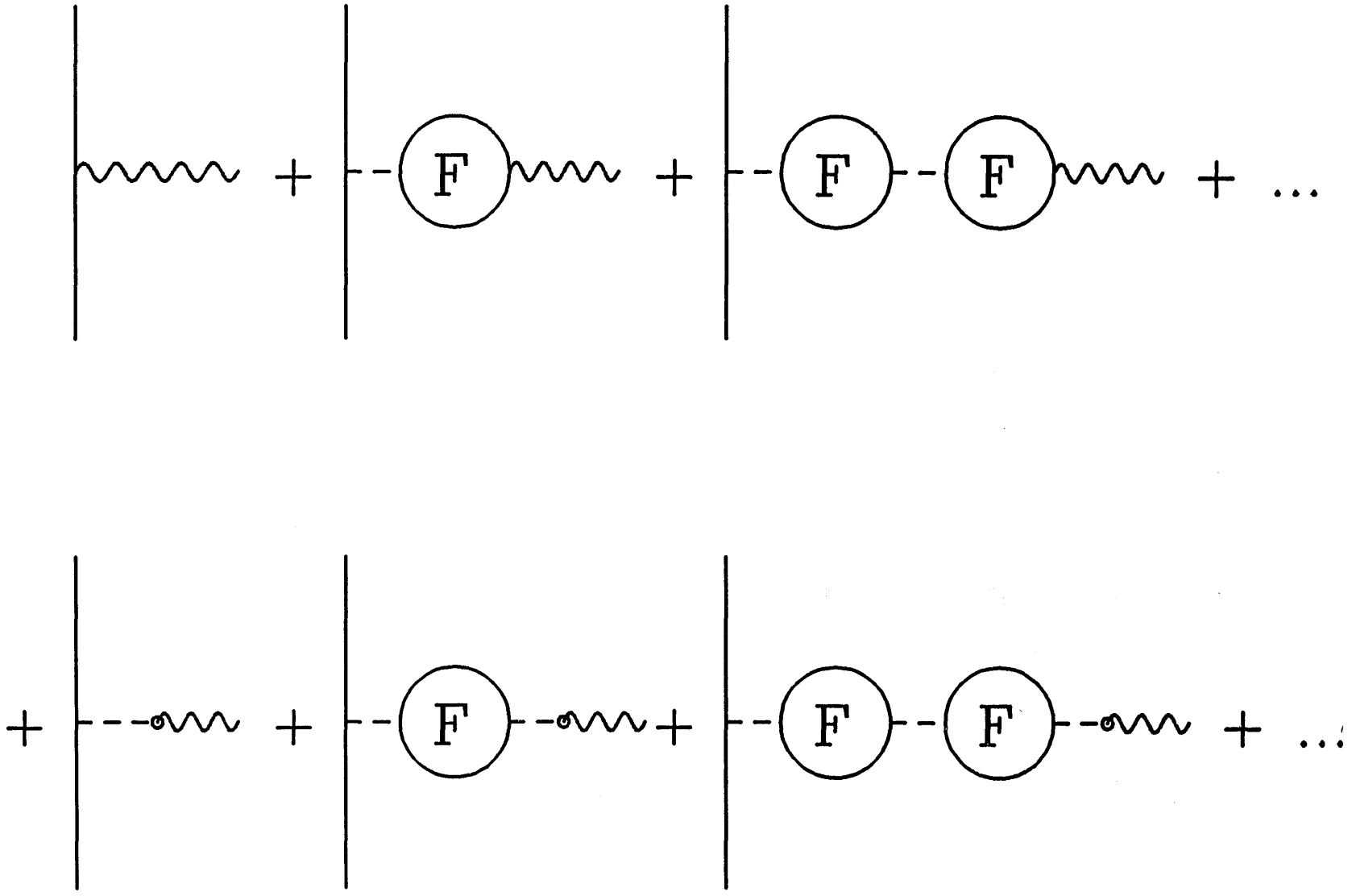

Figure 8

figure 9

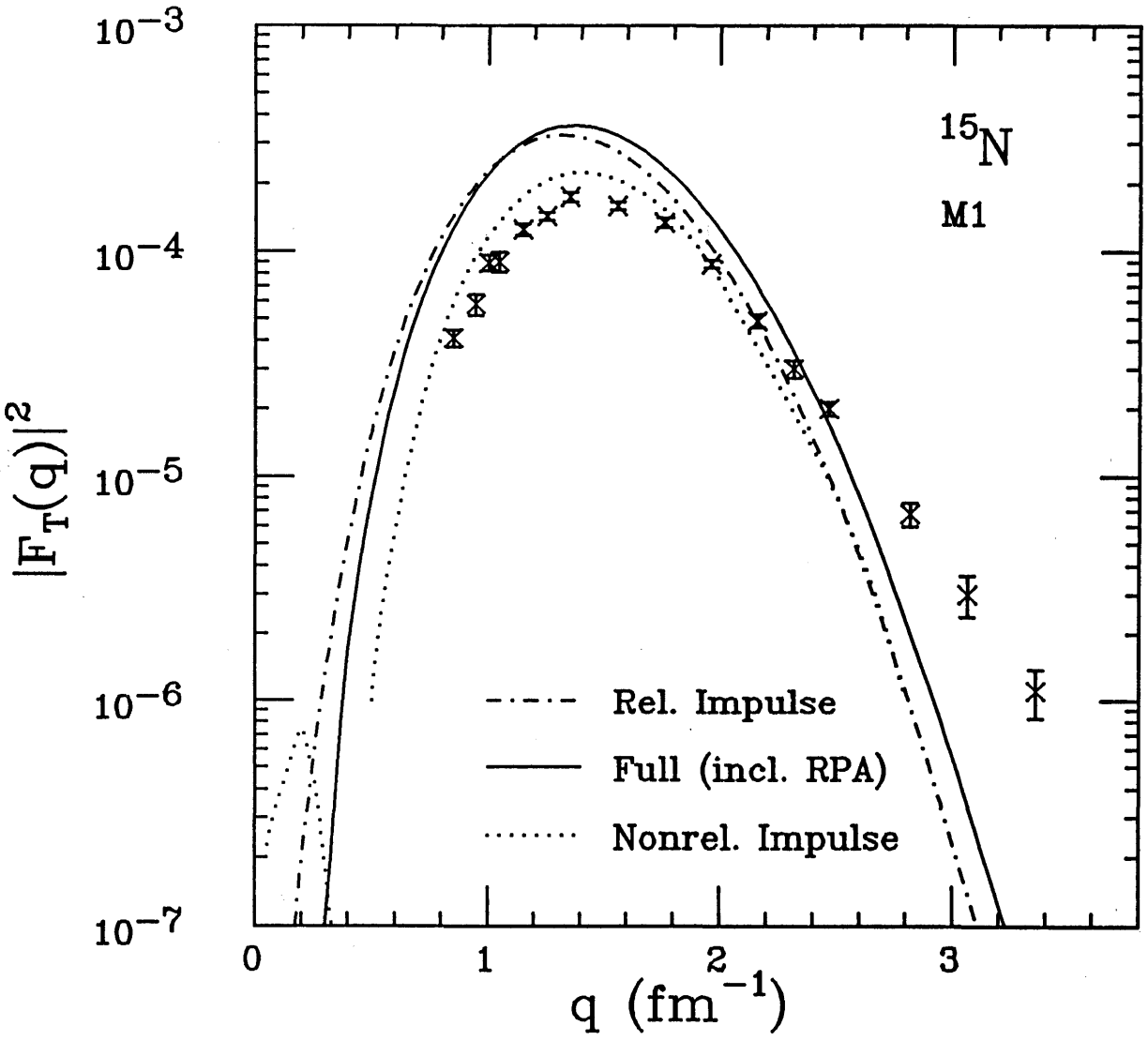
10^{-3}
10^{-4}
10^{-5}
10^{-6}
10^{-7}
$|F_T(q)|^2$
^{15}N
M1
Rel. Impulse
Full (incl. RPA)
Nonrel. Impulse
0
1
2
3
q (fm^{-1})

figure 10

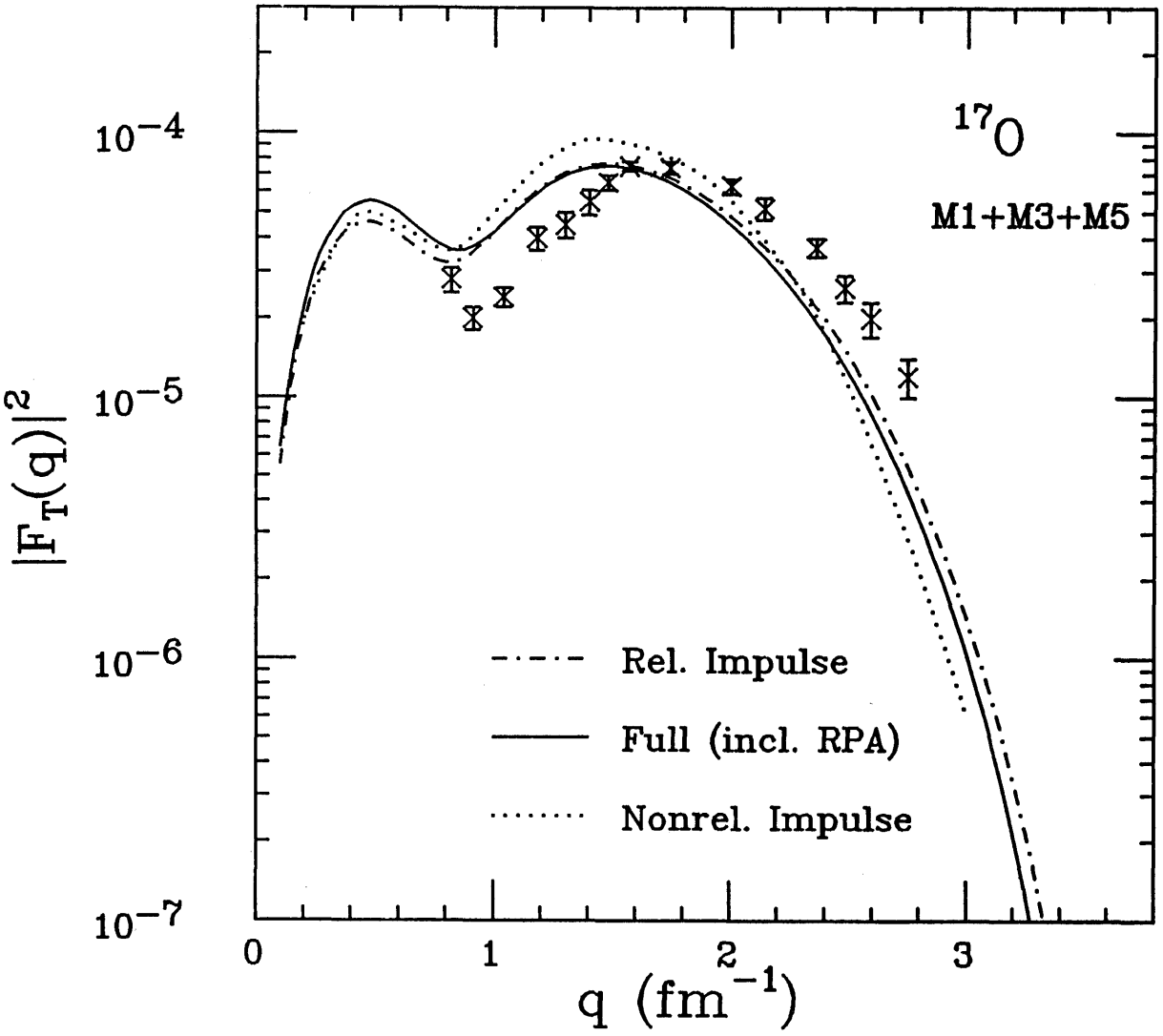
^{17}O
M1+M3+M5
Rel. Impulse
Full (incl. RPA)
Nonrel. Impulse
$|F_T(q)|^2$
10^{-4}
10^{-5}
10^{-6}
10^{-7}
0
1
2
3
q (fm^{-1})

figure 11

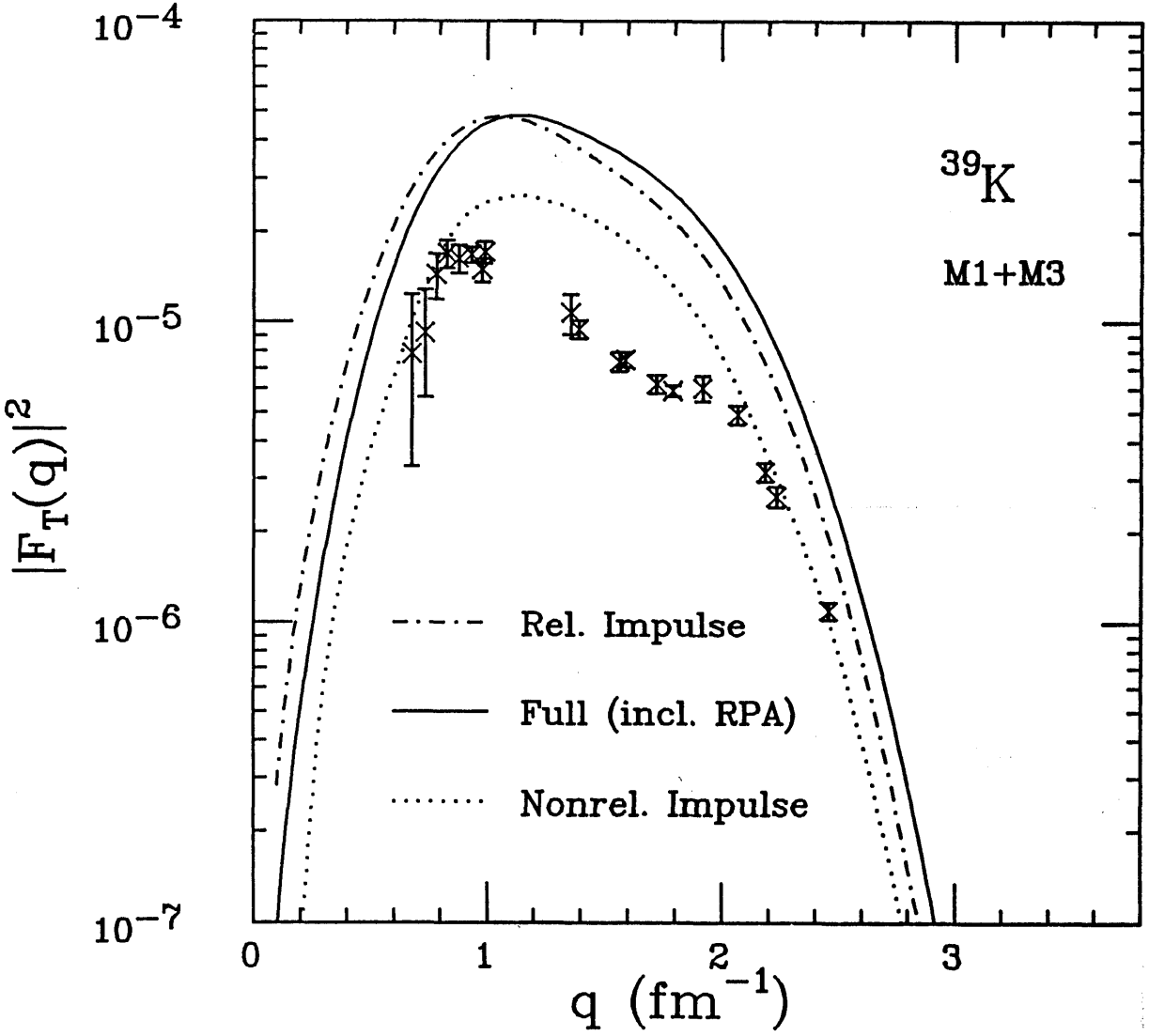
10^{-4}
10^{-5}
10^{-6}
10^{-7}
$|F_T(q)|^2$
^{39}K
M1+M3
Rel. Impulse
Full (incl. RPA)
Nonrel. Impulse
0
1
2
3
q (fm^{-1})

figure 12

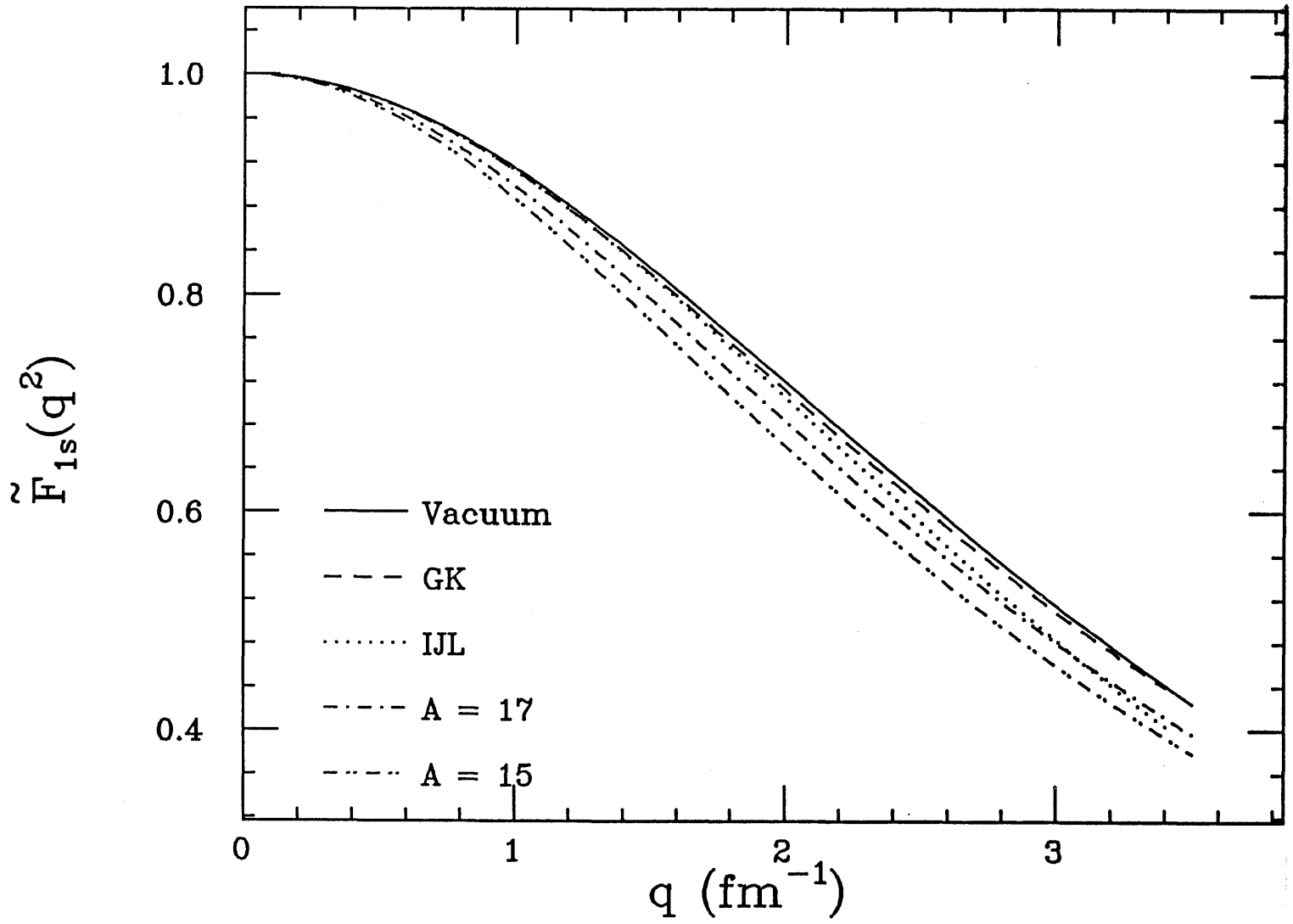

figure 13

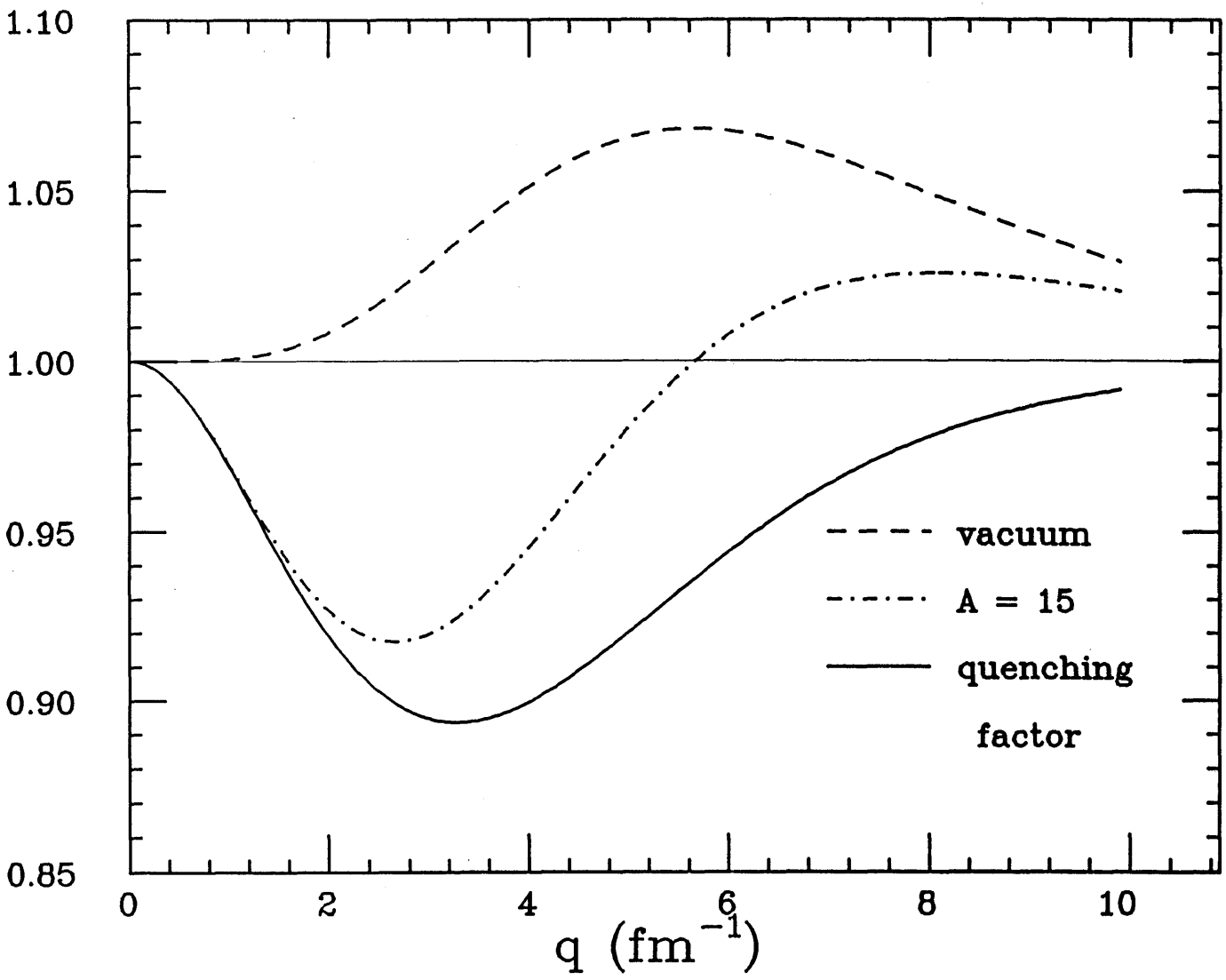
1.10
1.05
1.00
0.95
0.90
0.85
0
2
4
6
8
10
q (fm^{-1})
vacuum
A = 15
quenching
factor

figure 14

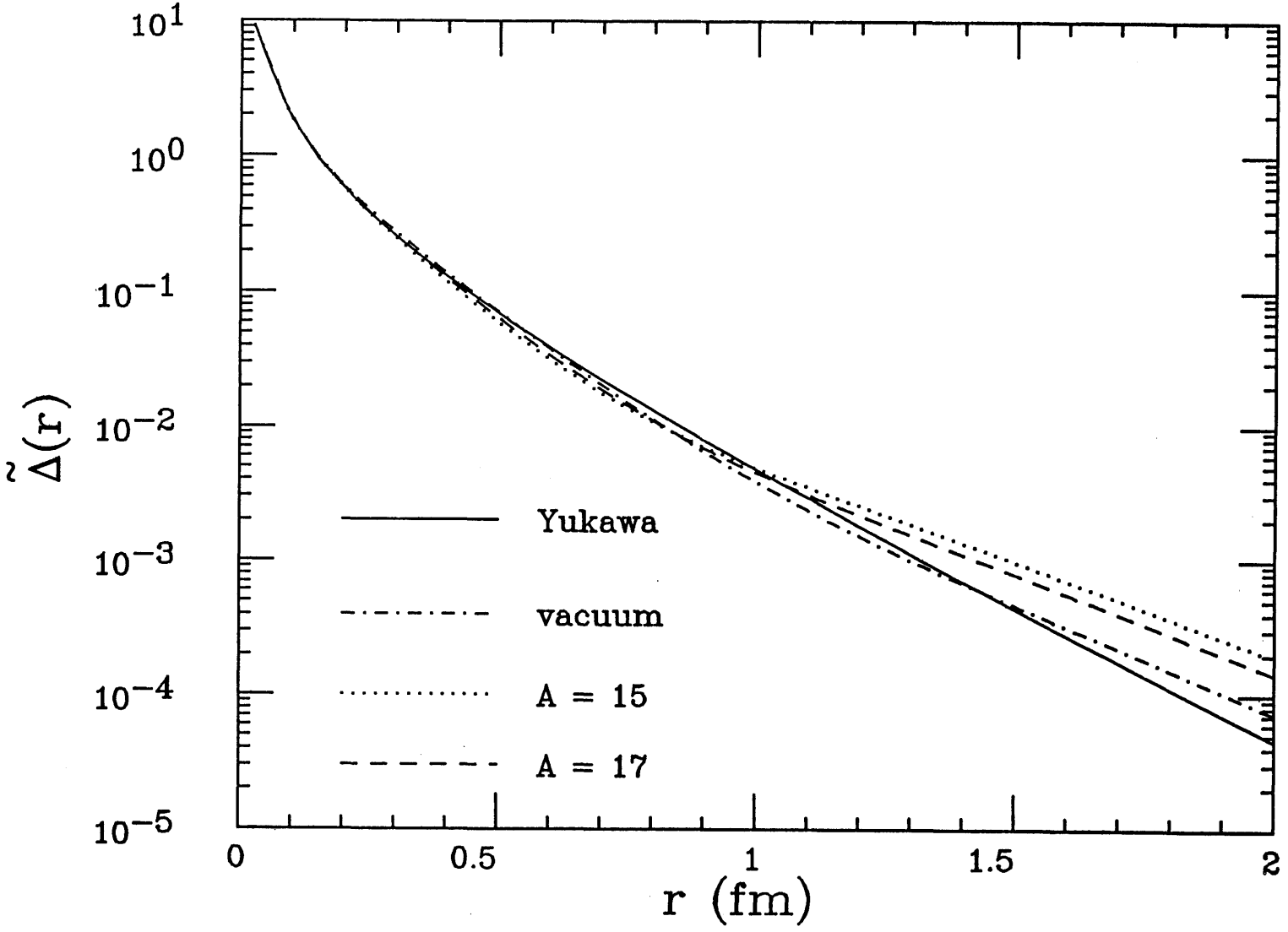
10^1
10^0
10^{-1}
10^{-2}
10^{-3}
10^{-4}
10^{-5}
$\tilde{\Delta}(r)$
Yukawa
vacuum
A = 15
A = 17
0
0.5
1
1.5
2
r (fm)

figure 15

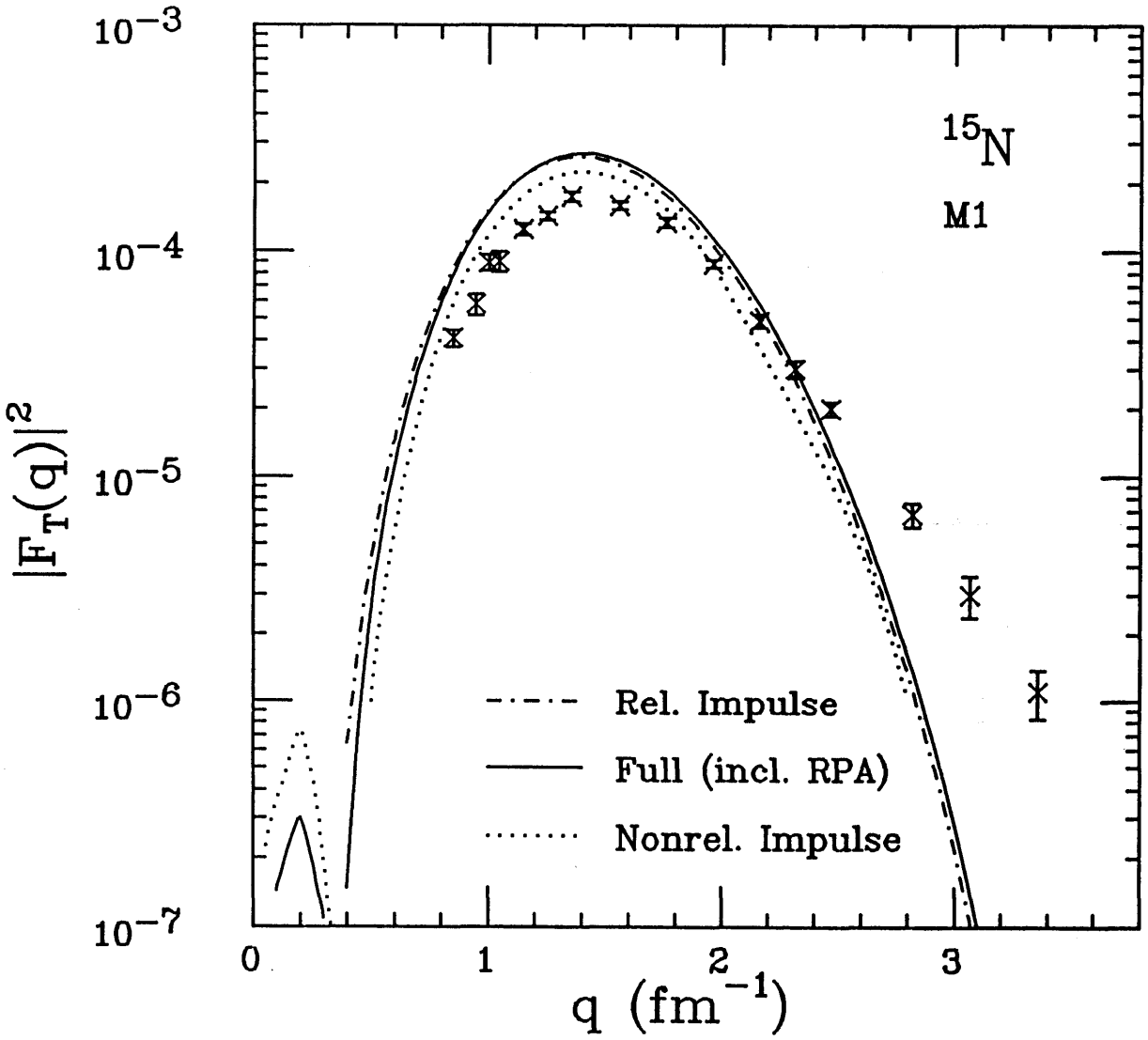
10^{-3}
10^{-4}
10^{-5}
10^{-6}
10^{-7}
$|F_T(q)|^2$
0
1
2
3
q (fm^{-1})
^{15}N
M1
Rel. Impulse
Full (incl. RPA)
Nonrel. Impulse

figure 16

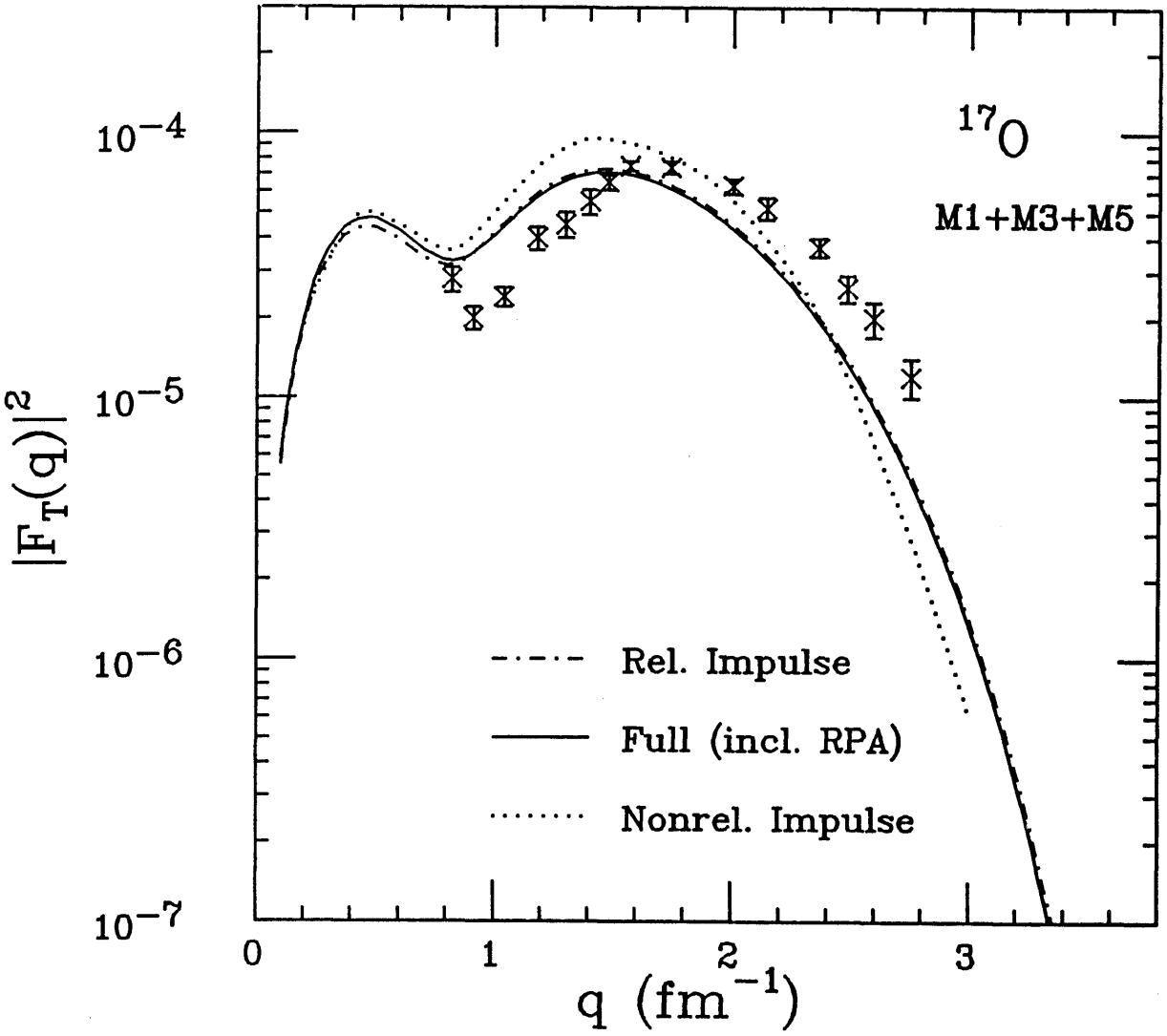
^{17}O
M1+M3+M5
Rel. Impulse
Full (incl. RPA)
Nonrel. Impulse
$|F_T(q)|^2$
10^{-4}
10^{-5}
10^{-6}
10^{-7}
0
1
2
3
q (fm^{-1})

figure 17

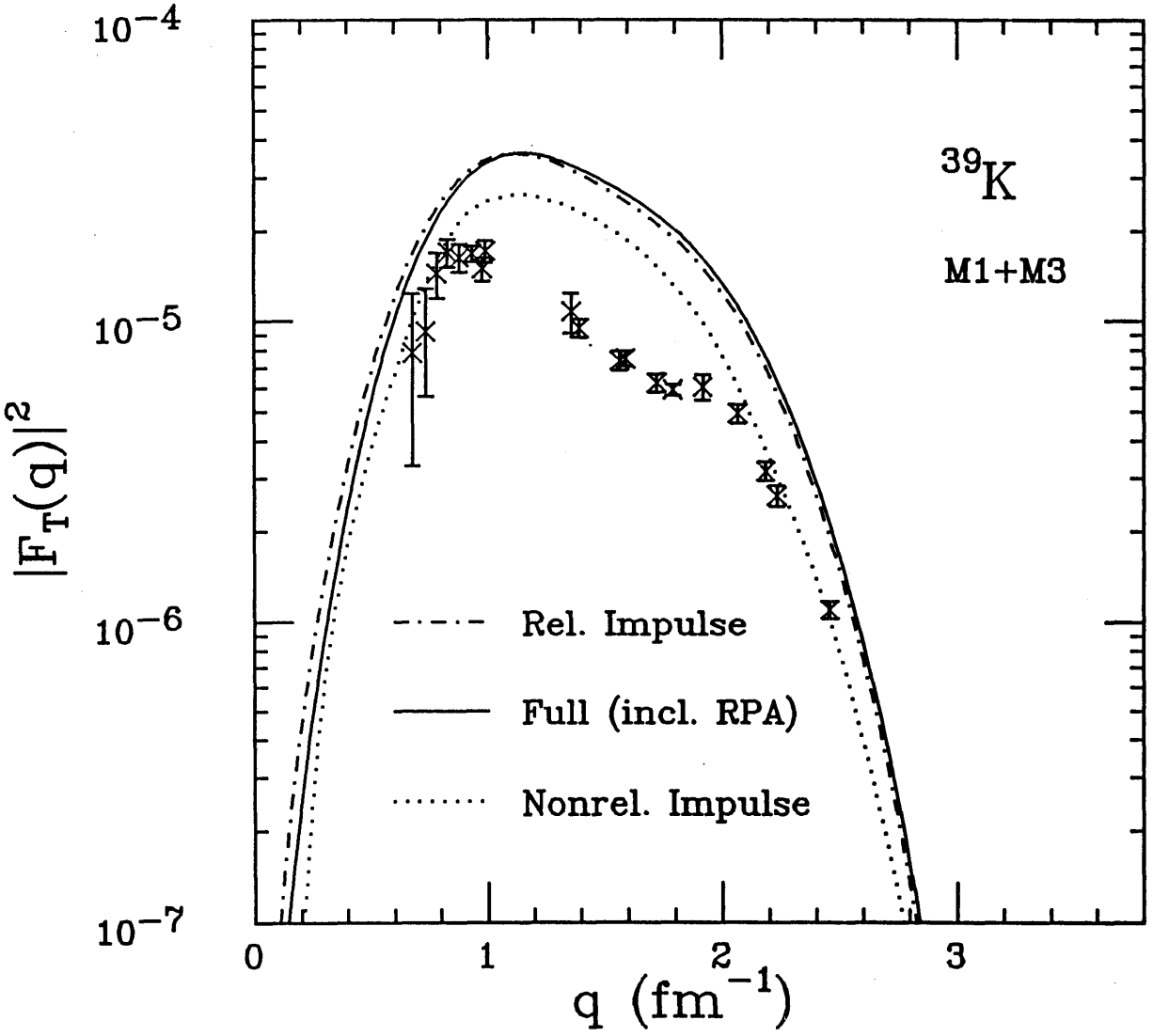
10^{-4}
10^{-5}
10^{-6}
10^{-7}
$|F_T(q)|^2$
^{39}K
M1+M3
Rel. Impulse
Full (incl. RPA)
Nonrel. Impulse
0
1
2
3
q (fm^{-1})

figure 18

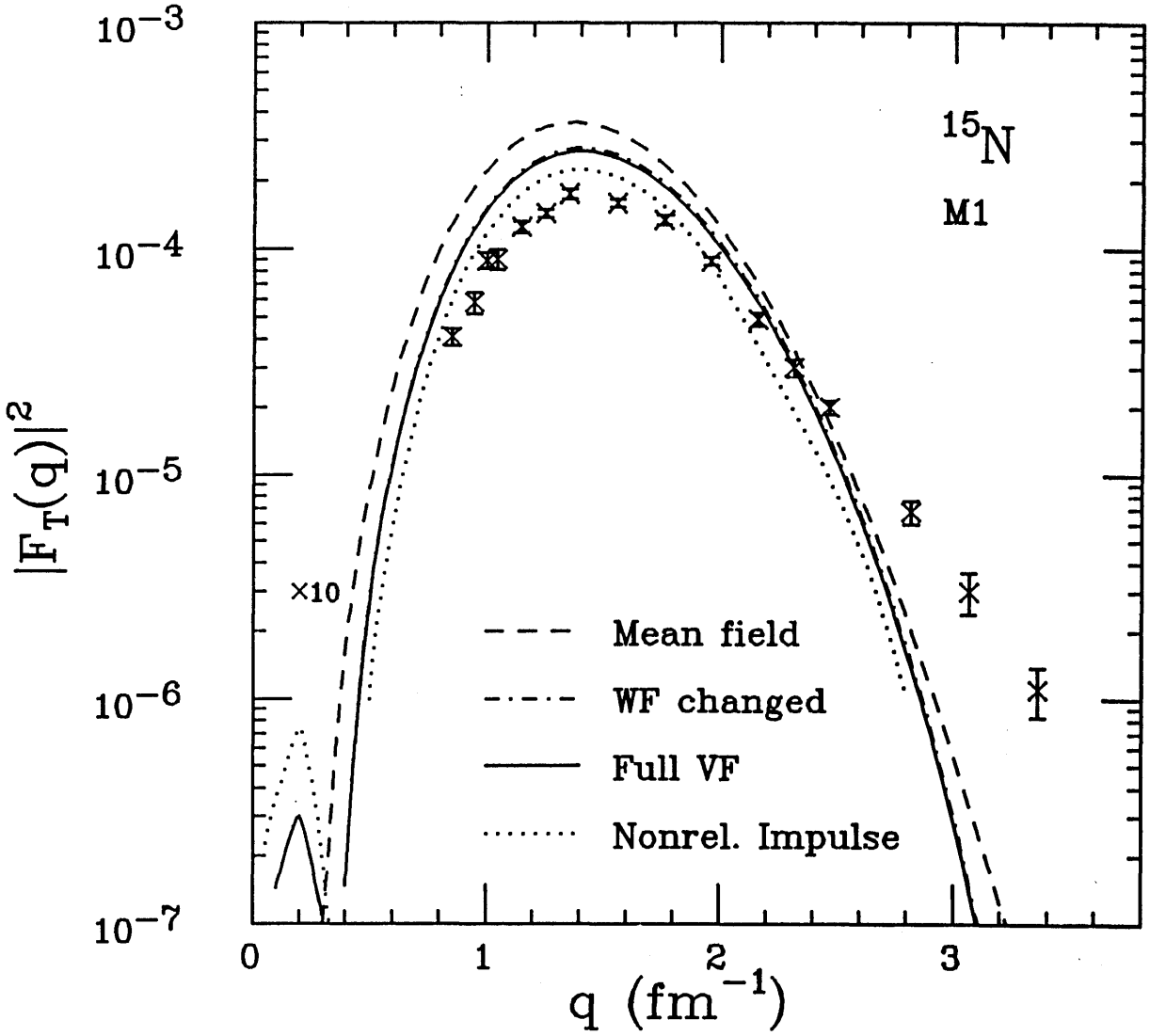
10^{-3}
10^{-4}
10^{-5}
10^{-6}
10^{-7}
$|F_T(q)|^2$
^{15}N
M1
×10
Mean field
WF changed
Full VF
Nonrel. Impulse
0
1
2
3
q (fm^{-1})

figure 19

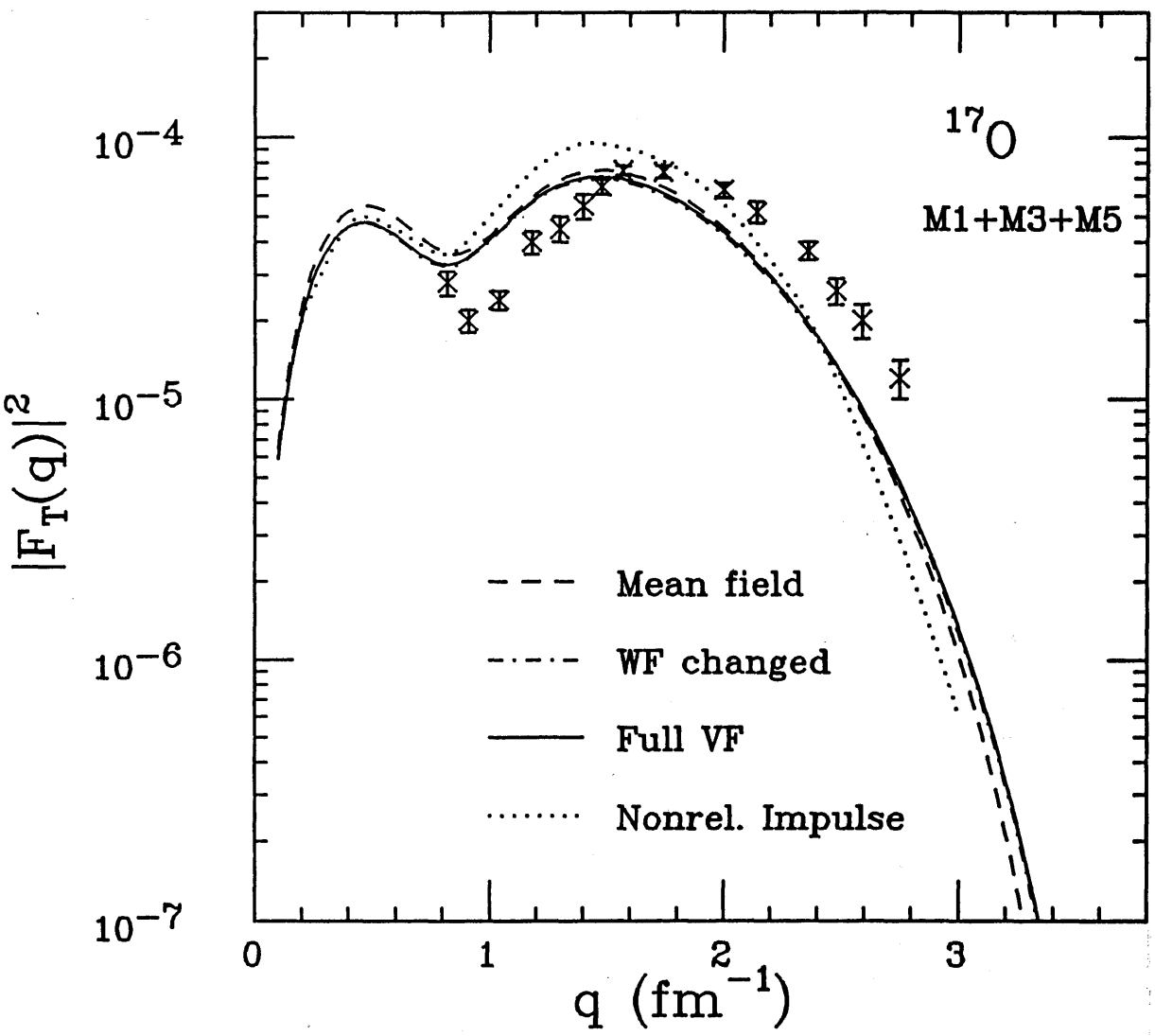
^{17}O
M1+M3+M5
Mean field
WF changed
Full VF
Nonrel. Impulse
$|F_T(q)|^2$
10^{-4}
10^{-5}
10^{-6}
10^{-7}
0
1
2
3
q (fm^{-1})

figure 20

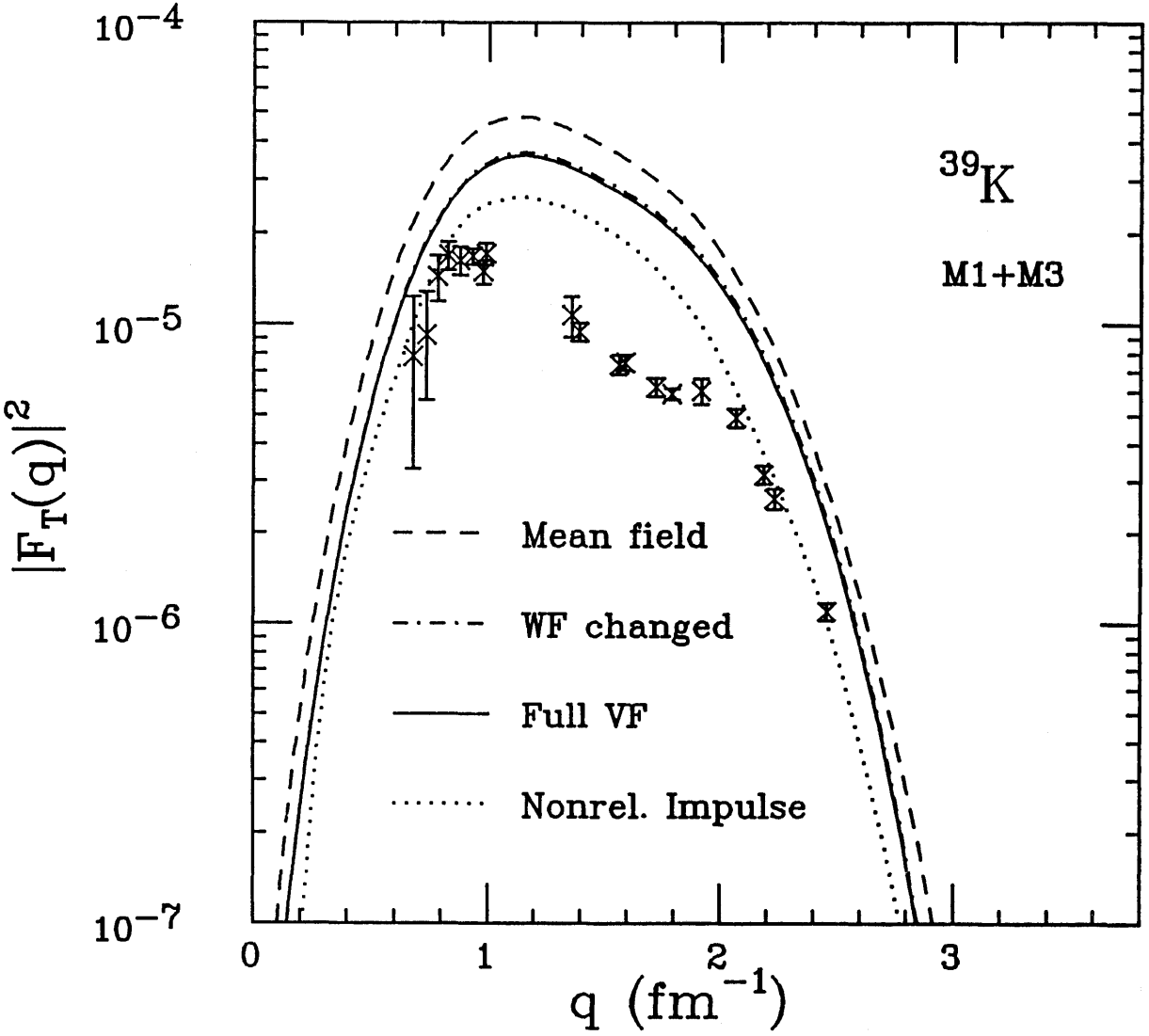
10^{-4}
10^{-5}
10^{-6}
10^{-7}
$|F_T(q)|^2$
^{39}K
M1+M3
Mean field
WF changed
Full VF
Nonrel. Impulse
0
1
2
3
q (fm^{-1})

figure 21